NASA CR-72320

BAC Report No. 8489-945001

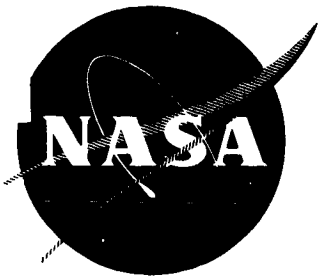

DESIGN REPORT

INVESTIGATION OF ADVANCED THRUST CHAMBER DESIGNS

By

C.H. Brown

Contributors: K. McIlroy, G. Sabak, D. Chizlett

Prepared For

NATIONAL AERONAUTICS AND SPACE ADMINISTRATION

Contract NAS 3-7968

BELL AEROSYSTEMS - A textron COMPANY

P.O. Box 1, Buffalo, New York 14240

NOTICES

This report was prepared as an account of Government sponsored work. Neither the United States, nor the National Aeronautics and Space Administration (NASA), nor any person acting on behalf of NASA:

(a) Makes any warranty or representation, expressed or implied, with respect to the accuracy, completeness, or usefulness of the information contained in this report, or that the use of any information, apparatus, method, or process disclosed in this report may not infringe privately owned rights; or

(b) Assumes any liabilities with respect to the use of, or for damages resulting from the use of any information, apparatus, method or process disclosed in this report.

As used above, "person acting on behalf of NASA" includes any employee or contractor of NASA, or employee of such contractor, to the extent that such employee or contractor of NASA, or employee of such contractor prepares, disseminates, or provides access to, any information pursuant to his employment or contract with NASA, or his employment with such contractor.

Requests for copies of this report should be referred to:

National Aeronautics and Space Administration
Office of Scientific and Technical Information
Attention: AFSS-A
Washington, D.C. 20546

NASA CR-72320
BAC Rept.No.8489-945001

DESIGN REPORT

INVESTIGATION OF ADVANCED THRUST CHAMBER DESIGNS

By

C. H. Brown

Contributors: K. McIlroy, G. Sabak, D. Chizlett

Prepared For:
NATIONAL AERONAUTICS AND SPACE ADMINISTRATION

February 1968

Contract NAS 3-7968

Technical Management
NASA, Lewis Research Center
Cleveland, Ohio
Chemical and Nuclear Rocket
Procurement Section

Rudolph A. Duscha

Bell Aerosystems
P. O. Box 1
Buffalo, N. Y.

CONTENTS

CONTENTS (CONT)

ILLUSTRATIONS

ILLUSTRATIONS (CONT)

TABLES

LIST OF SYMBOLS

A	area	$in.^2$
a	conduction path length	in.
b	conduction flow area	$in.^2$
C_p	specific heat	BTU/lb °R
D_H	hydraulic diameter	in.
F	Gray body radiation factor	- -
f	Fanning friction factor	- -
g	gravitational constant	$32.2\ ft/sec^2$
h	forced convection film coefficient	$BTU/in.^2$ sec °R
J	Joule constant	778 ft lb/BTU
k	thermal conductivity of wall material	BTU in./hr ft^2 °R
K	thermal conductivity of hydrogen	BTU in./$in.^2$ sec °R
P	static pressure	psia
$\dot{q}$	heat flux rate	BTU/sec $in.^2$
$\dot{Q}$	heat rate	BTU/sec
S	external surface area	$in.^2$
T	temperature	°R
V	velocity	ft/sec
$\dot{W}$	hydrogen flow rate	lb/sec
X	length	in.

GREEK

Δ	increment	- -
ϵ	emissivity	- -
μ	viscosity	lb/ft sec
υ	kinematic viscosity	ft^2/sec
ρ	density	lb/ft^3

σ	Stefan-Boltzmann constant	0.173×10^{-8} BTU/ft^2 hr $^\circ$R
ϕ	correction factor for asymmetric heating, curvature, and entrance length effects, considered unity for this analysis	- -
τ	wall thickness	inches

SUPERSCRIPTS

- time rate

SUBSCRIPTS

1, 2	. . . . .station locations
i, j	. . . . .arbitrary nodes
cw	cold wall
r	recovery
L	fluid
w	wall
o	outer

I. SUMMARY

This program is directed towards developing advanced designs and fabrication techniques for regeneratively cooled rocket thrust chambers. The selected design shall show promise of reducing fabrication cost and time, reducing heat flux to the coolant, and increasing thrust chamber life. The completed thrust chamber shall be delivered to NASA, LeRC where experimental evaluation will be conducted.

Detailed design studies and analyses led to the selection of TD nickel for the inner liner material. The inner liner contains the coolant flow channels which are produced by electrical discharge machining. The outer shell is produced by electroforming nickel on the lands of the inner liner.

Various design configurations consisting of tubular and milled channel flow passages were analyzed and compared. An extensive material study was conducted comparing the advantages and disadvantages of refractory metals, superalloys, and dispersion hardened alloys. Alternate fabrication methods for the inner liner, coolant passages and outer structural shell were evaluated i.e., High Energy Rate Forming (HERF), spinning and conventional forming. Chemical milling, electrochemical milling, electro discharge machining and conventional milling were compared for producing the flow passages. Electroforming, diffusion bonding, explosive welding, conventional welding and brazing were evaluated for the outer structural shell.

The effects of any particular fabrication methods upon the design were carefully evaluated to insure the objectives of the program were not unjustly compromised.

II. INTRODUCTION

A conventional regeneratively cooled rocket thrust chamber is generally constructed from a number of tubes that have been formed to the chamber shape and joined together by brazing or welding. The tubes have also been shaped such that the cross-sectional area is tailored to the thermal and pressure requirements at any particular axial station in the engine. Though this method of construction results in an efficient heat exchanger there are many shortcomings relative to fabricating such a design.

The fabrication of a conventional tube bundle consists first, of drawing and then intricate die-forming of the tubes to produce the desired cross-sectional areas and contour. The tubes are then layed up on a mandrel and further formed to insure intimate fit-up to one another. After locating manifolds, flanges, and other supporting members the assembly is brazed or welded. Leakage checks are performed and frequently reveal many areas that were not joined or bonded, making repair necessary by time consuming hand methods. These often produce local disturbances to fluid flow, heat transfer, and can create stress risers. Because the initial fabrication development of this type of thrust chamber requires considerable time and expense, changes in contour, diameters, propellants, and other new innovations are prohibitive.

This report will describe new design configurations, fabrication techniques, and materials of construction that show promise of reducing fabrication cost and time, reducing heat flux to the coolant, and increasing thrust chamber life.

A detailed heat transfer analysis demonstrated a considerably higher heat flux than was originally anticipated. The higher heat flux was found to have a profound influence on the pressure drop through the coolant passages. Since one of the primary objectives of the program is to reduce the heat flux to the coolant, an extensive effort was made to explore alternate design configurations and materials of construction that would satisfy this goal.

Various refractory metals, superalloys and dispersion hardened alloys for the inner thrust chamber liner, which is exposed to the combustion gas, were subjected to critical design analysis. Alternate coolant passage configurations, such as stepped diameter tubes constructed from refractories or stainless steel and coolant channels machined in the inner liner were studied, in an effort to obtain a simplified but efficient heat exchange medium.

Alternate methods of attaching the outer structural shell, which in some cases also served as part of the coolant passage container, were studied and compared. Various materials for the shell were also studied and optimized for each overall thrust chamber configuration.

Various methods of forming the inner liner were explored. These methods included:

(1) Drop hammered and welded sections
(2) High energy rate forming
(3) Spinning

These methods were compared for their structural integrity, economy and fabrication time.

III. GENERAL DISCUSSION

The designs and analyses performed were specifically for a nominally 8000 lb thrust hydrogen-fluorine engine, operating at a chamber pressure of 400 psia, with an oxidizer-to-fuel mixture ratio of 12, and having a nozzle expansion area ratio of 60. The chamber characteristic length is a minimum of 25. Based on these analyses, a thrust chamber will be fabricated and delivered to LeRC where experimental evaluation will be conducted.

The proposed preliminary design to be subjected to a detailed design analysis consisted of an inner columbium alloy liner to which a coating was applied internally, to prevent attack of the combustion products. An insulating fibrous metal was applied to the outer surface of the liner. Constant diameter stainless steel tubes, contiguous at the throat only, were joined to the fibrous metal (see Figure 1). The columbium inner liner would permit higher design wall temperatures, thereby lowering the heat flux to the coolant. The constant diameter tubes would then eliminate many of the shortcomings of conventional formed tubes.

A detailed heat transfer analysis resulted in an unforeseen high heat flux and a nonlinear reduction of heat flux with increasing gas sidewall temperatures. The higher heat flux was attributed largely to the thermal conductivity of the combustion gas at an average temperature between gas and wall. The original design conceived for this program a pressure drop through the coolant passages of 125 psi maximum. Since it was shown that the heat flux was substantially higher than originally predicted, it was obvious the coolant side heat transfer coefficient must be correspondingly increased to maintain the design wall temperature. It was found that the higher coefficient, caused the pressure drop through the coolant passages to rise far in excess of the design goal of 125 psi.

In an effort to alleviate the high pressure drop being encountered, a parametric analysis was initiated and extended to include:

(1) Lower driving total gas temperatures
(2) Higher wall temperatures

The original design wall temperature was 2700°F with a driving total temperature of 7500°R. Increasing the wall temperature (as suggested in 2) would require the use of higher temperature materials such as tungsten or its alloys, graphite, ablative materials, molybdenum, tantalum or its alloys. The original proposed material was to be a columbium alloy for the inner liner. Decreasing the driving total gas temperature (as suggested in 1) would require the injector to produce a lower mixture ratio gas along the chamber wall.

The first suggestion was disregarded after further consideration. It was believed that the injector design was capable of producing the full design mixture ratio of 12:1 along the wall, thus delivering the highest performance. Therefore, a concentrated effort was applied to increasing the wall temperature. A parametric analysis was performed maintaining the same basic design configuration, an inner metallic liner to which a fibrous metal and constant diameter tubes were attached, where the wall temperatures were varied to

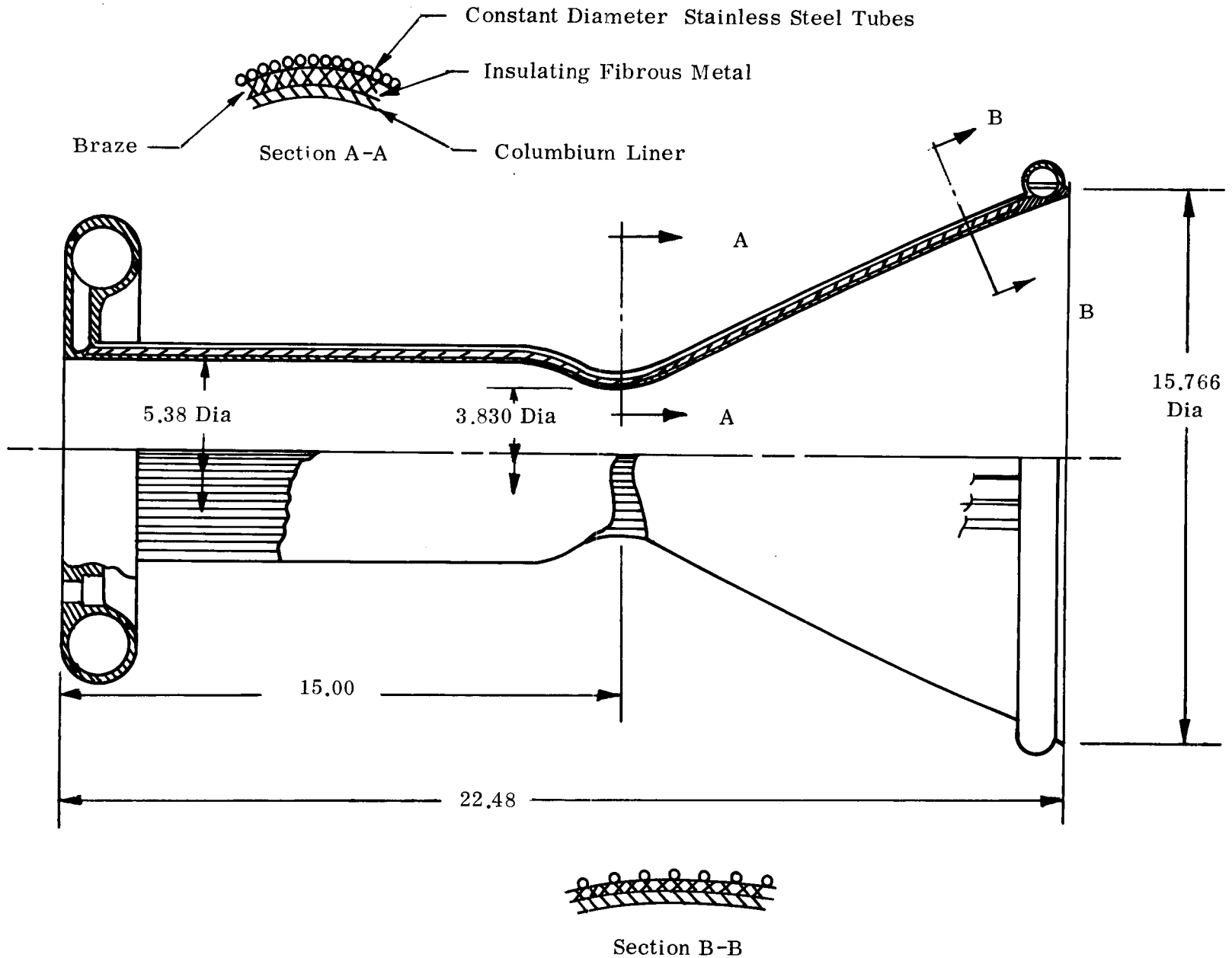

Figure 1. Proposed Preliminary Design

determine the effects upon the coolant passage pressure drop. The analysis indicated that even at higher gas sidewall temperatures, 4500°F, the pressure drop was far in excess of 125 psi using constant diameter tubes and maintaining a tube wall temperature low enough to permit the use of stainless steel tube material. These results suggested that three other alternatives be investigated:

(1) Vary the tube diameter in steps
(2) Utilize a high temperature material for the tubes
(3) A combination of (1) and (2).

The parametric and design analysis was further extended to evaluate the new alternatives. Varying the stainless steel tube diameter in a stepped manner still produced pressure drops much higher than desirable, 400 to 500 psi. Stepped diameter refractory metal tubing produced lower pressure drops, although still in excess of 125 psi. The high temperature stepped tubes would also present new fabrication problems. It was believed that forming the tube would be difficult and expensive, also joining the tubes to the inner liner would require significant development; the more ductile high temperature tube materials would require a special protective coating to the tube interior to prevent hydrogen embrittlement of the grain structure. A ductile material is desirable due to the severe imposed thermal stresses occurring during operation. Since tubes, even though simplified, seemed to offer no advantages over a conventional tube bundle design, it was decided to investigate other coolant passage concepts.

A design was conceived that contained flow channels of varying cross-section between an inner and outer liner. The flow channels would be machined in an inner liner; next an outer shell, made in two longitudinal sections, would be joined by brazing or other unique advanced joining techniques.

A new parametric heat transfer analysis was conducted where the wall temperatures and local flow channel sizes were varied so that the pressure drops could be determined. Many high temperature refractory metals were evaluated during this analysis but only two appeared to be suitable from a combined heat transfer and structural standpoint, the columbium and tantalum alloys. Of these two, the columbium alloy SCb-291 proved to be superior on a strength to weight basis at the operating temperature selected. The gas sidewall temperature selected was based upon a proven coating to protect the liner from the products of combustion. Though the pressure drop, 195 psi, through the coolant passages was still in excess of the 125 psi goal, it was believed that the design had been optimized within the limitations of fabrication techniques and materials of construction, also the 195 psi probably represented a more realistic value. The columbium liner channeled chamber was then subjected to a detailed design and fabrication analysis.

As a part of the detailed analysis, coatings or platings to prevent the interior surfaces of the flow channels from becoming embrittled by hydrogen were thoroughly evaluated. Very limited development work has been done in this area and it was believed that the only coating material that would offer complete protection to hydrogen embrittlement and still be compatible with subsequent fabrication operations is tungsten. The method of applying the tungsten coating has been developed for single shapes, surfaces and relatively small overall sizes. A development program would be required for a part the size of the subject thrust chamber with intricate flow channels to insure adequate and uniform surface coverage.

The required thickness of tungsten would also have to be determined by preparing specimens and performing tests in hydrogen. An estimate was prepared to accomplish the above development program along with an estimate to complete the entire design efforts and fabricate the thrust chamber. At this point, the program was closely scrutinized in an effort to determine the risks involved in obtaining a truly satisfactory and reliable tungsten coating at a reasonable cost and in a reasonable time.

A design review was conducted at the NASA, LeRC. The design and analysis leading up to the columbium liner, channeled chamber concept was presented in detail. It was decided that the objectives of the overall program may be jeopardized by attempting to develop a satisfactory protective coating against hydrogen embrittlement. It was also felt that the 125 psi pressure drop goal may be unrealistic with respect to materials available today. The concept of milled channels, however, appeared to offer flexibility in design changes with minimum cost and change-over time in fabrication. It was, therefore, decided to continue the basic channeled chamber concept, but increase the pressure drop limitation so that lower gas sidewall temperatures could be used and lower temperature metals not prone to hydrogen embrittlement could be investigated.

Previous parametric heat transfer analyses indicated that pressure drops between 300 and 400 psi might be obtained with the channeled chamber, if the gas sidewall temperature was held between 2000 and 2500°F. Materials known as superalloys and dispersion hardened alloys fall in this temperature range and most are not susceptable to embrittlement by hydrogen. It was then decided that two such materials, Hastelloy X, a superalloy, and TD nickel, a dispersion hardened alloy, would be subjected to a preliminary heat transfer, structural and fabrication analyses. Upon completion of these analyses, tradeoffs would be made and one material selected for final analysis.

The results of the analyses indicated that TD nickel was far superior to Hastelloy X from the standpoint of heat transfer, strength and fabrication tolerances. The TD nickel thrust chamber has a pressure drop of 292 psi where the Hastelloy X has a pressure drop of 375 psi. During the fabrication analysis it was found that the Hastelloy X chamber would require manufacturing tolerances beyond the realm of practicality. These design tolerances were necessary to prevent structural failure by local overheating. Hastelloy X was originally selected for comparison to TD nickel because:

(1) It is considerably cheaper per pound than TD nickel
(2) Welds present less of a problem in Hastelloy than they do in TD nickel

However, Hastelloy X did not possess the properties required to meet the objectives of the program therefore, TD nickel was considered to be the best candidate material.

A final heat transfer and stress analysis was performed on the thrust chamber using TD nickel as the inner liner material. This analysis optimized the flow channels and wall thicknesses.

A study was made in an effort to optimize the fabrication techniques for the TD nickel thrust chamber and is discussed in detail under Section VII of this report. Alternate methods for forming and joining the inner liner, producing the flow channels and attaching the outer shell and manifolds were compared from a cost, time and reliability standpoint. It was concluded that the inner liner would be spun in two sections and welded, the flow channels would be machined by the electrodischarge machining method and the outer shell and manifolds would be formed by the electroforming process using pure nickel as the base material. Figure 2 is the design layout which depicts this concept.

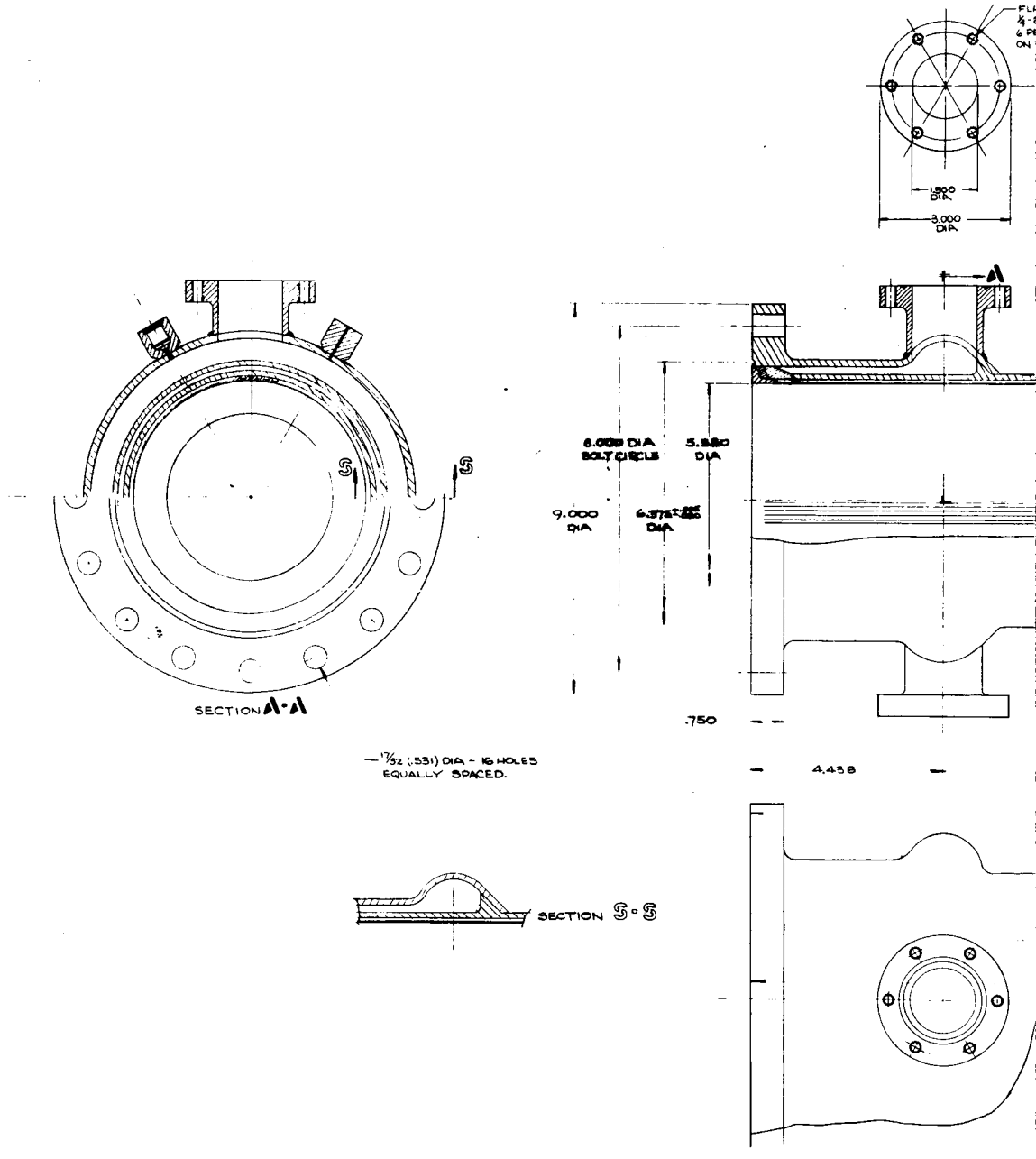

Figure 2. Final Design Layout

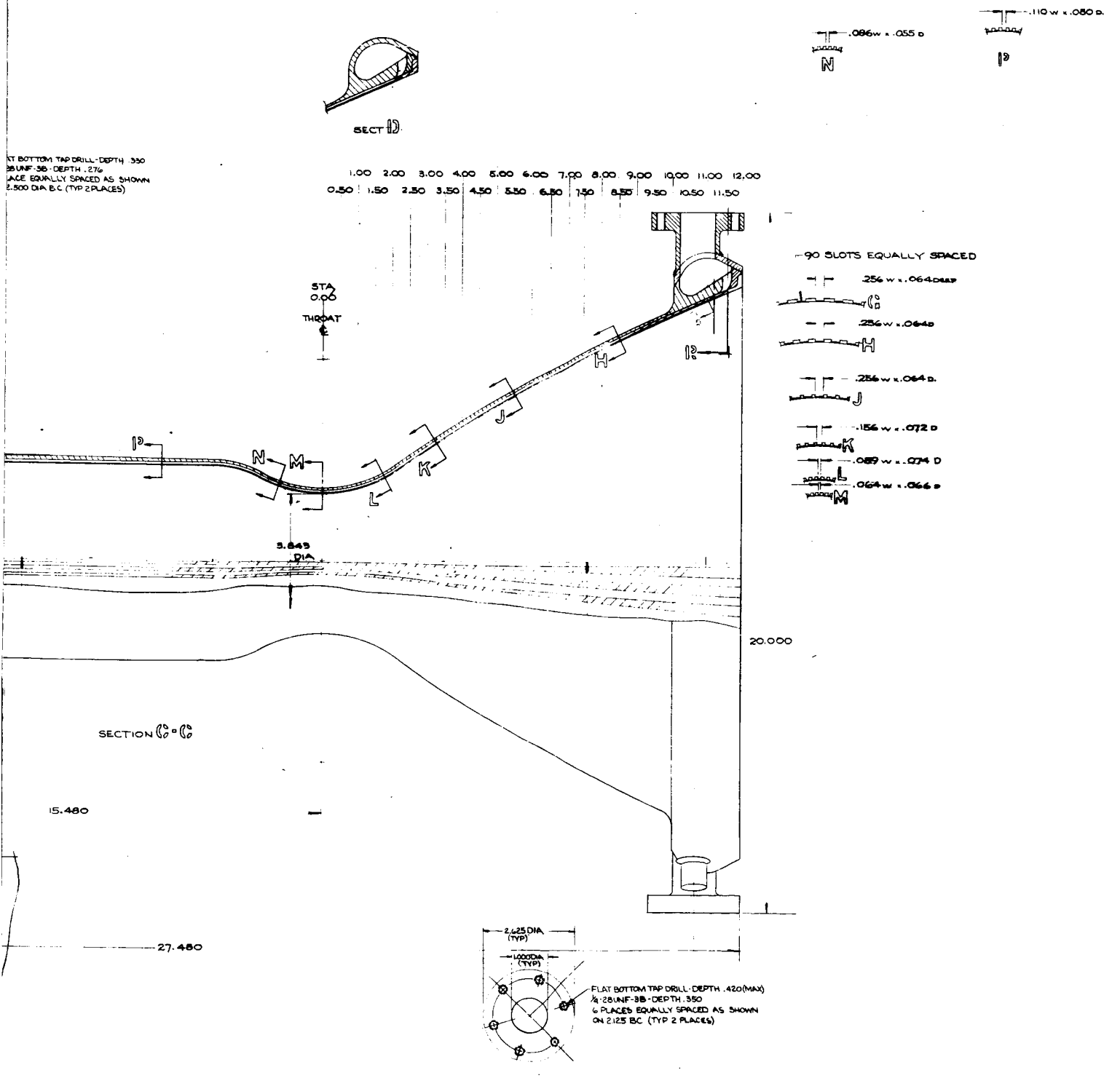

T BOTTOM TAP DRILL-DEPTH .350
8UNF-3B-DEPTH .276
ACE EQUALLY SPACED AS SHOWN
2.500 DIA B.C (TYP 2 PLACES)

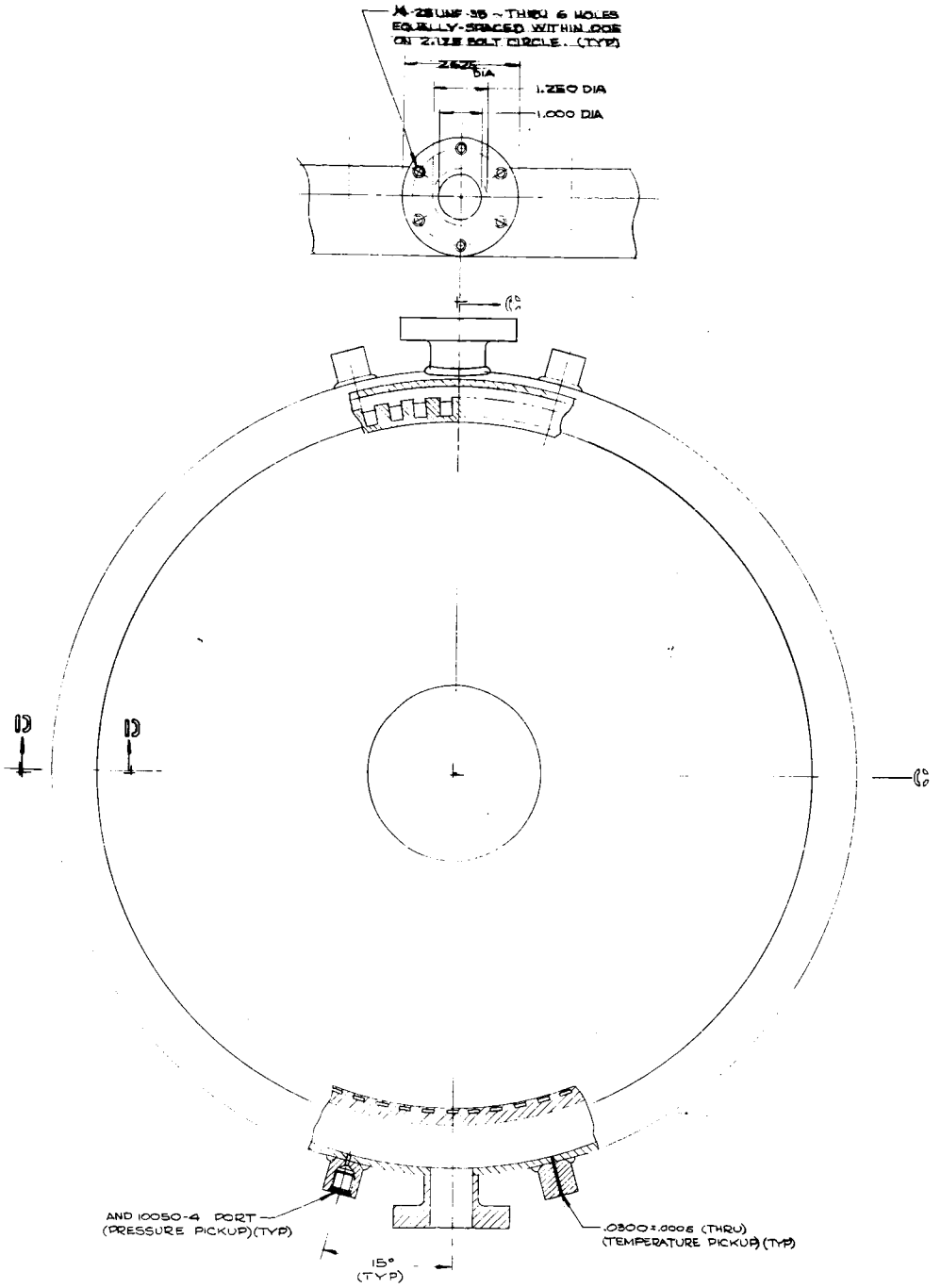

Figure 2. Final Design Layout (Cont)

IV. GENERAL DESIGN ANALYSIS

A. DESIGN REQUIREMENTS

Thrust (F)		8000 lb
Chamber Pressure (P_c)		400 psia
Propellants	Fuel --------	Hydrogen
	Oxidizer -----	Fluorine
Mixture Ratio	Oxidizer/Fuel	12.0
Characteristic Length (L*)		25 in.
Nozzle Expansion Area Ratio (A_E/A_T)		60:1
Driving Gas Temperature		7500°R

B. THRUST CHAMBER DESIGN

1. Performance

The performance analysis was based on the F_2/H_2 injector design furnished by NASA, Lewis which has the following characteristics:

Mixture Ratio = 12.0 (uniform across face)
c* Efficiency = 98.0%

The combustion and chamber heat transfer losses were accounted for by adjusting the chamber total enthalpy such that the calculated c* was equal to the reported delivered c* based on the 98% efficiency. The recombination losses and friction losses were calculated using the Bray program and influence coefficient correlation respectively. The nozzle heat transfer losses were calculated using a Rayleigh line type solution considering a variable area duct. The results of these calculations are summarized below:

c* - 7945 ft/sec (98% c* efficiency)	
I_{sp} (non-equilibrium corrected for c*)	450.2
ΔI_{sp} heat transfer	3.2
ΔI_{sp} 3D	3.2
ΔI_{sp} friction	17.9
I_{sp} delivered	425.9

2. Throat Area and Flow Rate

The flow rate, $\dot{W}_T = \frac{F}{I_{sp}}$

Where W_T = Flow Rate, lb_m/sec, Total

F = Thrust, lb_f

I_{sp} = Specific Impulse, $\frac{lb_f - sec}{lb_m}$

and $\dot{W}_T = 18.80$ lb/sec

The throat area, $A_T = \frac{c^* W}{P_c g}$

where A_T = Area throat, in^2

c^* = Characteristic Velocity ft/sec

$\dot{W}$ = Flow Rate, lb_m/sec

P_c = Chamber Pressure, lb/in^2

g = Gravitational Constant, 32.2 ft/sec^2

$A_T = 11.60$ $in.^2$

The throat diameter then is 3.843 in.

3. Chamber Geometry

The characteristic length, (L*) of the thrust chamber was specified by NASA-Lewis as 25.0 in. minimum. The thrust chamber diameter was also specified by NASA, Lewis to be 5.380 inches.

The $L^* = \frac{V_c}{A_T}$

where V_c = Chamber volume in^3

L* and A_T (same as before)

$V_c = 290.0$ in^3 which is the total minimum volume for the cylindrical and convergent sections. The minimum length of the chamber then from the injector face to the throat is 15.0 in.

C. NOZZLE DESIGN

The thrust produced by an exhaust nozzle primarily depends upon the mass flow and exit area of the nozzle. Maximum thrust for a given exit area can be obtained when the divergent portion of the nozzle is such that the exit flow is uniform and parallel to the nozzle axis. Such nozzles, generally known as ideal or one-dimensional, would be excessively long and heavy. Conical nozzles of shorter length than the ideal would suffer a loss in thrust since the exit flow is not entirely in the axial direction. Logically, one would seek a contoured nozzle so as to minimize the thrust loss due to the above mentioned flow divergence.

1. Theory

The losses due to nonaxial flow for contoured nozzles may be investigated parametrically in terms of nozzle exit area ratios and nozzle length. The latter variable, length, is commonly identified in a relative manner as percent bell comparing it with a 15° conical nozzle of the same area ratio.

Quantitative evaluation of the losses associated with the nozzle geometry are obtained by application of the method of characteristics. The flow of the gases is assumed to be inviscid, irrotational and isentropic. The nozzle is maximized for performance by use of G. V. Rao's equations with which he related conditions at the lip of the nozzle exit in terms of the flow angle, Mach number and ambient pressure as

$$\text{Sin } 2\theta = \frac{(P_e - P_a)}{\frac{1}{2}\rho_e V_e^{\,2}} \quad \cot \alpha$$

where

θ = Exit lip angle

ρ_e = Gas density at exit

V_e = Gas velocity at exit

P_e = Gas pressure at exit

P_a = Ambient pressure

α = $\sin^{-1} \frac{1}{M_e}$

M_e = Mach No.

A physical conception of Rao's method is simple to visualize. Consider a nozzle of a given length and assume that the flow at the exit is uniform and parallel. If the exit area is increased (with no increase in length) the exit Mach number will increase and the flow will become slightly divergent. With the increase in Mach number, the thrust is increased, but the flow divergence reduces the effectiveness of this thrust improvement.

As the area is increased further, the thrust improvement with an increase in area will be exactly balanced by the thrust loss due to the flow divergence. This corresponds to the maximum thrust nozzle defined by Rao's method when, (P_a=0). If (P_a) is not zero, an increase in exit area of the uniform flow nozzle results again in a thrust increase due to the increased Mach number, but the thrust decrement is now due not only to divergence, but also to the pressure force, ($-P_a A_{ex}$) acting on the nozzle. Obviously, the optimum thrust nozzle for this situation will have a smaller exit area than that for (P_a=0). In the limit, if, (P_a=P_E) for the uniform-parallel-flow nozzle, any change in the exit area will result in a thrust loss.

In reality, the ratio of specific heats, (γ) of the actual exhaust gas changes with nozzle area ratio and is determined from thermochemical computations of the rocket exhaust expansion process. The Model 8489 nozzle profile was computed to include this feature.

The variable properties of the exhaust were found using Bell Computer Program 2184 which defines the ratio of specific heats of a thermally perfect gas at any state point in terms of the change in local pressure and density as:

$$\gamma = \left[\frac{\partial \ln P}{\partial \ln \rho} \right]_s$$

The particular expression for γ is required by the nozzle contouring computer program as it solves the method of characteristics matrix, the law of continuity and the change in momentum flux all of which are mutually dependent on pressure, velocity temperature and molecular weight. Figure 3 indicates the functionality with respect to the state pressure used for the Model 8489 nozzle.

PROGRAM NUMBER 2027

CONSTRUCTION OF AERODYNAMICALLY OPTIMUM (RAO) CONTOURED ROCKET NOZZLE

This program computes by means of the method of characteristics, the wall profile from a specified wall profile in the vicinity of the nozzle throat to a specified exit area ratio and receiver or ambient pressure. The flow condition at the exit lip is defined by Rao using variational calculus to be:

$$\sin^2 \theta_E = \frac{P_E - P_a}{\frac{1}{2} \rho V_E^2} \cot \mu_E$$

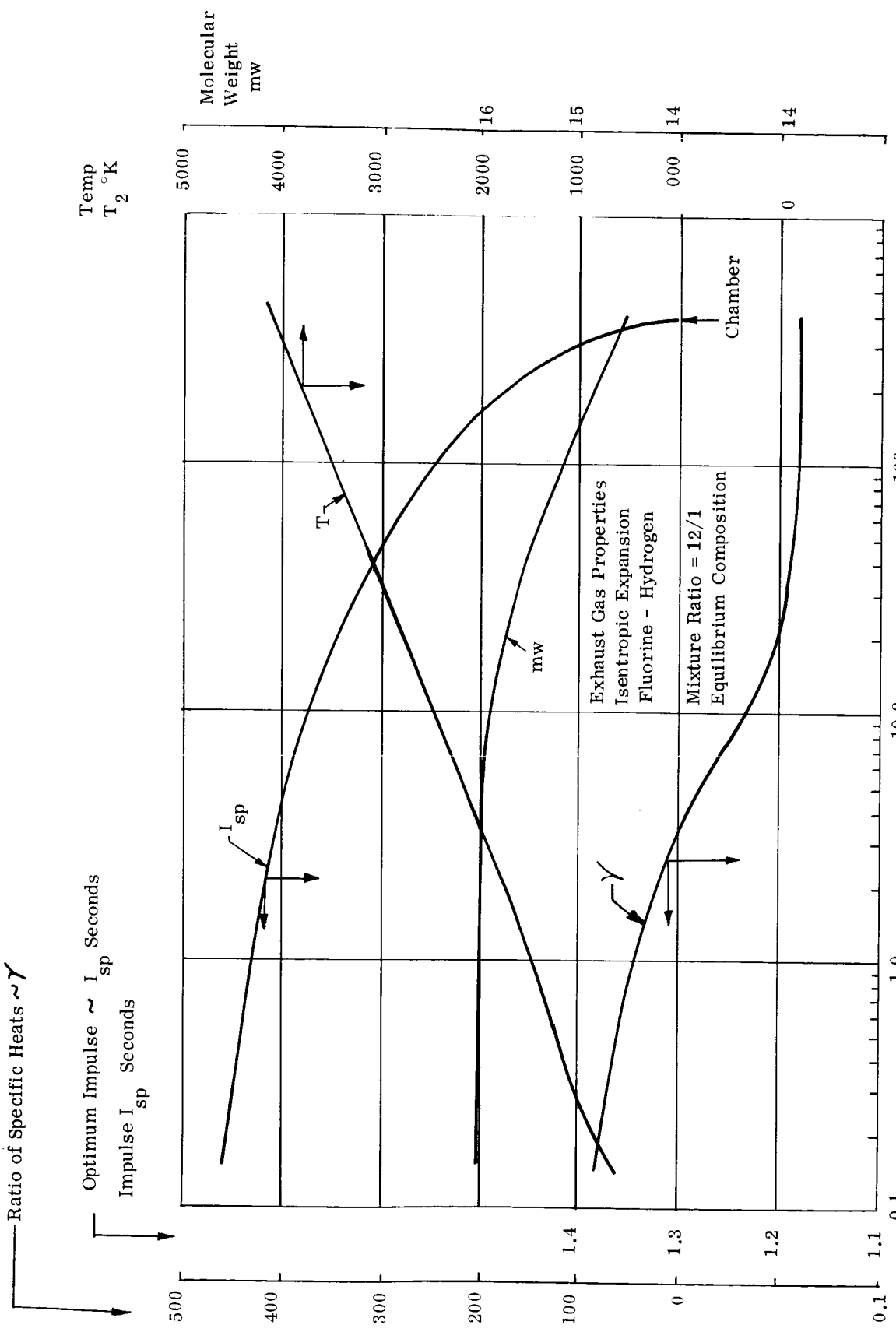

Figure 3. Exhaust Gas Properties

θ_E = Flow angle

P_E = Exit pressure

P_a = Ambient pressure

μ_E = Mach number angle at exit

ρ = Gas density at exit

V_E = Exit velocity

Rao also postulated that the flow across the last left running characteristic must be identical to that passing through the throat, hence is able to establish the nozzle length for a given pressure and exit area ratio.

The program updates the ratio of specific heats used for constructing the characteristics mesh in terms of the gas pressure that best represents the exhaust gas being considered for the propulsion medium. The nozzle performance is found by integrating the momentum thrust and pressure thrust along the last left running characteristic from axis to nozzle lip. The feature of the variable property gas is handled in a manner similar to that prescribed by Neuman and Guenther in NASA Technical Report R-33 (computer program 2184). The basic nozzle construction equations of Rao appear in "Jet Propulsion", Vol. 28, June 1958.

The program then provides the nozzle profile giving the maximum thrust for the specified exhaust gas, chamber pressure, and ambient pressure. Design drawings then use these coordinates for fabrication into high performance flight nozzles. A typical nozzle will convert 98.6% of the theoretical one dimensional thrust to usable thrust with a nozzle of 75% bell length.

COMPUTER PROGRAM 2184

THEORETICAL BRAY PERFORMANCE FOR DETERMINATION OF NOZZLE PROFILE

This computer program, used to determine the reaction rate limited performance of rocket propellants by means of the Bray approximation, is an adaptation of Reference 9, developed at the NASA, Lewis Research Center.

The Bray approximation is based on the hypothesis that during the expansion process, the rates of recombination of chemical species in the exhaust gas progressively decrease due to lowering pressure and temperature, while the rates required to maintain thermodynamic equilibrium progressively increase due to the increased gas velocity. It is postulated that at some point during the expansion process known as the "breakpoint" the recombination rate obtainable will equal the minimum required. Beyond that point the recombination will fall behind the rate of expansion. The Bray method then treats all expansion upstream of the breakpoint as equilibrium flow and all downstream as frozen composition flow.

Program 2184 locates the reaction rate breakpoint by determining the point in the nozzle where the net rate of change in the number of molecules is equal to the recombination rate. As an input to the program, a nozzle contour is described in terms of the flow cross-section area (A_x) versus the station (x) measured from the nozzle inlet.

2. Design Point

The contract specified that the nozzle shall be bounded within an envelope of a 60:1 area ratio and an 80% bell length nozzle. The wall contour in the vicinity of the throat is assumed to be formed by a radius equal to the throat diameter.

Assumption of the wall radius is based upon a technique for estimating the transonic flow conditions put forth by Sauer in NACA TM 1147. He developed a series solution for solving Mach number and flow angle in terms of the contour to throat radius ratio and ratio of specific heats.

If the resulting pressure and momentum flux at variable Mach number is integrated across the throat radius from the axis to the wall and compared to the one dimensional thrust coefficient at the critical pressure ratio, the entrance loss to the nozzle may be found. Such a functionality is indicated in Figure 4. Negligible losses occur with this proportion of wall radius to throat radius.

From this transonic zone, a method of characteristics solution is performed by digital computer so to join it with the nozzle exit. The assumptions for the input variables are summarized in Table 1.

The resulting aerodynamically optimum profile is listed in Table 2 and portrayed on Figure 5. Included in the table are flow conditions at the wall and the integrated surface area which might be useful for structural and weight analyses.

It should be noted that the optimum vacuum nozzle length is 75.2% for P_a = 0 in Rao's optimum equation for setting the nozzle exit conditions. The 80% bell length as in Table 2 was found by setting the P_a = 0.042 psia in Rao's previously optimizing equation.

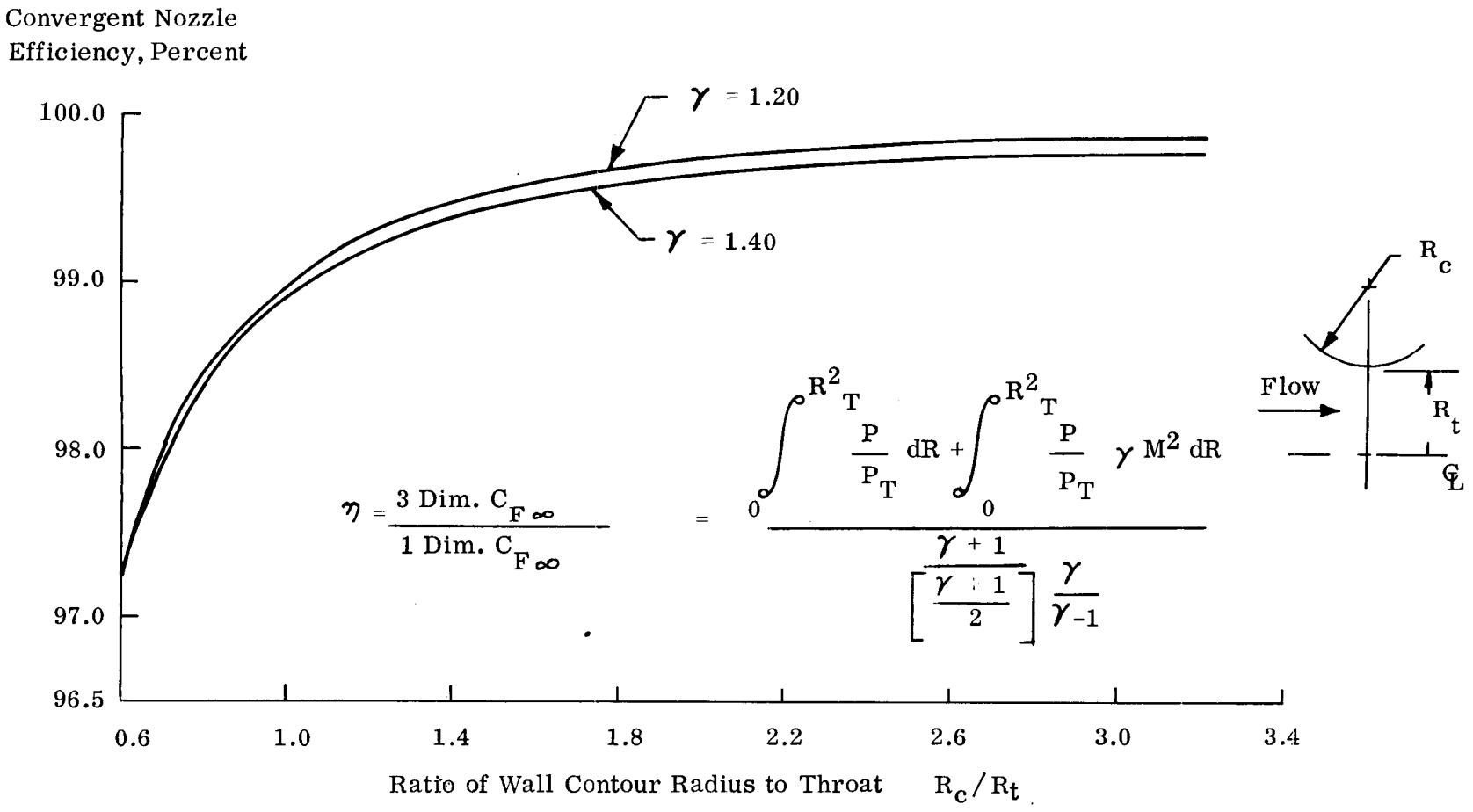

Figure 4. 3-Dimensional Convergent Nozzle Efficiency versus Throat Radius Ratio

TABLE 1

DESIGN PARAMETERS

ENVELOPE:

Nozzle exit area ratio	60:1
Nozzle length, percent bell	80.0
Throat diameter, inches	3.843
Throat wall contour radius, inches (upstream and downstream)	3.843

EXHAUST GAS:

Equilibrium state properties	
Fluorine/Hydrogen	
Chamber pressure, psia	400.0
Mixture ratio	12:1

TABLE 2

DIVERGENT NOZZLE PROFILE PARAMETERS
MODEL 8489

Axial Distance From Throat Inches	Wall Radius Inches	Wall Angle Degrees	Pressure at Wall psia	Mach Number at Wall	Ratio of Specific Heats of Gas	
0.791	2.0039	11.88	116.21	1.518	1.182	
1.256	2.133	19.09	77.097	1.778	1.185	
2.25	2.655	35.98	22.94	2.452	1.202	
4.699	4.220	30.94	11.47	2.781	1.226	
5.269	4.557	30.18	10.49	2.847	1.232	
6.282	5.134	28.86	8.51	2.949	1.243	
8.090	6.092	26.62	6.23	3.10	1.262	
10.121	7.064	24.39	4.67	3.25	1.281	
12.039	7.897	22.53	3.71	3.37	1.295	
14.240	8.770	20.67	2.96	3.49	1.307	
16.052	9.428	19.32	2.51	3.58	1.315	
18.132	10.126	17.91	2.12	3.68	1.322	
20.084	10.734	16.69	1.84	3.77	1.328	
22.140	11.330	15.55	3.85	3.85	1.333	
24.062	11.851	14.58	1.43	3.93	1.336	
26.092	12.365	13.63	1.28	4.00	1.339	
28.000	12.808	12.81	1.16	4.06	1.342	
30.002	13.246	12.02	1.06	4.13	1.344	
32.105	13.678	11.30	0.96	4.19	1.347	
34.011	14.044	10.58	0.88	4.25	1.349	
35.981	14.405	9.89	0.82	4.30	1.351	
38.683	14.883	9.01	0.74	4.37	1.353	Exit

Chamber Pressure = 400 psia
Total Surface Area (Throat to Exit) = 2474 sq in.

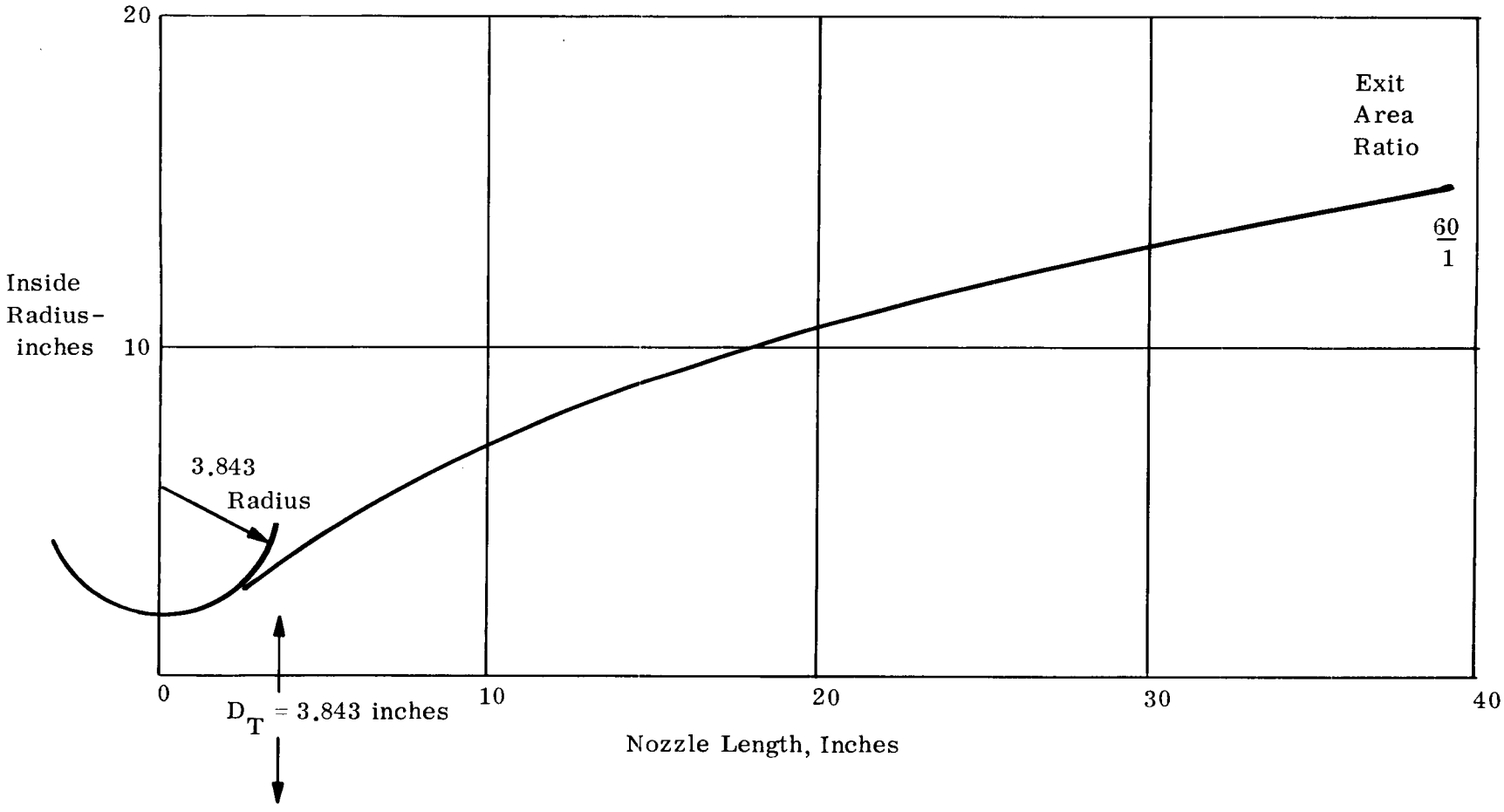

Figure 5. Optimum Nozzle Profile Model 8489

V. HEAT TRANSFER ANALYSIS

A. SUMMARY

This section describes the thermal analysis performed on the regeneratively cooled thrust chamber and radiation cooled nozzle extension. It summarizes the temperature and pressure distribution when the engine is operating at a 12:1 mixture ratio for three different design configurations and materials. Tolerance studies have been made to determine the sensitivity of temperature and pressure to "off-design" hydrogen coolant passages and wall thicknesses. TD nickel was selected as the material for the regeneratively cooled section and SCb-291 columbium for the radiation cooled nozzle extension.

B. GENERAL DISCUSSION OF THE EVOLUTION OF DESIGN CONFIGURATIONS

In the initial concept of the regeneratively cooled hydrogen/fluorine 8K engine, the means of cooling the engine was to flow the hydrogen through constant diameter tubes attached to a liner, the tube contiguous at the throat but separating at the divergent and chamber sections.

The heat flux at any area ratio was obtained by means of the Reference Enthalpy method (Reference 1). Computer Program Number 5002 utilizes this method and is documented in Appendix B. The resultant computed heat flux at various area ratios (based on a mean $\bar{K}_G$) and gas sidewall temperatures (T_{WG}) for the combustion side driving temperature 7500°R, are presented in Figure 7. $\bar{K}_G$, the gas film coefficient, is defined on Figure 6.

There is speculation based on the results of experimental data from other programs that the mixture ratio at the walls will be considerably less than the overall mixture ratio of the engine (12:1). The possible resultant reduction in local driving temperature (reduced from 7500°R to 6115°R) equivalent to a local 6:1 mixture ratio, will reduce the heating rates to the walls.

By judicial design of the injector, it is possible to obtain by increasing the fuel flow in the periphery of the injector, a barrier mixture ratio at the chamber walls equivalent to a local mixture ratio of 6:1 with insignificant loss in overall performance.

The full driving temperature of 7500°R was used to determine the heating loads to the engine. Thus, if the gas layer temperature adjacent to the liner is reduced, the design will be conservative.

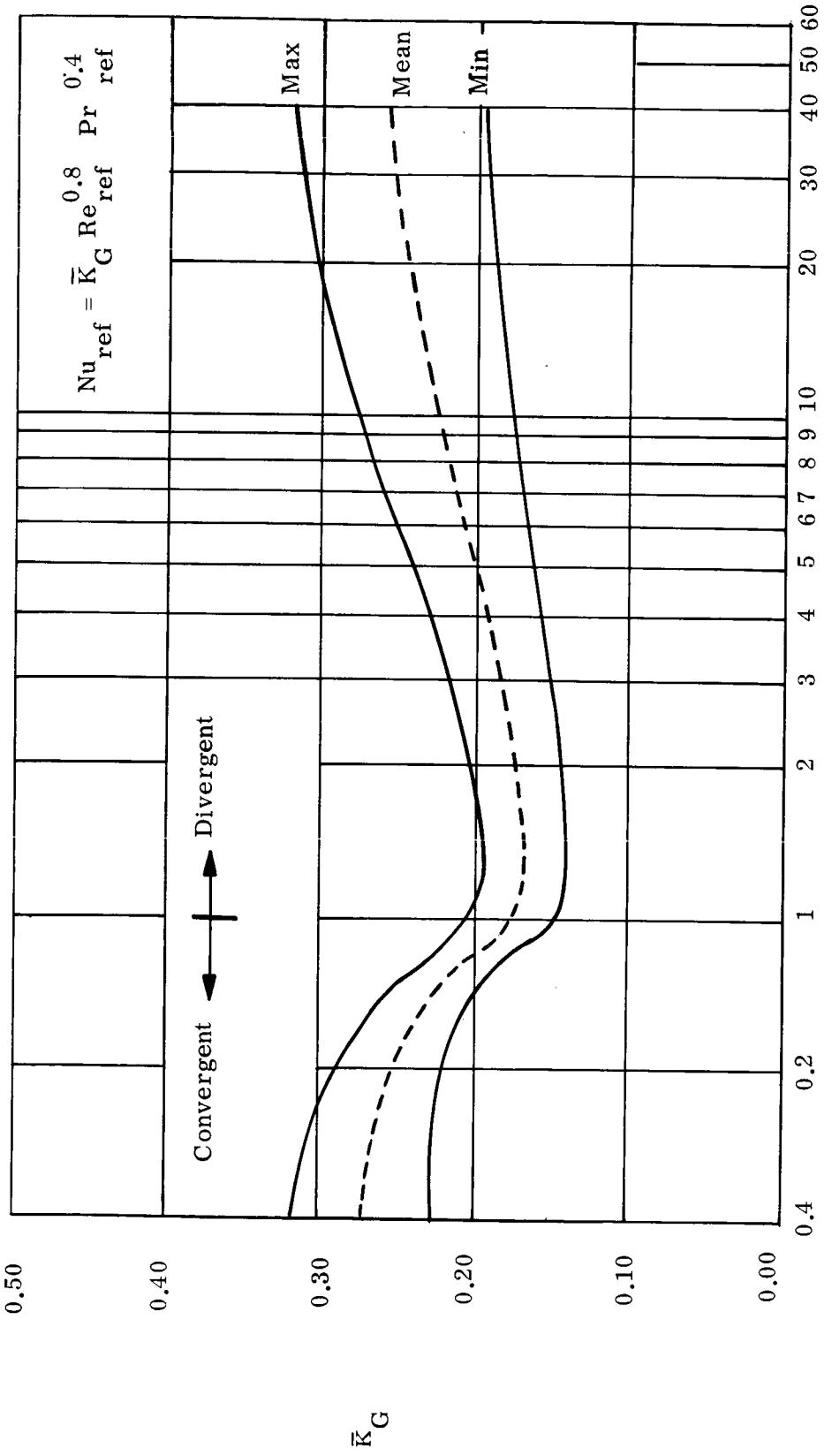

Figure 6. Gas Film Coefficient Distribution

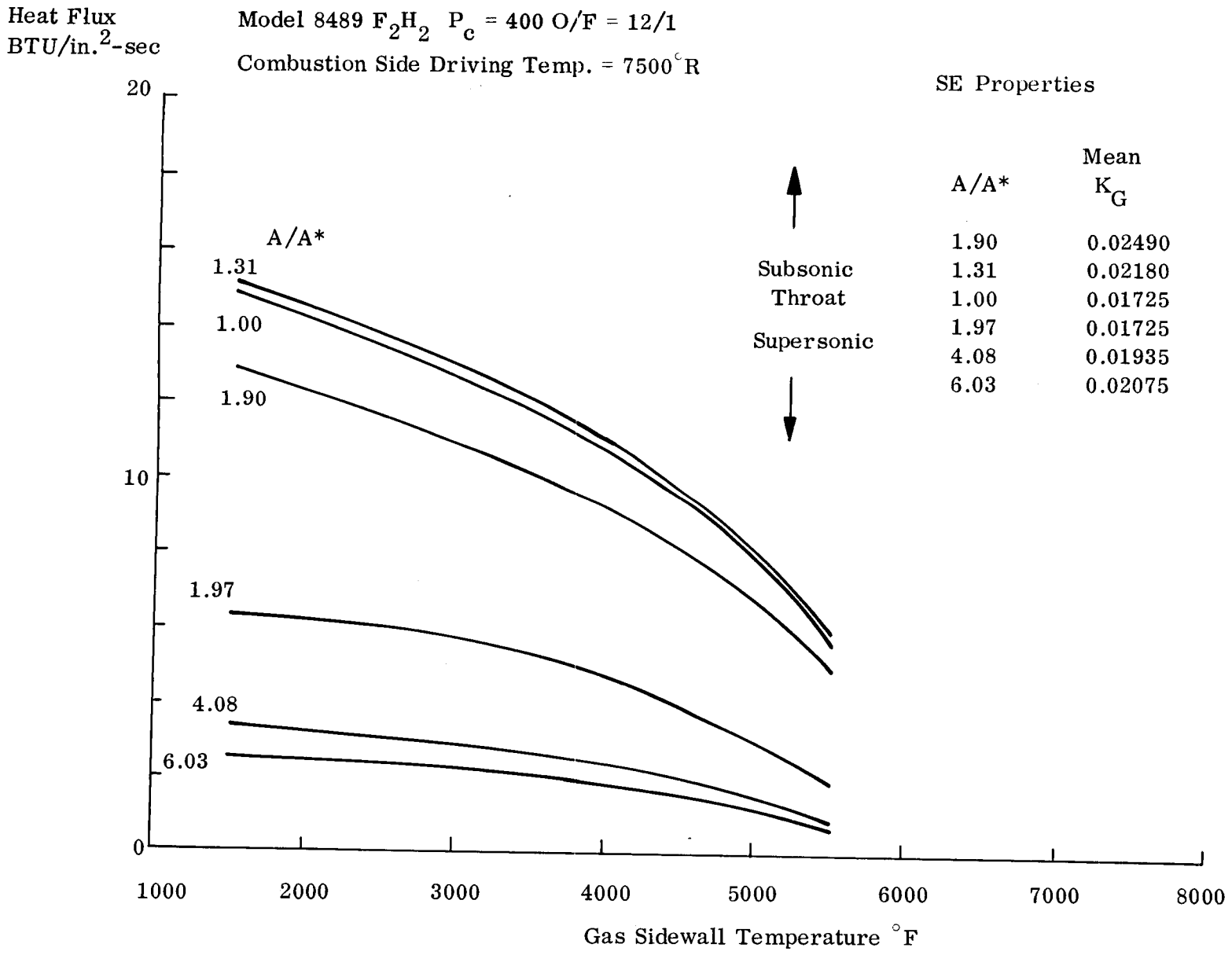

Figure 7. Heat Flux versus Wall Temperature

By selecting a constant tube diameter and assuming a tube wall thickness of 0.016 in., the maximum number of tubes which can be made contiguous at the throat is calculated. Having determined the heat flux at the throat for any gas sidewall temperature (T_{WG}) and tube size, the resultant coolant sidewall temperature (T_{WL}) can be determined. Figure 8 shows the results of a parametric study varying gas sidewall temperature and coolant sidewall temperature versus required wall thickness resistance (t/K in^2 sec °F/BTU). Tube sizes from 0.10 to 0.06 inch ID are considered.

If T_{WG} is limited to 3500°F, the coolant sidewall temperature will be 2125°F using 147 stainless steel tubes of 0.06 inch ID. (See Figure 8). The resulting wall resistance t/K is 110 in^2 sec °F/BTU. The value of t/K for the 0.016 inch stainless steel tube is 65 in^2 sec °F/BTU resulting in an allowance of 45 in^2 sec °F/BTU for the inside liner and felt-metal material. For Tantalum-Tungsten material, the t/K for a 0.10 inch wall thickness which is structurally required to carry the chamber hoop load, is 144. Thus, the liner resistance is almost three times the allowable value of 45 in^2 sec °F/BTU and obviously impossible even if a felt-metal insulator was not used. Also, with 147 constant cross section tubes of 0.06 in. ID, the pressure loss is predicted to be in excess of 500 psi. It is, therefore, determined that the concept of using constant diameter tubes is prohibitive because the tube must be sized by the conditions of maximum heat flux and throat geometry. These preliminary analyses do not consider conduction effects around the tube periphery and hence are slightly conservative in the determination of coolant sidewall temperature.

In an effort to reduce pressure losses due to the penalty in using constant diameter tubes, the possibility of using stepped diameter tubes, such that a number of different tube diameters are joined in series and are selected dependent upon the local heating rate. Table 3 summarizes the data obtained with various analysis using combinations of tube sizes and numbers for the three regions of the engine. The analysis was made using computer program No. 3855 as detailed in Appendix D. The analysis assumed that the gas sidewall temperature was constant at 3500°F and consulting Figure 7 the appropriate heat fluxes at any area ratio are determined. The resulting heat fluxes are boundary conditions for the computer program which was used initially for preliminary analysis. The program is useful for simple parametric type studies and is low in computation costs. It may be noted, in some cases, the coolant wall temperature distribution T_{WL} will be such that there is very little possible temperature allowance available for tube wall resistance. In fact, one location exists at the inlet to the chamber where a required T_{WL} of 4084°F exists, which indicates that T_{WG} must be considerably higher than the assumed value of 3500°F.

It can also be noticed that the coolant sidewall temperatures T_{WL} (See Table 3) vary greatly along any section of constant size tube and, therefore, the tubes are poorly optimized. In the wrapped tube concept tubes of constant diameter are wound at variable pitch angles in an attempt to cover a larger area of chamber wall, i.e. by having the tubes close together in the chamber section, the resulting heat flux per square inch of coolant passage is reduced and therefore the necessary thermal gradient through the wall is also reduced. Thus, it may be possible to maintain a constant longitudinal wall temperature by varying the pitch angles of the wound tubes. The wrapped tube, by its nature is longer than the conventional axial tube and this increased length results in a in a higher pressure drop, which offsets the advantage of the reduced heat flux.

Prevailing Conditions:
Coolant, out, pressure 550 psia
Combustion Gas Temperature 7500°R
Combustion Efficiency 98%
Single Pass Tubes of Constant Diameter

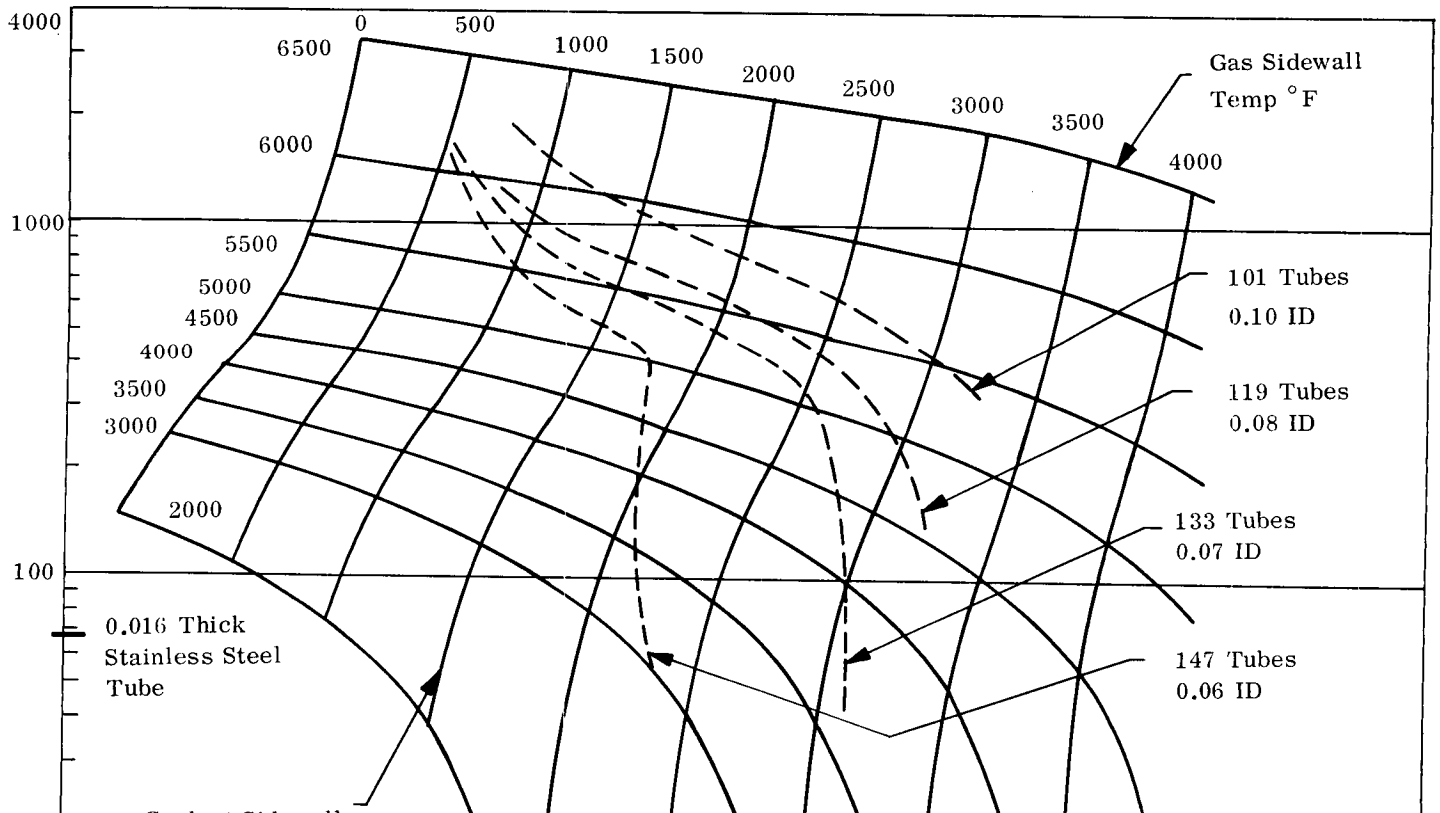

Figure 8. Required Wall Thickness as a Function of Gas Side and Coolant Sidewall Temperatures at Throat Station

TABLE 3

SUMMARY OF RESULTS OF STEPPED TUBE ANALYSES

		Total	Chamber Section				Throat Section				Divergent Section			
T_G °R	T_{WG} °F	ΔP Psi	Tubes/Dia	T_{WL} at Inl °F	T_{WL} at Outl °F	ΔP Psi	Tubes/Dia	T_{WL} at Inl °F	T_{WL} at Outl °F	ΔP Psi	Tube/Dia	T_{WL} at Inl °F	T_{WL} at Outl °F	ΔP Psi
7500	3500	284	120/0.08	3198	1894	193	147/0.06	1094	2130	95	100/0.10	2583	1697	16
7500	3500	204	162/0.08	2799	1815	93	147/0.06	1094	2130	95	100/0.10	2583	1697	16
7500	3500	195	144/0.095	4084*	2325	72	144/0.06	699	1644	110	144/0.10	1850	1386	13
7500	3500	415	144/0.07	2366	1613	289	144/0.06	595	2451	116	144/0.10	2184	1217	10
7500 *1	3500	705	64 at 58°/0.09	1325	1100	615	64 at 54°/0.09	500	2150	90	NO ANALYSIS			

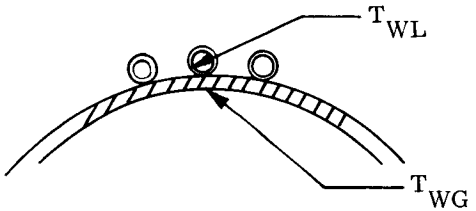

Chamber Section

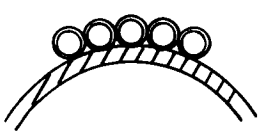

Throat Section

*1 Wrapped tube concept

T_G Combustion gas temperature

T_{WG} Gas sidewall temperature °F

T_{WL} Coolant sidewall temperature °F

P Coolant pressure loss psi

* T_{WL} is indicated to be above T_{WG} for the heat flux for a T_{WG} of 3500°F

Since it was apparent that neither the stepped diameter tube nor the wrapped tube resulted in a low pressure drop, it was concluded that the flow passage must be optimized at incremental locations.

This can be accomplished by having variable diameter tubes or varying cross-section passages. If a conventional tube bundle design is not acceptable, the obvious solution is to have variable cross-section channels. Another concept by which the area ratio in the chamber was increased to 3.0 (versus A/A* of 1.9 in the present design) was examined. Pressure loss in the chamber was substantially decreased (30%) because of the shorter chamber length required to maintain the same L*. However, an increase in chamber diameter would not be compatible with the NASA, Lewis injector for which the chamber is being designed.

At this time in the study, it was decided that a concept of channels milled in the liner held much greater promise than a tube-on-liner concept. It was obvious that by varying the width and depth of a channel that pressure losses can be minimized and also that liner temperatures could be optimized as in the case of a tube bundle design.

In order to minimize the pressure loss of hydrogen through the thrust chamber, it is necessary to operate at as high a wall temperature as permitted by the material being considered. This results in lower heat fluxes to the coolant. Tantalum-Tungsten, which could operate at temperatures as high as 3500°F, was selected as the candidate material. Columbium can operate effectively at a temperature of 3000°F and has the same thermal conductivity as Tantalum-Tungsten, but has a better strength-to-weight ratio at these temperatures.

Fifty-six channels were selected based on 0.20 in. wide channel and 0.05 in. land in the chamber section which it was felt is close to an optimized value from the standpoint of manufacturing, stress and weight requisites. In order to obtain the least pressure loss in the system it is required that the channel width be as large as possible. It was also considered that a land width of 0.05 in. was sufficient for attachment of the outter shell. Thus, using this criteria, the channel width variation is determined by calculating the periphery at any location and subtracting 56 lands x 0.05 in. wide and dividing the remaining dimension by 56.

In the divergent section of the engine, it is not feasible to have 56 channels and 0.05 in. wide lands, because the channel width would become large and the wall thickness under the channel would increase in thickness resulting in a weight penalty. It was therefore decided that the inlet manifold be located at a position 2.5 in. from the throat and have double pass flow in the divergent section equivalent to a total of 112 channels.

Having fixed the channel width, it is now necessary to select appropriate channel depths and liner thicknesses. From preliminary computer analysis considering conduction through the walls, it was found that the lands act as effective fins. It had been decided to try to optimize the design such that $T_{WG} = 3500°F$ and that the liner

material would be Tantalum-Tungsten. The high wall temperature of 3500°F was selected in order to reduce the heat flux to the engine and hence reduce the pressure loss in the system. Because of the ability of the land to transfer the heat to the hydrogen, it was found that the wall temperatures (T_{WG}) could be maintained at 3000°F and yet have pressure losses of the order of 200 psi in the system. However, because of the 2:1 ratio of density of Tantalum-Tungsten compared to Columbium SCb-291, it was decided to use the latter (the thermal conductivity of the two materials being equal).

C. DISCUSSION OF A COLUMBIUM DESIGN

The wall thicknesses of the liner for a columbium design were set by preliminary stress requirements (material properties, temperature and differential pressure loading). It was decided from previous knowledge that 56 channels of 0.25 in. wide would allow a land width of 0.05 in. It was thought that this would achieve the most effective direct coolant area and also give an almost equal temperature distribution under the channel and the land.

Preliminary stress estimates required the liner thickness in the chamber and divergent sections to be 0.055 and 0.020 in. respectively. In order to have minimum weight in the divergent section, the channel depth was set at 0.08 in. If the wall temperature (T_{WG}) was optimized in the divergent section (i.e. at the desired elevated temperature), the depth of channel would be prohibitive with a resultant increase in weight. The chamber and throat channel widths are determined from the land geometry by maintaining an 0.05 in. land between each of the 56 channels. The channel depth is determined by the required convective heat transfer coefficient on the hydrogen side to maintain a gas sidewall temperature (T_{WG}) of about 3000°F which is the desired maximum operating temperature for columbium. Figures 9 and 10 illustrate the flow passage size as a function of X; the axial distance in inches measured from the throat station 0.0 in. Table 4 summarizes the geometry for the SCb-291 columbium design. Table 5 shows the wall temperature distribution at each fluid node and the hydrogen temperature and pressure distribution through the thrust chamber. Figure 11 illustrates the general alphabetical nodal distribution of approximately half of a channel. In the thermal analysis it is necessary to analyze only half of a channel because lines of thermal symmetry can be drawn through each of the centerlines of the channel and the land.

Thus, it can be seen that an acceptable design from a thermal standpoint (wall temperature less than 3100°F) can be achieved using columbium, and the overall pressure loss through the channel is 177 psi.

Columbium however, requires a protective coating to prevent hydrogen embrittlement through the grain. Considerable expense and time is required to develop such a coating, and it was felt that the overall program might be jeopardized. In an effort to alleviate or eliminate this problem superalloys and dispersion hardening alloys were examined. Two alloys, Hastelloy X and TD nickel were thoroughly investigated.

TABLE 4

COLUMBIUM SCb-291 CHANNEL CONFIGURATION

Fluid Node	Outlet Axial Location	Liner Thickness (Mean)	Channel Depth (Mean)	Half Channel Width	Land Thickness Inches
1	+ 4.0	0.020	0.080	0.068	0.05
2	+ 7.0	0.020	0.080	0.108	0.05
3	+10.0	0.020	0.080	0.153	0.05
4	+12.0	0.020	0.080	0.185	0.05
5	+10.0	0.020	0.080	0.185	0.05
6	+ 7.0	0.020	0.080	0.153	0.05
7	+ 4.0	0.020	0.080	0.108	0.05
8	+ 2.5	0.020	0.080	0.068	0.05
9	+ 1.0	0.030	0.075	0.114	0.05
10	- 1.0	0.041	0.070	0.087	0.05
11	- 2.0	0.052	0.064	0.104	0.05
12	- 7.0	0.055	0.065	0.124	0.05
13	-11.0	0.055	0.072	0.124	0.05
14	-15.0	0.055	0.084	0.124	0.05

Material Columbium SCb-291, Outer Liner = 0.06 in.

56 Channels Chamber and Throat Sections

112 Channels (2 Pass) in Divergent Sections

TABLE 5

COLUMBIUM SCb-291 DESIGN-THERMAL ANALYSIS SUMMARY

56 Channel chamber and throat
112 Channel divergent section

Fluid Node	Node Length in.	Outlet Temp °F	Outlet Press. psia	Corresponding Wall Temperature °F								
				A	B	C	D	E	F	G	H	I
1	1.65	-398.6	720.3	1026	810	824	569	74	-61	-383	-271	-145
2	3.30	-366.4	719.3	541	465	399	303	-52	-133	-376	-372	-163
3	3.30	-339.8	718.2	354	296	242	167	-113	-182	-349	-331	-223
4	2.20	-321.3	717.6	289	220	192	107	-139	-198	-328	-319	-232
5	2.20	-302.5	716.2	300	220	206	107	-139	-198	-309	-303	-232
6	3.30	-273.4	711.9	377	296	269	167	-113	-182	-286	-278	-223
7	3.30	-241.9	697.7	504	465	356	303	-52	-133	-254	-235	-164
8	1.65	-223.8	666.1	774	810	537	569	74	-61	-227	-198	-145
9	1.65	-183.2	648.7	2365	1853	1977	1297	586	375	-175	-89	202
10	2.20	-115.8	626.4	2878	2529	2072	1507	811	433	-105	-9	265
11	1.10	-76.0	627.7	2993	2716	1997	1465	889	518	-54	24	339
12	5.00	114.1	595.5	2957	2648	2025	1463	970	597	63	114	450
13	4.00	272.1	509.2	2965	2678	2034	1512	970	635	232	266	514
14	4.00	428.5	543.6	3065	2772	2160	1628	996	691	386	409	593

Hydrogen inlet temperature = 50°R

Hydrogen pressure loss = 177 psi

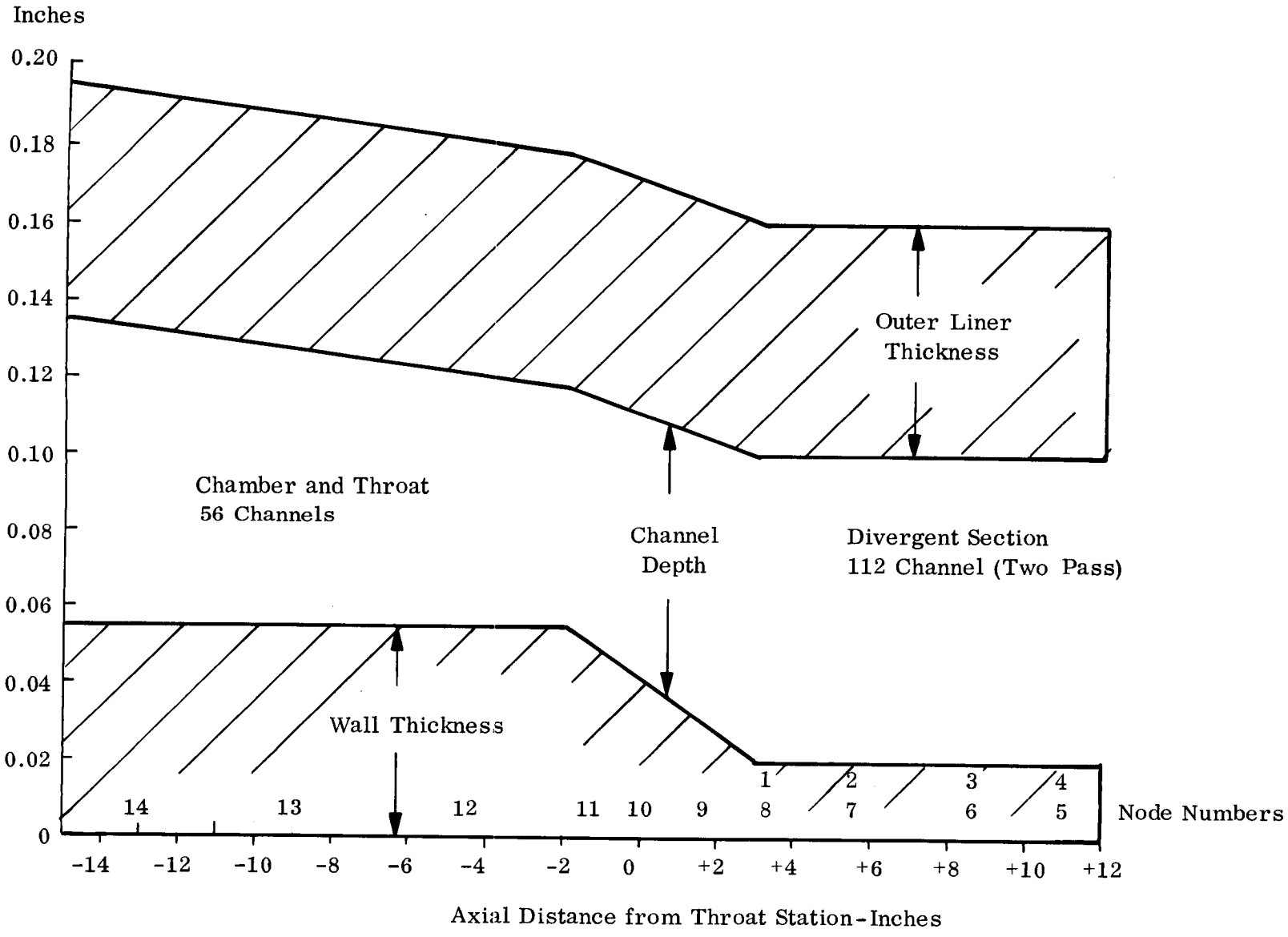

Figure 9. Columbium SCb-291 Design
Wall Thickness

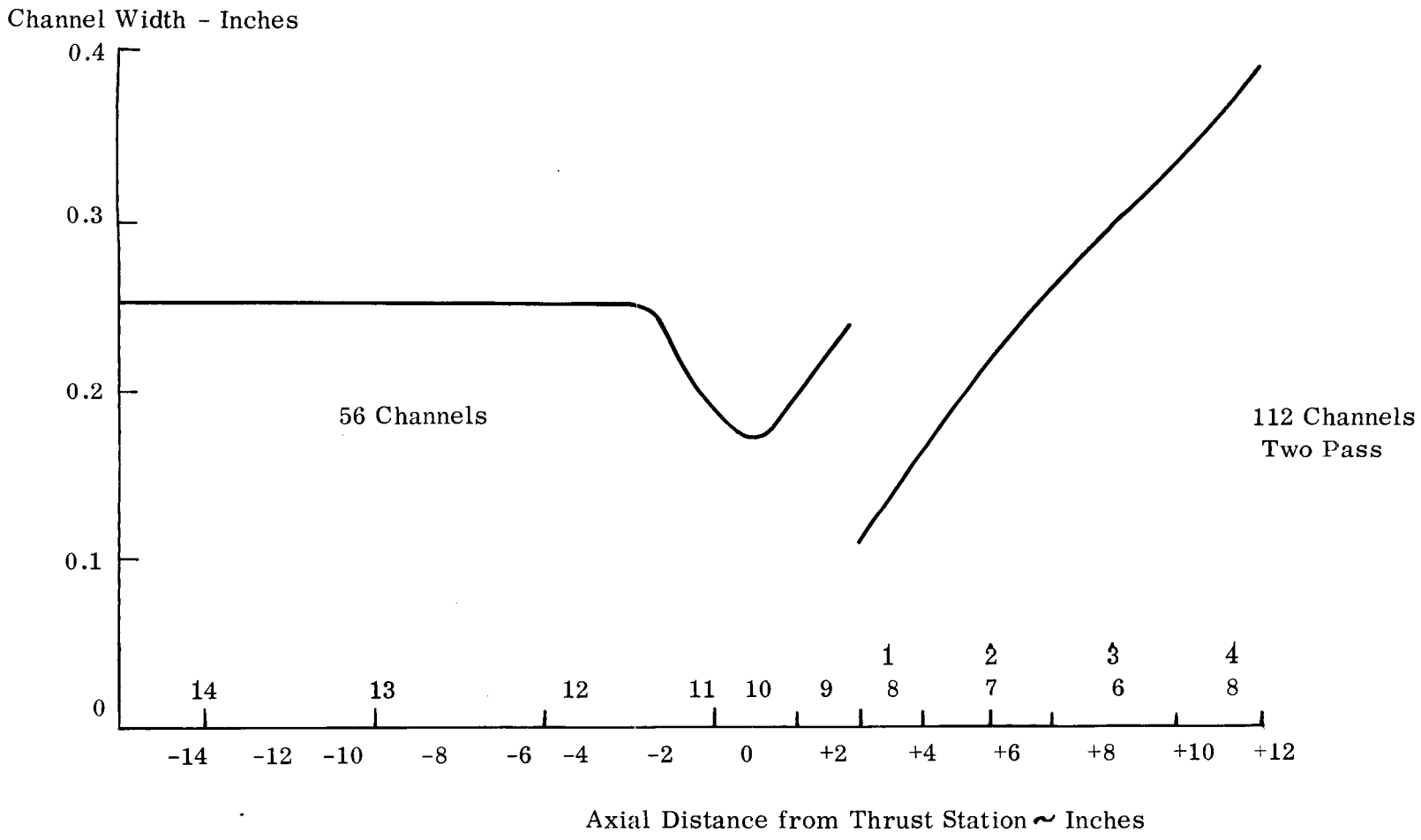

Figure 10. Columbium SCb-291 Design Channel Width

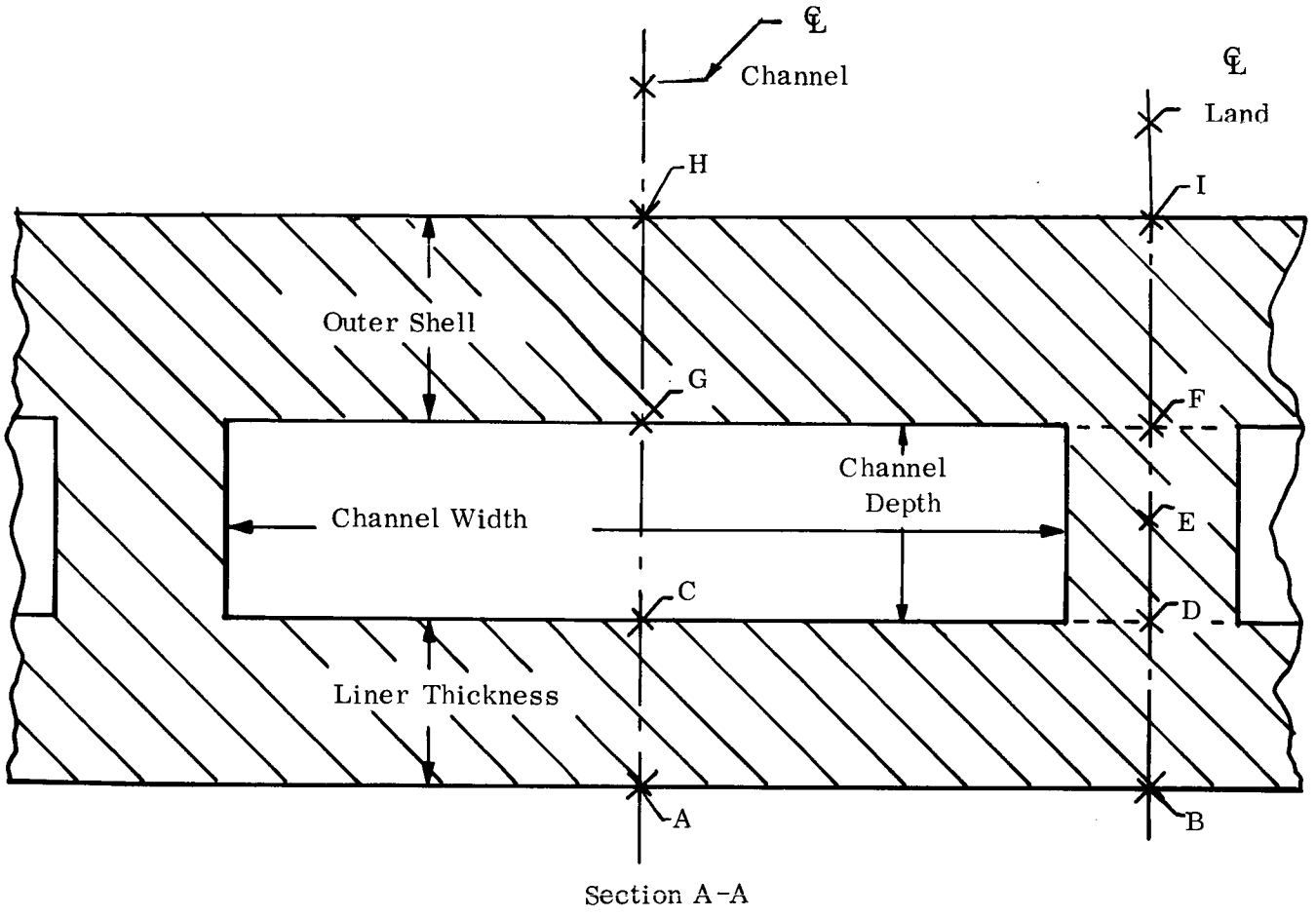

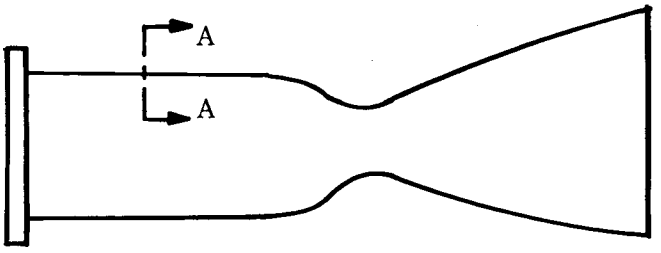

Figure 11. Alphabetical Nodal Distribution about Any Flow Channel

D. DISCUSSION OF A HASTELLOY X DESIGN

The Hastelloy X design was developed utilizing experience gained with the columbium design. Since the thermal conductivity of Hastelloy X is approximately half that of columbium SCb-291, it is necessary to reduce the liner thickness to a minimum in the chamber and throat sections (where heat fluxes are maximum), so as to provide minimum wall thermal resistance. This was primarily achieved by increasing the number of channels from 56 to 112. Thus, the span of each channel is reduced and the beam thickness (liner wall thickness) can be reduced directly.

It was the intent of the selection of channel geometry to maintain a wall temperature of 2200°F, maximum. Figures 12 and 13 show the channel depth, wall thicknesses and channel widths for the Hastelloy X design. Table 6 summarizes the geometry. Table 7 shows the wall temperature distribution and hydrogen temperatures and pressures. A pressure loss of 360 psi occurs as the hydrogen flows through the channel and is much greater than desired. With this design, the temperatures under the land are in excess of the desired value of 2200°F in the chamber sections. In order to reduce these temperatures the channel depth must be further reduced with a resultant additonal pressure loss.

In the selection of channel depth variation through the entire thrust chamber, it was apparent that a very small change in physical dimensions (wall thickness, channel depth or width) can result in significant changes in wall temperatures.

Since tolerances appeared to be of such importance to pressure loss and wall temperatures, a study was made to examine the sensitivity of temperature to channel depth and wall thickness. Figures 14 and 15 show that for a small change in wall thickness (0.002 inch above nominal), the wall temperature under the land will reach 2300°F with 0.060 in. channel. If the maximum limit is set at 2300°F, it can be see that this limit can quite easily be exceeded for a very small variation in geometry, and have a possible structural failure. Also to be considered is the pressure change for a change in channel depth. In Figure 16 it can be seen that the pressure loss in the chamber section is greatly increased (140 psi) when the channel depth is decreased by 0.005 in. from the nominal value of 0.060 in.

Thus, it is proven that the Hastelloy X design is marginal in that the design points are very close to the maximum values, and overheating and rupture of the chamber would result if a tight tolerance was not maintained.

At this time an alternate material, TD Nickel, was investigated which has much better properties at these elevated temperatures than Hastelloy X.

E. FINAL DESIGN - TD NICKEL

The final design using TD nickel as the inner liner with a deposited nickel outer cover, has evolved from the material analysis described in another section of this report. In this design it is required to have gas sidewall temperatures less than or equal to 2200°F and also minimize the hydrogen flow pressure loss.

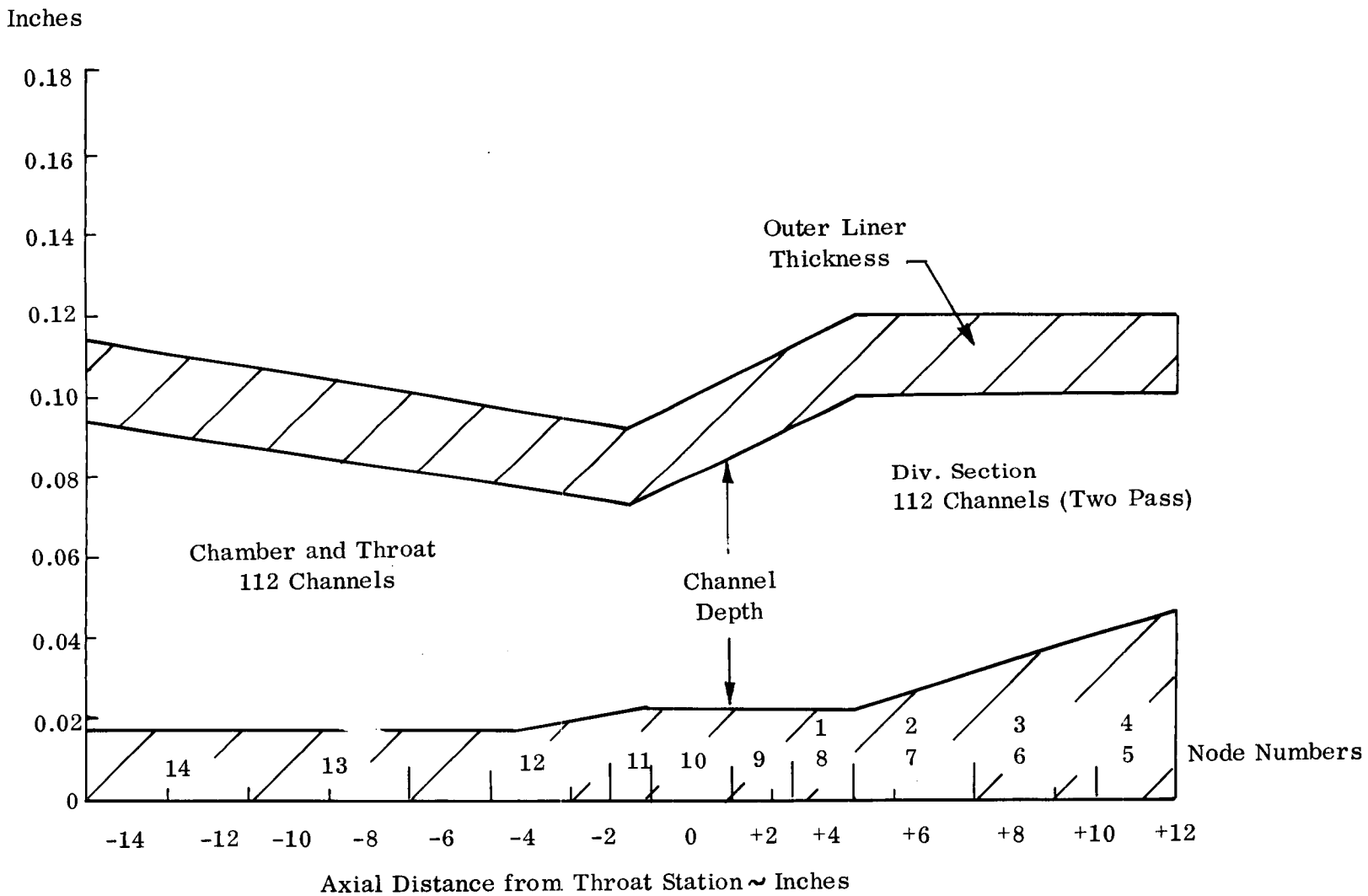

Figure 12. Hastelloy X Design Wall Thickness

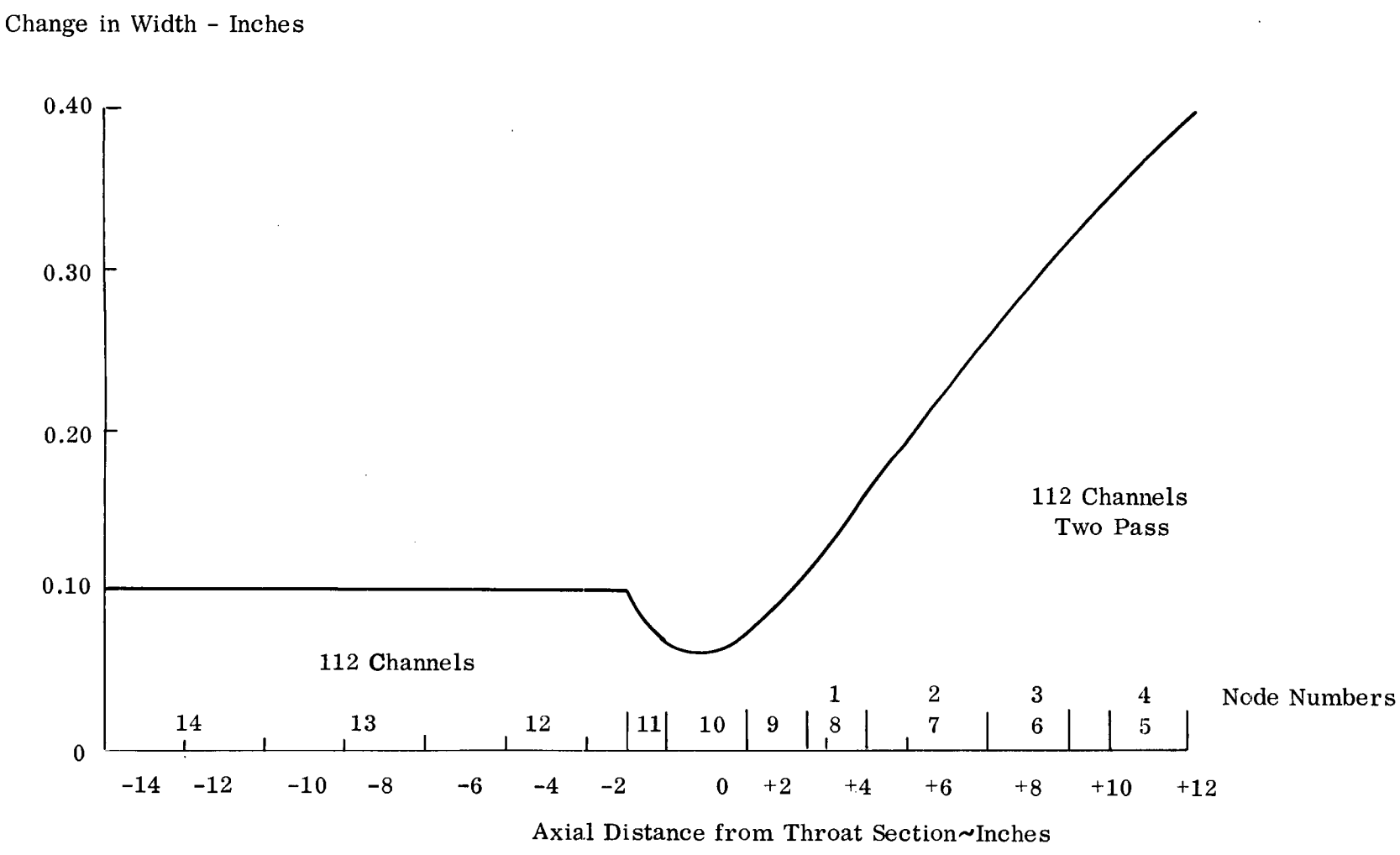

Figure 13. Hastelloy X Design Channel Width

TABLE 6

HASTELLOY X CHANNEL - CONFIGURATION

Fluid Node	Outlet Axial Location	Liner Thickness (Mean)	Channel Depth (Mean)	Half Channel Width	Land Thickness Inches
1	+ 4.0	0.020	0.080	0.068	0.05
2	+ 7.0	0.027	0.073	0.108	0.05
3	+10.0	0.035	0.065	0.053	0.05
4	+12.0	0.043	0.057	0.185	0.05
5	+10.0	0.043	0.057	0.185	0.05
6	+ 7.0	0.035	0.065	0.153	0.05
7	+ 4.0	0.027	0.073	0.108	0.05
8	+ 2.5	0.020	0.080	0.068	0.05
9	+ 1.0	0.022	0.066	0.042	0.05
10	- 1.0	0.022	0.058	0.031	0.05
11	- 2.0	0.022	0.050	0.040	0.05
12	- 7.0	0.017	0.060	0.050	0.05
13	-11.0	0.017	0.067	0.050	0.05
14	-15.0	0.017	0.074	0.050	0.05

Material Hastelloy X

Outer Shell = 0.04 in. Const.

112 Channels Throughout Engine

TABLE 7

HASTELLOY X THERMAL ANALYSIS SUMMARY

112 Channels Inlet Temperature -4001°F

Fluid Node	Node Length in.	Outlet Temp °F	Outlet Press. psia	Corresponding Wall Temperature °F								
				A	B	C	D	E	F	G	H	I
1	1.65	-382.6	900.4	1196	1257	771	870	110	-52	-382	-302	-107
2	3.30	-359.0	898.9	777	877	333	494	1	-111	-368	-336	-149
3	3.30	-337.0	897.0	505	597	63	232	-76	-154	-347	-335	-180
4	2.20	-324.2	896.2	348	437	-91	90	-122	-181	-329	-324	-201
5	2.20	-311.3	894.1	348	437	-93	90	-122	-181	-317	-312	-201
6	3.30	-285.7	890.1	498	597	50	232	-76	-154	-298	-291	-181
7	3.30	-253.4	878.9	740	877	279	494	1	-111	-268	-256	-149
8	1.65	-234.1	858.9	1069	1257	583	870	110	-52	-238	-213	-1
9	1.65	-217.8	806.2	1523	1771	657	1141	330	100	-217	-130	19
10	2.20	-104.6	719.7	2211	2239	1377	1529	675	355	-143	32	222
11	1.10	-84.9	731.7	2199	2341	1361	1609	879	557	-73	100	389
12	5.00	122.0	662.8	2122	2209	1576	1703	832	572	46	226	445
13	4.00	286.5	604.9	2129	2262	1583	1777	860	624	230	357	524
14	4.00	448.7	538.6	2194	2321	1668	1856	884	561	418	461	522

ΔP = 360 psia

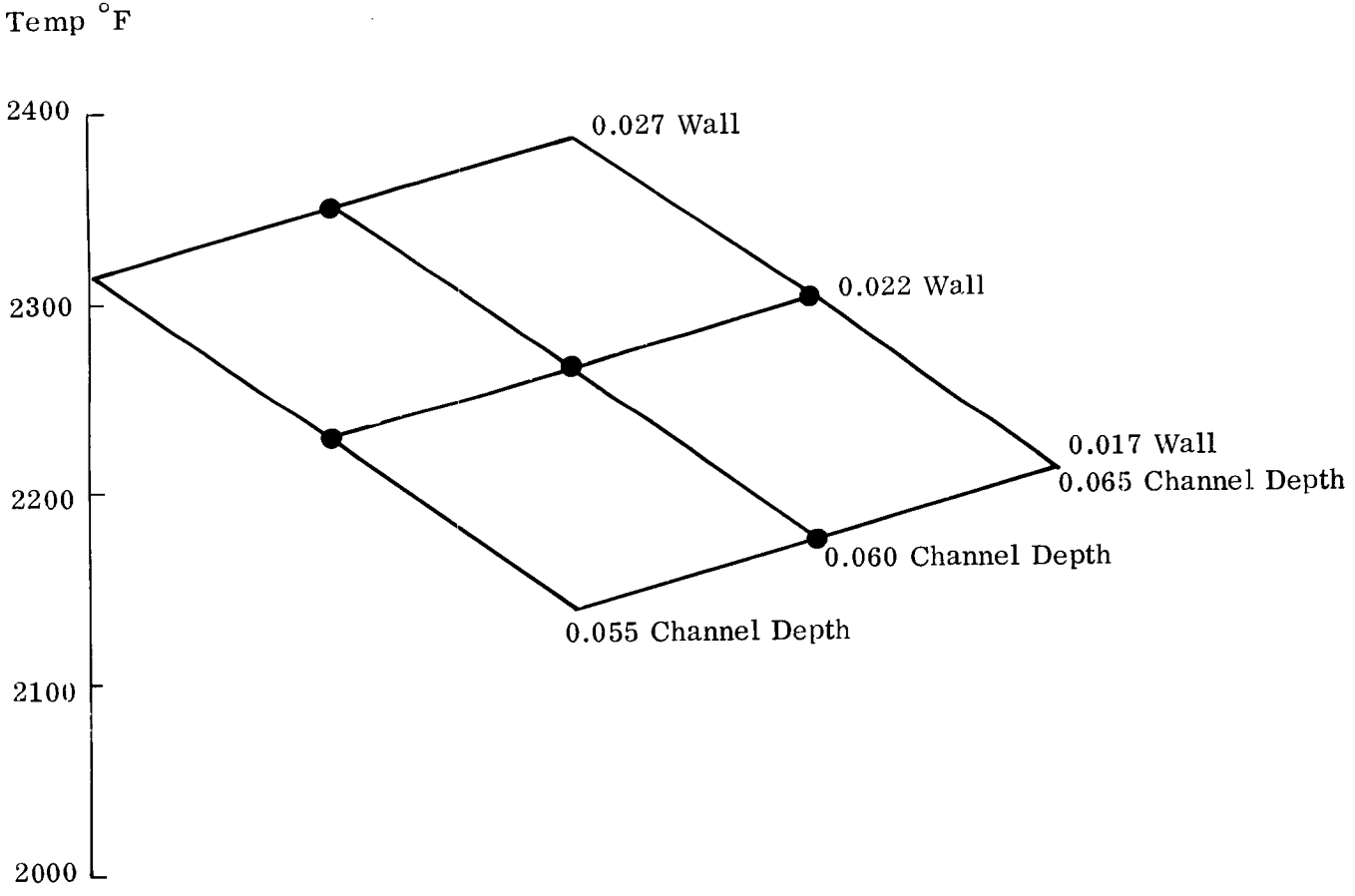

Figure 14. Hastelloy X Design ~ Tolerance Study
Land Temperatures (Chamber)

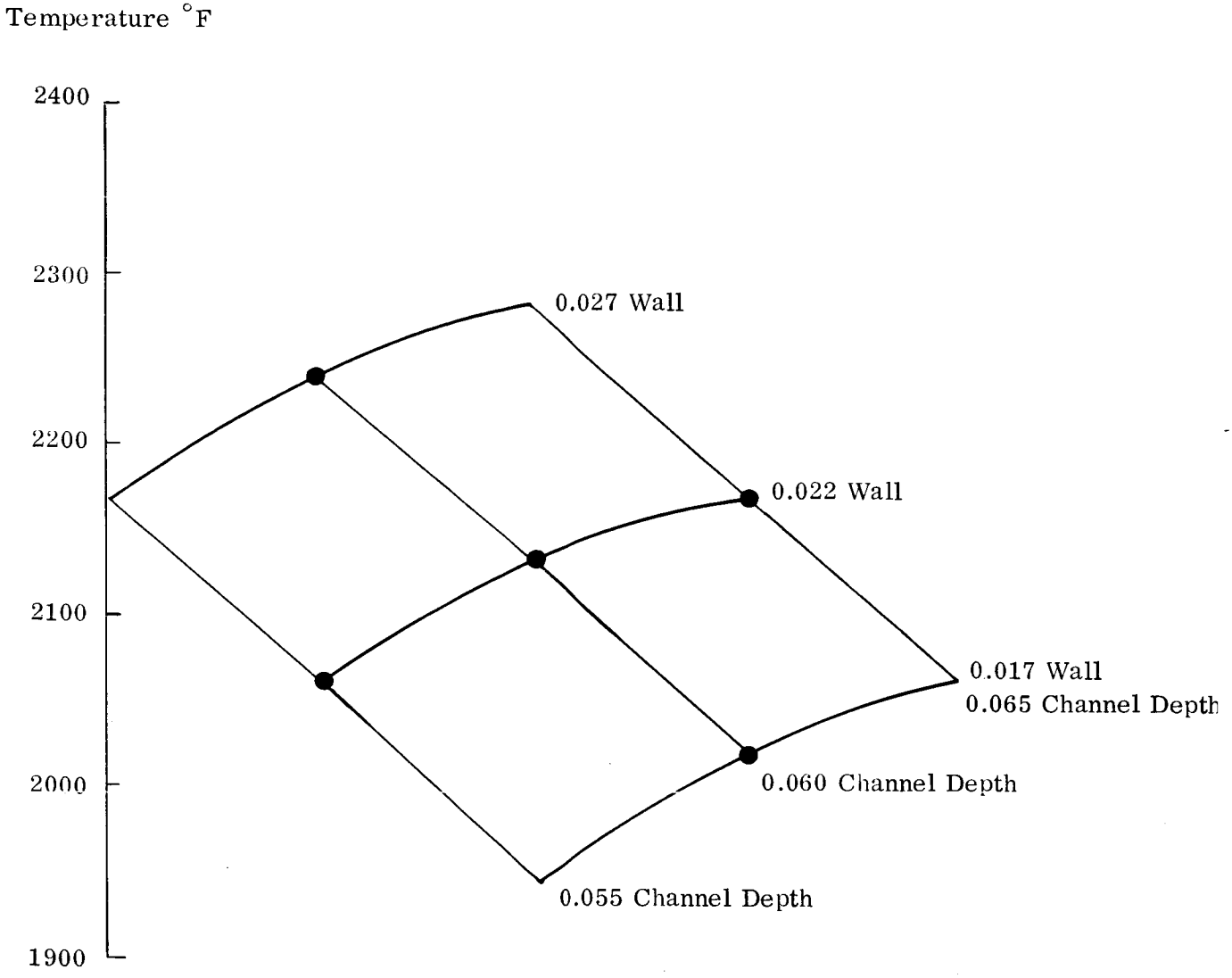

Figure 15. Hastelloy X Design ~Tolerance Study
Wall Under Channel Temperature (Chamber)

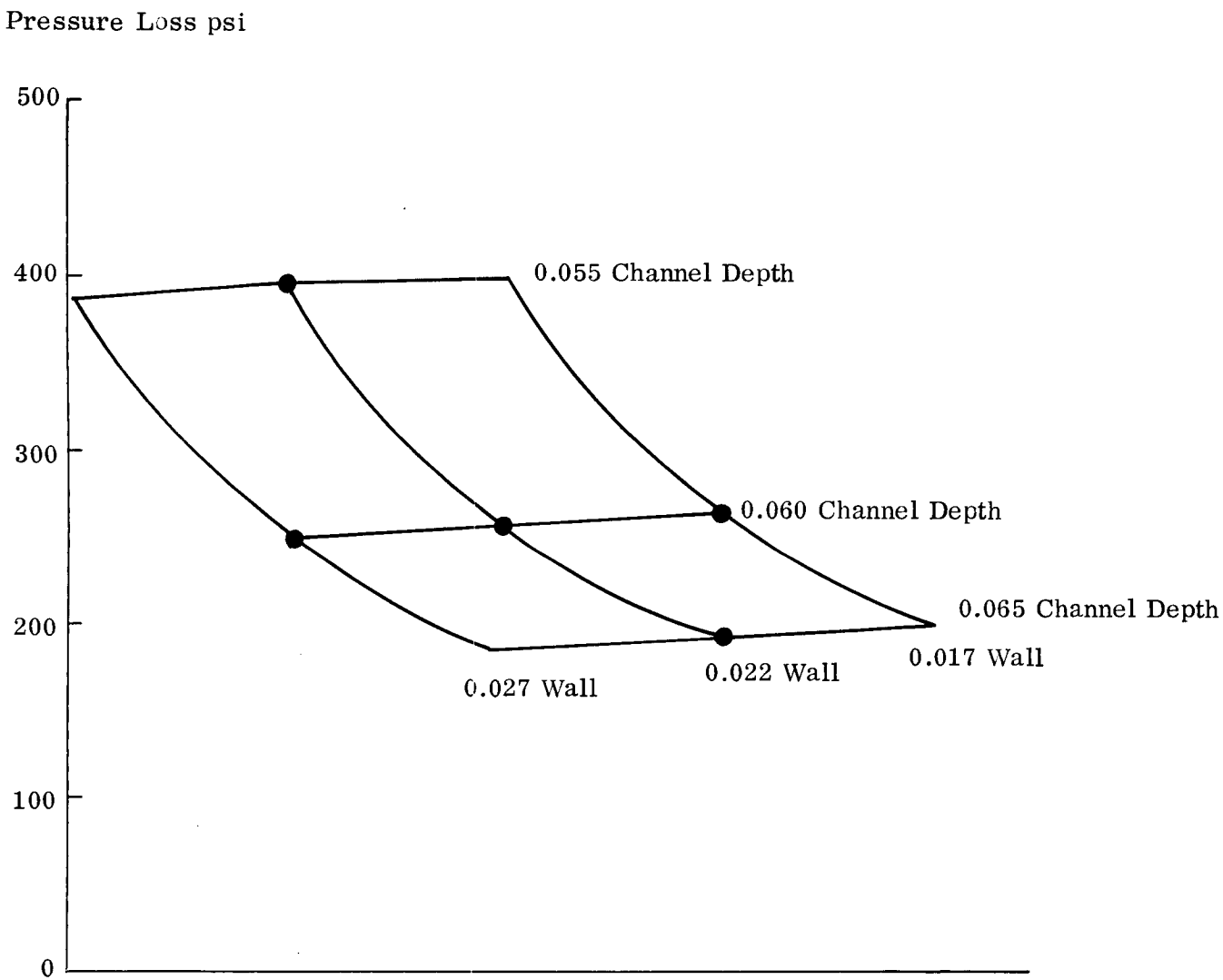

Figure 16. Hastelloy X Design ~ Tolerance Study
Pressure Loss (Chamber Only)

Previous to the selection of 90 channels for the design, some analyses were made of the chamber section using 56 channels and TD nickel material with 0.10 in. wide lands. From these results the temperature under the land was 2400°F and under the channel 2200°F, and the pressure loss was 320 psia through the entire thrust chamber (196 psia in chamber). Another analysis was made with 112 channels and 0.05 in. wide land for the chamber section, resulting in channel and land temperatures of 2060°F and 1830°F respectively (and pressure loss of 121 psia in the chamber section). Much is to be gained by having 112 channels (with half the channel width of the 56 channel design.) The reduced beam width permits the wall thickness to be reduced which lowers the thermal resistance. Thinner lands (0.05 in. vs 0.10 in.) act as better fins resulting in the reduction of the land temperatures. The combination of these effects result in a reduced pressure loss through the chamber.

In consideration of manufacturing processes an 0.075 in. land width is desired. It was therefore realized that an optimum number with 0.075 in. lands lay between 56 and 112 channels and hence 90 channels were selected.

From the manufacturing point of view, 112 channels would require longer fabrication time than 56 channels, because of the increased number of channels and required deeper cut. The shallower depth of wall thickness will be more difficult to hold within tolerance because it is required to halve the thickness of the 56 channel design. The hydrogen inlet manifold was relocated at the end of the regeneratively cooled section in the nozzle and the flow is single passed to the injector. The flow passage depth is adjusted to the local conditions, heat flux, hydrogen temperature and pressure. The resultant geometry for the final design is shown in Table 8 and the associated temperature and pressure distributions are listed in Table 9. The predicted pressure loss for this case is 292 psi (about 70 psi less than the Hastelloy X design). Figures 17 and 18 show the geometrical profiles of the channels. A tolerance study similar to that of the Hastelloy X design was conducted for the chamber section and Figures 19 and 20 show the gas sidewall temperature under the lands and channels for a typical fluid node (No. 8). If the upper limit is also 2300°F, as in the case of Hastelloy X, it can be seen that if the tolerances are 0.005 in. from the design value for both wall thickness and channel depth, that the maximum temperature is 2258°F. Figure 21 illustrates the pressure loss change for a channel depth 0.005 in. different from the nominal value of 0.080 in. It can be seen that if the channel depth is reduced to 0.075 in. throughout the channel section, the pressure loss will increase by 50 psi. Table 10 makes a comparison of tolerance for TD nickel and Hastelloy X. The effect of wall thickness inaccuracy for the TD nickel is much less than for the Hastelloy X design (because of the better thermal conductivity of the former).

Two major considerations led to the selection of TD nickel rather than Hastelloy X: (1) pressure loss in the coolant channels and (2) operating wall temperature versus melting point of the material. The former, pressure loss, differs by a factor of nearly three considering channel depth tolerances. Referring to Table 10, the Hastelloy X design shows that for every 0.001 in. decrease in channel depth, the pressure loss increases 28.0 psi, where the TD nickel pressure loss is 9.6 psi for the same decrease in channel depth. The latter, wall temperature versus melting point of the material, is even a more critical consideration. Table 10 shows that for

TABLE 8

TD NICKEL CHANNEL CONFIGURATION

Fluid Node	Outlet Axial Location	Liner Thickness (Mean)	Channel Depth (Mean)	Half Channel Width	Land Thickness in.	Outer Shell Thickness
1	+10.0	0.032	0.069	0.128	0.266	0.065
2	+ 7.0	0.032	0.069	0.128	0.186	0.065
3	+ 4.0	0.032	0.069	0.128	0.075	0.065
4	+ 2.5	0.028	0.072	0.078	0.075	0.065
5	+ 1.0	0.026	0.074	0.0445	0.075	0.065
6	- 1.0	0.026	0.066	0.032	0.075	0.065
7	- 2.0	0.026	0.055	0.043	0.075	0.065
8	- 7.0	0.026	0.080	0.055	0.075	0.110
9	-11.0	0.026	0.080	0.055	0.075	0.110
10	-15.0	0.026	0.080	0.055	0.075	0.110

Material TD Nickel

90 Channels, One Pass.

Outer Shell - Nickel

TABLE 9

TD NICKEL THERMAL ANALYSIS SUMMARY

90 CHANNEL-NICKEL COVER
One Pass System
New Inlet Pressure = 830 psia (rerun of 900 psia case)

Fluid Node	Node Length in.	Outlet Temp °F	Outlet Press. psia	Corresponding Wall Temperature °F								
				A	B	C	D	E	F	G	H	I
1	2.20	-376.9	829.1	222	309	179	266	227	201	-193	-144	172
2	3.30	-334.1	827.2	339	331	272	264	205	167	-199	-150	126
3	3.30	-270.2	821.5	765	424	628	282	150	77	-209	-171	8
4	1.65	-229.4	812.3	1241	862	996	592	306	183	-95	-38	89
5	1.65	-179.1	771.2	1704	1514	1292	1030	491	299	0	88	183
6	2.20	-102.4	669.1	1827	1834	1211	1223	612	382	51	167	255
7	1.10	-44.0	729.9	1895	1938	1278	1349	817	573	100	226	372
8	5.00	160.4	671.6	2161	2039	1717	1542	816	584	193	308	367
9	4.00	322.6	614.2	2105	2071	1641	1592	923	713	344	458	517
10	4.00	481.1	532.2	2097	2120	1627	1659	1034	834	487	600	656

Est. required inlet press. = 842 psia to exit at 550 psia
ΔP = 292 psi

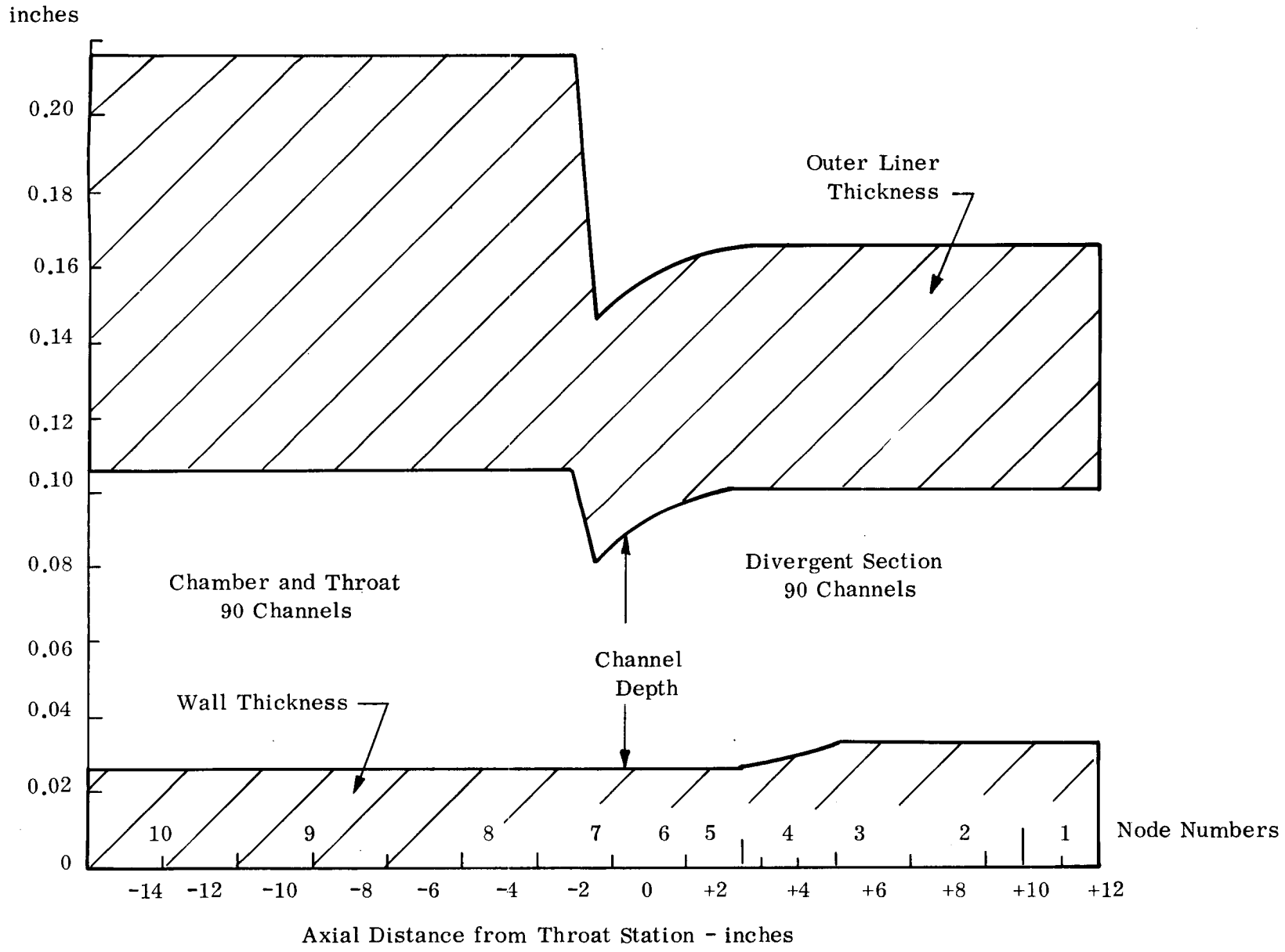

Figure 17. TD Nickel Design Wall Thickness

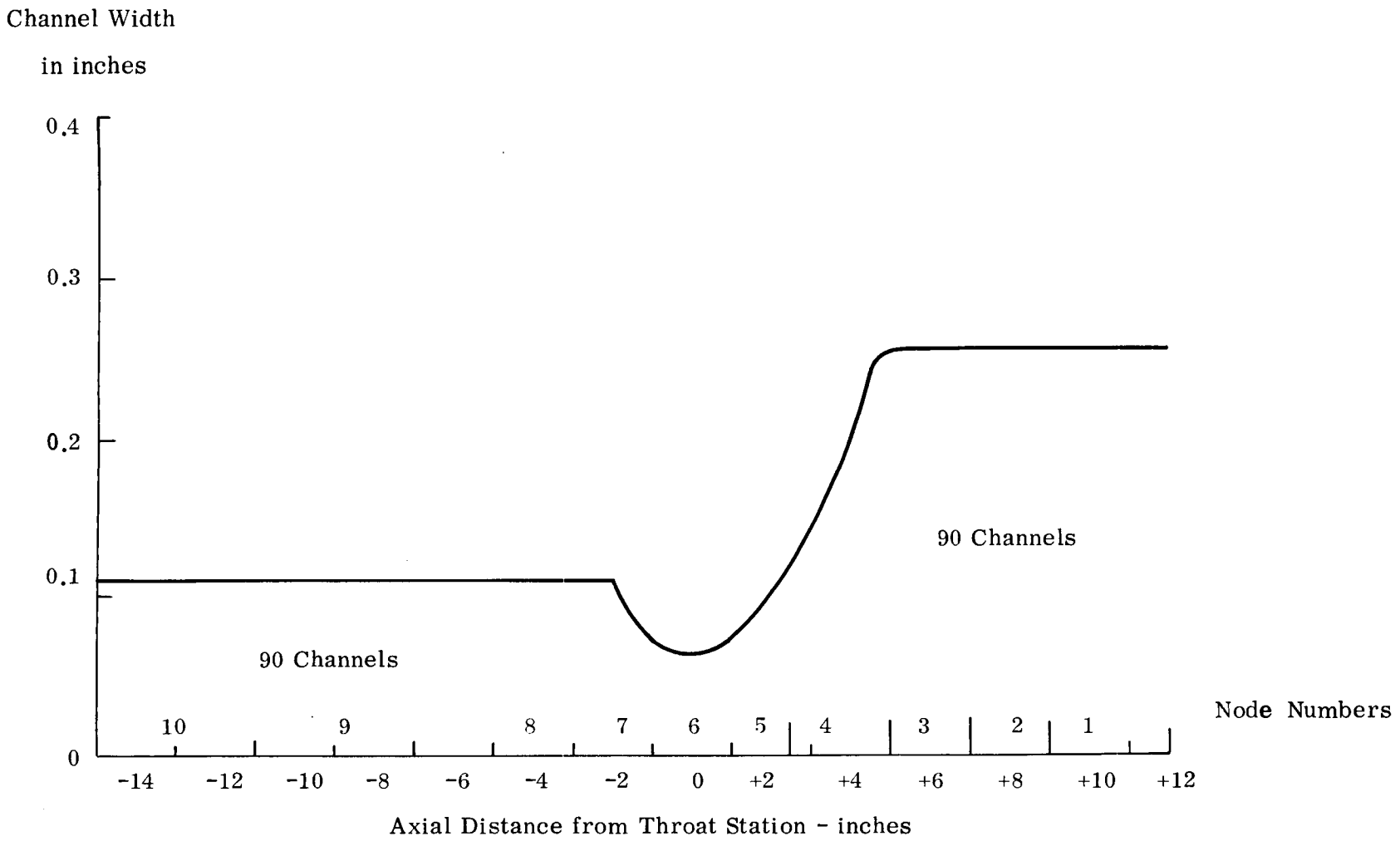

Figure 18. TD Nickel Design Channel Width

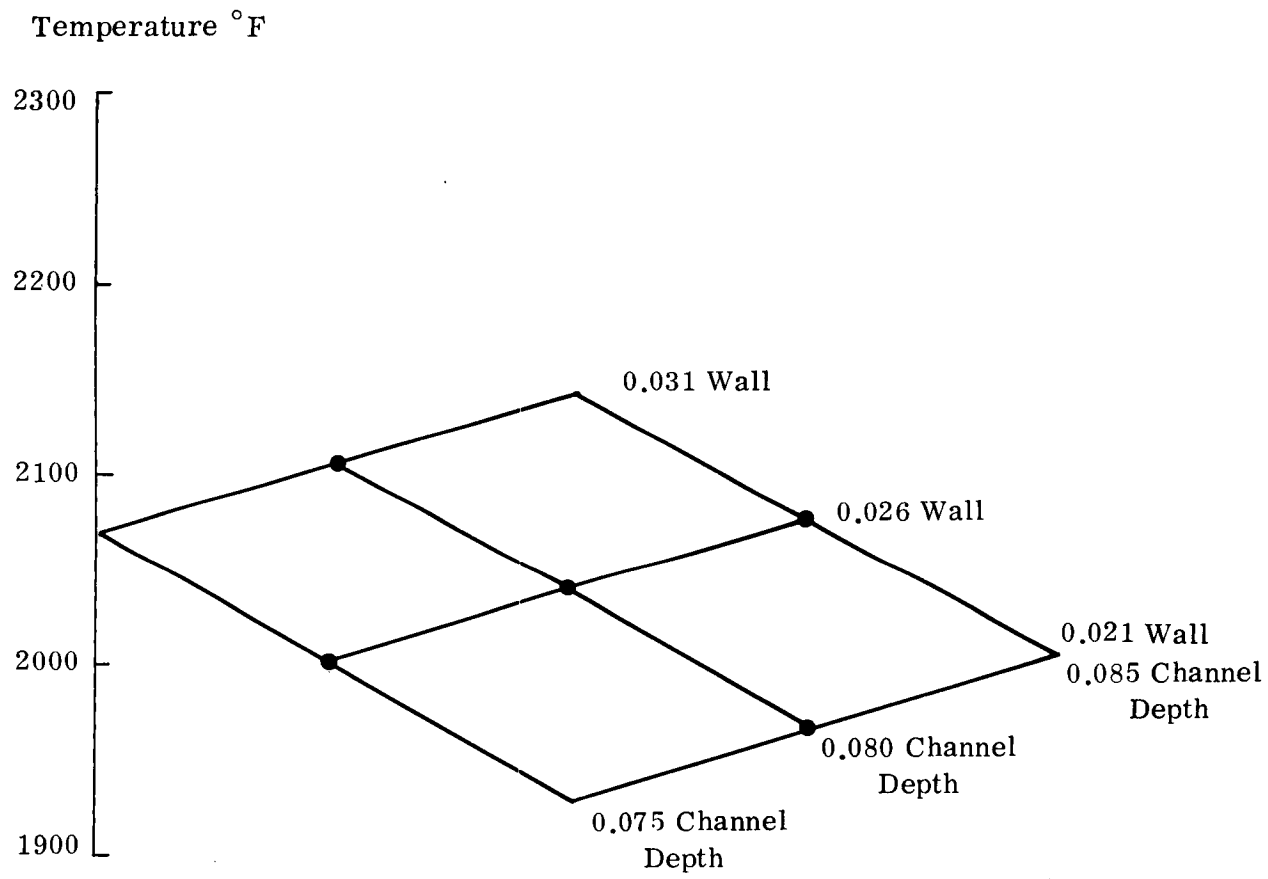

Figure 19. TD Nickel Design ~Tolerance Study
Land Temperatures (Node 8)

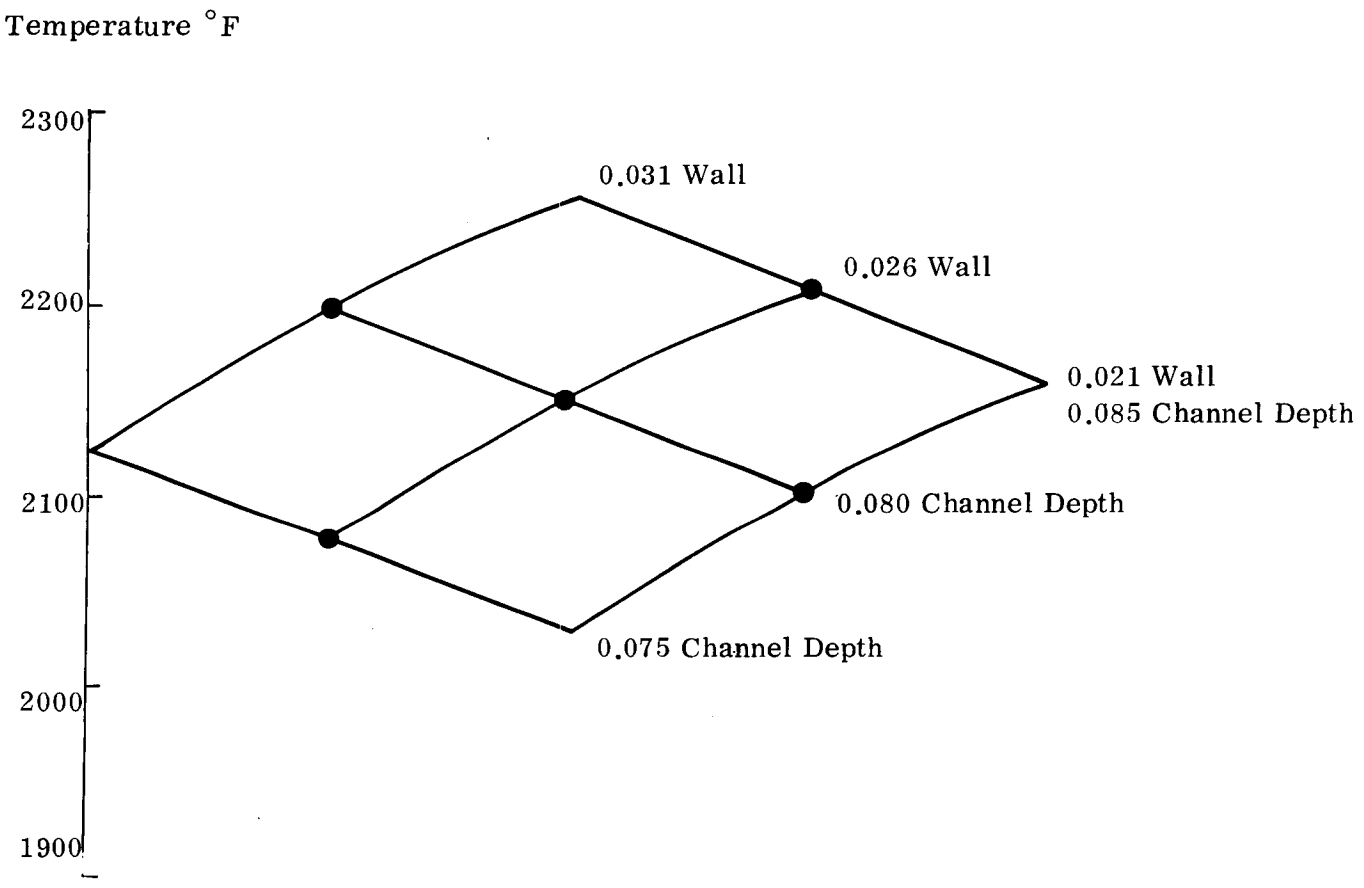

Figure 20. TD Nickel Design~Tolerance Study
Wall Under Channel Temperature (Node 8)

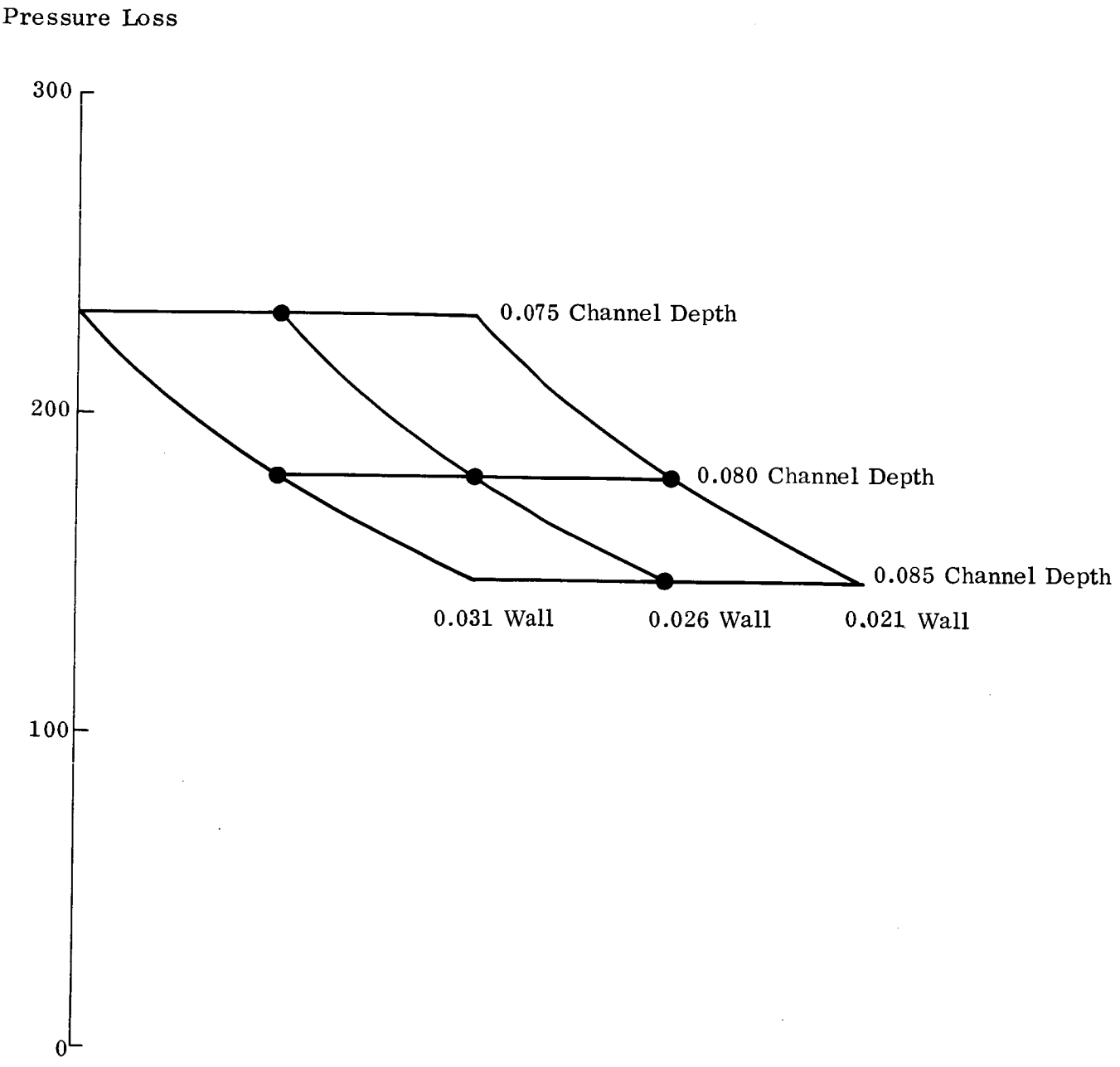

Figure 21. TD Nickel Design ~ Tolerance Study
Pressure Loss (Chamber Only)

TABLE 10

DIMENSIONAL TOLERANCE EFFECTS ON TEMPERATURE AND PRESSURE COMPARISONS BETWEEN TD NICKEL AND HASTELLOY X

	TD Nickel		Hastelloy X	
	Temperature Change °F	Increase in Press. Loss (Cham. Sect) psi	Temperature Change °F	Increase in Press. Loss (Cham. Sect) psi
Decrease of Channel Depth by 0.001 in., under Channel with Constant Wall Thickness	-14.1	9.6	-16.0	28.0
Decrease of Channel Depth by 0.001 in., under Land with Constant Wall Thickness	- 7.4	9.6	- 8.2	28.0
Increase of Wall Thickness by 0.001 in., under Channel with Constant Channel Depth	+ 9.3	No Change	+20.6	No Change
Increase of Wall Thickness by 0.001 in., under Land with Constant Channel Depth	+13.8	No Change	+18.1	No Change

NOTE: Temperature variation is on the hot gas side surface, either at the land or channel as stated.

every 0.001 in. increase in wall thickness under the channel, the wall temperature increases 9.3° for TD nickel and 20.6° for Hastelloy X. Referring to Table 9, it can be seen that the highest wall temperature (using nominal dimensions) is 2161°F for the TD nickel design. Now, if the nominal wall thickness is increased by 0.005 in. (fabrication tolerance), the wall temperature becomes 2207°F. Since TD nickel melts at 2650°F, a relatively safe difference (443°F) remains. Table 7 shows a nominal wall temperature of 2211°F (under the channel) for the Hastelloy X design. Increasing the wall thickness by the same amount, 0.005 in., brings the wall temperature to 2314°F. Since Hastelloy X melts at 2350°F, the wall is only 36° from the melting point.

The reason the Hastelloy X wall temperature was designed for 2211°F nominally was for lowest possible pressure loss. A safer Hastelloy X design is possible at a nominal design wall temperature below 2000°F but the pressure loss (overall) would be in excess of 500 psi. It was believed that the goals of the program would be unjustly compromised with this design since the original pressure loss goal was 125 psi. Considering the shortcomings of Hastelloy X in this application, TD nickel was selected on the basis of the above analysis and study.

F. CRITERIA TO BE CONSIDERED IN THE DESIGN OF RECTANGULAR COOLANT PASSAGES FOR A REGENERATIVELY COOLED THRUST CHAMBER

From this study of a regeneratively cooled thrust chamber, much experience has been gained which is applicable to future designs of this type and not necessarily limited to hydrogen cooling. In order to design a regeneratively cooled chamber, it is necessary once a nozzle profile is selected to optimize the geometrical configuration from a viewpoint of chamber weight, coolant pressure loss and manufacturing costs.

The parameters of importance are chamber material, engine operating pressure, coolant properties, number of channels, land width, channel width, channel depth and wall thickness under the channels. It is obvious that a method of analysis must be established to arrive at suitable designs.

The following is an outline which will explain the steps to be followed:

(1) The combustion gas temperature is obtained for the engine mixture ratio and propellants.

(2) A maximum operating gas sidewall temperature is selected based on the properties of the wall material under consideration.

(3) Heat fluxes to the chamber walls are calculated knowing the gas driving temperature, state properties of the combustion gases and gas sidewall temperature, etc.

(4) The land width is selected based on the minimum acceptable value compatible with the manufacturing process and stress requirements.

(5) At this time a number of channels is selected which will result in a channel width approximately equal to the land width, at the thrust chamber throat station. This arbitrary method permits a starting point for a parametric analysis.

(6) Thus knowing the channel width, coolant pressure, the maximum allowable wall temperature and the structural properties of the selected material, the requisite wall thickness under the channel can be determined by a simple beam analysis.

(7) Channel depths are selected at each station which are basically dependent upon the required coolant heat transfer coefficient. The mathematical model is then analyzed using computer program No. 3812 (See Appendix D). From the resulting temperature distribution, the channel depths are then adjusted to attempt to approach the maximum required gas sidewall temperature. Thus, a number of computer runs are required to optimize the design.

(8) A different number of channels is selected and by the same procedure, a new design is obtained.

(9) Step (8) is repeated and thus three slightly different designs are generated which are compatible with temperature limits.

(10) Each thrust chamber is examined with regard to coolant pressure loss, chamber weight and manufacturing costs. From the overall mission requirements these related factors must be examined and a tradeoff study made.

(11) It is presumed that an optimum number of channels can then be selected for the original land width chosen. In order to determine if the overall design is optimized the land width should be increased and the entire procedure outlined above repeated.

(12) A thorough stress analysis is performed on the optimized design.

(13) Thus, a final optimized design has been verified for a selected material. Such a procedure would have to be repeated for other material selections.

G. NOZZLE UNCOOLED EXTENSION

The regenerative portion of the nozzle was terminated at an area ratio of 18.0, twelve inches from the throat station. Initially it was estimated that the radiative equilibrium temperature would be about 3200°F.

The uncooled extension to the engine was analyzed for two assumed emissivities, 0.65 and 0.85. It is found that for the full driving flux of a 12:1 mixture ratio engine that the temperature at the joint will be 3280°F (ξ = 0.65) and 3110°F (ξ = 0.85). Figure 22 shows the theoretical axial temperature distributions for the radiation cooled extension.

The analysis required the use of two computer programs. The internal radiation interchange factors were calculated by using Program No. 1593 (see Appendix A) and the external surface of the nozzle extension is assumed to be viewing deep space. These factors were then used as boundary conditions for computer program No. 3940 (see Appendix A) and the resultant wall temperature through the extension were obtained.

COMPUTER PROGRAM 1593

GRAY BODY RADIATION TOTAL INTERCHANGE FACTORS WITHIN AN ENCLOSURE FORMED BY A BODY OF RESOLUTION

The digital computer program was developed to calculate the total interchange factors between axial zones within an enclosure formed by a body of revolution of arbitrary profile, e.g., a rocket nozzle. The program will calculate the radiating surface area, geometrical view factor, and total interchange factor of each element within the enclosure based on a given input of:

(1) number of zones

(2) profile table and,

(3) local surface emissivity.

The program is unique in that the solution accounts for multiple reflection of thermal radiation within the enclosure as well as direct emission from the gray surfaces.

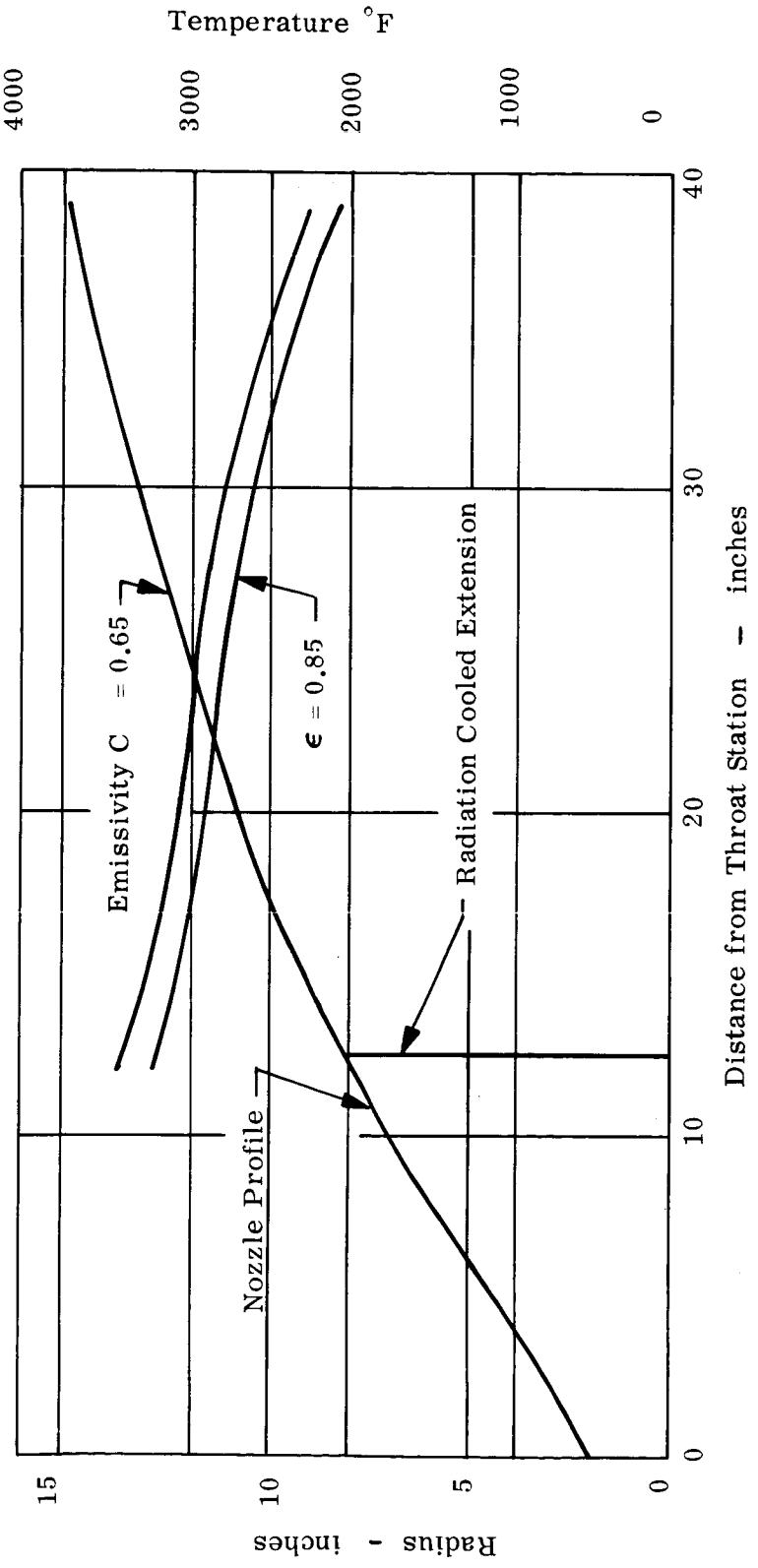

Figure 22. Temperature Distribution in Radiation Cooled Extension

COMPUTER PROGRAM 3940

THREE-DIMENSIONAL STEADY-STATE HEAT TRANSFER PROGRAM WITH ARBITRARY BOUNDARY CONDITIONS

This program is a generalized heat transfer program for computing steady-state temperature distribution within a simple or complex network made up of as many as 80 nodes. Any or all nodes may be involved in the transfer of heat by conduction and/or radiation interchange with any or all other nodes in the same network. Conduction between nodes includes the effect of temperature dependent values of thermal conductivity. Boundary conditions are imposed by relating nodes in the network to control nodes of known temperatures by any or all modes of heat transfer; conduction, convection, and radiation. Convection film coefficients between nodes in the network and control nodes may be dependent upon the resulting temperatures of the network nodes concerned. Known levels of heat flux also may be applied to the network.

H. SHUTDOWN EFFECTS (THERMAL)

From the temperature distribution as shown in Table 9 and from the relative thermal mass of each node, it is estimated that the resultant soak temperature of the chamber will occur within two seconds of shutdown and will be less than 1000°F. The heat flux from the chamber to the injector will decrease from an initial value at shutdown of 0.17 BTU/in.^{2} sec at two seconds and thereafter until an equilibrium temperature is reached as the whole system slowly radiates to the environment. For a complete thermal analysis to be made, information concerning the injector would be required (mass, dimensions, material, etc.).

I. CONCLUSIONS

After a large number of investigations, it has been shown that TD nickel will be the best material with rectangular coolant passages to be used for the thrust chamber design from the overall design aspect. TD nickel has better thermal conductivity than Hastelloy X; does not require a protective coating against hydrogen embrittlement (as required by columbium SCb-291), has less sensitivity to manufacturing tolerances, and finally has a high strength capability at the design temperature.

Table 11 summarizes the temperature limits and pressure loss for the three materials considered for the design. Figure 23 is a graph illustrating the probable trend of pressure loss (based on the limited data) as a function of the maximum operating wall temperature and thermal conductivity of the material. This figure is applicable only to this type and size of engine.

TABLE 11

SUMMARY OF RESULTS OF THREE DESIGNS

Material	Max. Gas Side Wall Temp. Limit (°F)	Regeneratively Cooled Chamber Pressure Loss psi	Material Thermal Conduct. K BTU in./ft^2 hr°F
Columbium or tantalum-tungsten	3065	177	354
Hastelloy X	2341	360	205
TD Nickel	2161	292	360

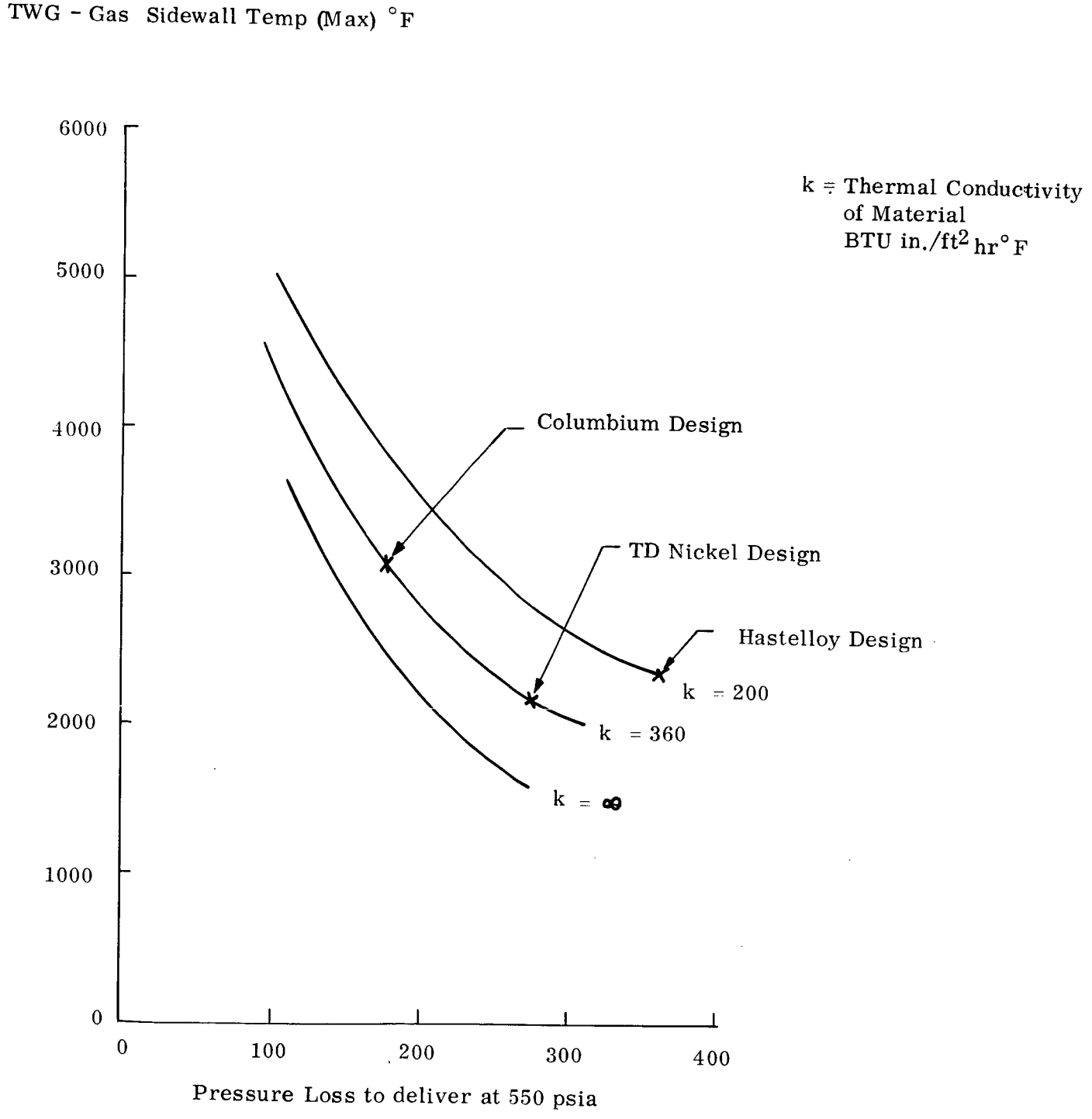

Figure 23. Pressure Loss Trend as a Function of Gas Sidewall Temperature and Thermal Conductivity of Material

VI. MATERIAL SELECTION

A. INTRODUCTION

The original design configuration selected for this program has been discussed in previous sections of this report. It was shown in the detailed analysis that the original configuration and materials employed were not capable of satisfying the design requirements. In an effort to meet these requirements, a materials study was initiated along with a parametric heat transfer and flow analysis.

In order to reduce the heat flux to the coolant, one of the primary goals of the program, the thermal analysis indicated that the wall temperature should be operated at as high a temperature as permitted by the material employed. Refractory materials, if compatible with all design requirements, would sustain wall temperatures in excess of 3000°F and would appear attractive from the standpoint of producing low heat fluxes relative to a regenerative engine made from materials such as stainless steel. Refractory materials were known to possess mechanical properties which would permit their use at the temperatures under consideration. Other characteristics of the materials must be considered, however, before a particular material can be matched to a design configuration with its many requirements. The five main areas to be considered when selecting a material for a rocket engine thrust chamber are:

1. Strength
2. Thermal properties, such as conductivity
3. Chemical compatibility
4. Fabricability
5. Cost

All the known refractory metals and alloys were investigated for this application but none appeared to optimize the design, considering the objectives of the program. The results of this investigation follow in the discussion.

After extending the parametric heat transfer analysis down to wall temperature of 2000°F, superalloys and dispersion hardened alloys were investigated. TD nickel was finally selected as the material for this liner and it is believed that the objectives of the program have been met as closely as today's materials state-of-the-art permits.

B. DISCUSSION

This section will compare the advantages and disadvantages of the materials evaluated for this program (See Table 12).

TABLE 12

MATERIAL SELECTION SUMMARY CHART

Inner Liner	Thermal Conductivity	Strength Above 2000°F	General Fabricability	Raw Matl Cost	Compatibility to Hydrogen Coolant	Compatibility to Combustion Prod.	Comments
Dispersion Hardened Alloys: i.e., TD Nickel	Medium	Medium	Medium	Medium	Good	Good	Best material for this application.
Copper	Excellent	Melts at 1980°F	Good	Low	Good	Good	Eliminated due to low melting point.
Nickel	Medium	Poor	Good	Low	Good	Good	Very poor strength.
Stainless steel	Poor	Poor	Good	Low	Good	Good	Poor strength and poor thermal conductivity.
Superalloys, Nickel base, Iron-Nickel base and Cobalt base: i.e., Hastelloy X	Poor	Poor	Good	Low	Good	Good	Poor strength and poor thermal conductivity.
Refractory Metals and Alloys							
Tungsten	Good	Good	Poor	Med. to High	Good	Good	Ductile/brittle transition temp. Could cause premature failures. Difficult to fabricate. heavy.
Tungsten Alloys i.e., Tungsten and Rhenium	Good	Good	?	Very High	Good	Good	Very costly material. Little known about its fabricability. heavy.
Molybdenum	Good	Good	Poor	Med. to High	Good	Medium	Ductile/brittle transition temp could cause premature failures. Difficult to fabricate.
Molybdenum alloys i.e., TZM	Good	Good	?	High	Good	Medium	Ductile/brittle transition temp could cause premature failures. Difficult to fabricate.
Tantalum alloys	Medium	Good	Good	High	Poor	Poor	Would require coating development program for protection against H_2 embrittlement. heavy.
Columbium alloys	Medium	Good	Good	High	Poor	Poor	Would require coating development program for protection against H_2 embrittlement.
Graphites	Can be varied	Good	*Med. to Poor	Low	Porosity Problem	Medium	*Difficult to attach flow passages and manifolds.

1. Columbium Alloy SCb-291 (Cb + 10W + 10 Ta)

a. Design Application

Thrust Chamber Inner Liner

b. Basis for Initial Selection

1. Alloy combines good mechanical properties at elevated temperature with excellent fabrication characteristics.

c. Problems Associated with Use or Application of Selected Material

1. Like most refractory alloys, requires protection against products of combustion and with the milled channel design requires protection to prevent hydrogen embrittlement of the grain structure.

d. Methods of Overcoming Specific Problems

1. A tungsten or tungsten aluminide coating could be applied to protect the liner attack by the combustion products.

2. Protection against hydrogen embrittlement in the flow channels would be difficult to achieve because of: (1) the complex geometry associated with the design of the channels and fabrication problems in attaching the outer cover and (2) limited development work in the area of protection against hydrogen embrittlement of columbium alloys. While tungsten appears to offer good protection, application of the tungsten to the large, complex surface, and evaluation of the resultant coating would require in itself an extensive development program. It was decided, therefore, to consider other candidate materials for the liner application.

2. Fibrous Metal

a. Design Application

Thermal and mechanical coupling between liner and external coolant tubes (external tube design).

b. Basis for Initial Selection

1. Fibrous nickel felt appeared to combine low structural modulus with relatively good heat transfer characteristics.

c. Problems Associated with Use of Selected Material

1. Sizes and shapes of the nickel felt required were beyond those commercially available.

2. Problems were encountered in brazing the fibrous nickel felt. The required thickness of the nickel felt was too thin to allow practical usage of conventional stop-off materials and the brazing alloy could not be kept from filling the fibrous material.

3. The nickel felt oxidized severely at relatively low temperatures, destroying its usefulness as a structural material.

d. Methods of Overcoming Specific Problems

1. Producers were willing to supply large sizes of material on a "best effort" basis. Special shapes could be fabricated by pressing and piecing.

2. Problems with brazing might be solved by cladding the nickel felt between foil; however, this in turn introduced new problems in manufacture of the material. Additionally, cladding would materially change the modulus of the coupling material and transmit undesirable structural loads into the outer tube structure.

3. Protecting the fibrous metal against oxidation could be accomplished by cladding, coating the individual nickel particles in the felt, or by changing the fibrous material to a more oxidation resistant alloy. Cladding has been discussed in (2) above. Coating the particles of nickel for protection against oxidation as well as changing the alloy would have a serious effect on the heat transfer characteristics of the fibrous material and destroy its usefulness as a coupling between liner and cooling tubes.

Because of inherent difficulties in solving these more or less basic problems, the use of fibrous nickel felt was not considered feasible for this program.

3. Stainless Steel Tubing

a. Design Application

1. Coolant Tubes (external tube design)

b. Basis for Initial Selection

1. Availability - Constant diameter tubing is readily available in stock or from redraw houses.

2. Stainless steel tubing is compatible with hydrogen and fluorine propellants, is readily formed, and can be joined to itself and other materials by conventional welding and brazing techniques.

c. Problems Associated with Use of Selected Material

1. No fabrication problems anticipated with the use of constant diameter stainless steel tubing in this application.

2. Stepped diameter stainless steel tubing can be readily fabricated, however, changes in contour and/or cross-section become costly and time consuming.

4. Refractory Tubing

a. Design Application

1. Coolant tubes (external tube design)

b. Basis for Initial Selection

1. Refractory tubing would allow the use of higher gas sidewall temperatures in the thrust chamber.

c. Problems Associated with Use of Selected Material

1. Drawing constant diameter, thin walled, refractory tubing within the sizes required for this application ranges from difficult to virtually impossible depending upon the particular alloy involved.

2. Compatibility with propellants severely limits selection of useable refractory alloys.

3. Joining of refractory tubing to itself and other materials could present difficult fabrication problems.

d. Methods of Overcoming Specific Problems

Solution of problems associated with the production and use of refractroy tubing for this application would require an extensive development effort.

5. Hastelloy X

a. Design Application

1. Thrust Chamber Inner Liner (channel design)

b. Basis for Initial Selection

1. Use of Hastelloy X shows a sizeable cost advantage over refractory alloys.

2. Hastelloy X does not require protection against high temperature oxidation, is compatible with both propellants, and is not subject to the problem of hydrogen embrittlement encountered with a columbium liner.

3. This nickel base alloy is readily machinable, can be spun, and is weldable to itself and other materials using conventional techniques.

4. Hastelloy X has adequate strength at operational temperature providing gas sidewall temperatures are held below 2000°F.

c. Problems Associated with Use of Selected Material

1. Heat transfer characteristics of Hastelloy X (as well as most other nickel base superalloys) are marginal for this application. The use of such a material would seriously compromise the flexibility of the chamber.

d. Methods of Overcoming Specific Problems

1. There is no practical means of solving the heat transfer problems with Hastelloy X in this application.

6. TD Nickel

a. Design Application

1. Thrust Chamber Inner Liner. (channeled design)

b. Basis for Initial Selection

1. Good heat transfer characteristics combined with good mechanical properties at elevated temperatures.

2. Good machinability and fabrication potential by spinning.

3. Compatible starting material for build-up of electroformed nickel.

c. Problems Associated with Use of Selected Material

1. Material requirements (size) beyond those commercially available.

2. TD nickel is difficult to join to itself by fusion welding processes without a serious reduction in joint strength at elevated temperatures.

3. Limited commercial experience in spinning TD nickel.

4. The mechanical properties of large sheet sizes of TD nickel have not been evaluated.

d. Methods of Overcoming Specific Problems

1. Manufacturer will fabricate material in sizes needed on a "best effort" basis.

2. Use of high temperature filler materials such as waspalloy, nichrome, etc., has been shown to increase elevated temperature strength of TD nickel weld joints.

3. TD nickel has been successfully spun into small thrust chambers and there is no technical reason why larger spun applications would not be feasible.

4. Manufacturer estimates mechanical properties of large TD nickel sheet to be in excess of 75% of available sheet properties. Review of existing design indicates 75% of available sheet properties is adequate for this application.

7. Outer Structural Shell

Four different materials were evaluated for the outer structural shell. This shell also serves as the enclosure for the flow channels.

a. Shell Material for the Columbium Inner Liner Design

For the columbium inner liner channeled chamber design, two materials were evaluated for the outer structural shell, SCb-291 columbium and stainless steel. Because the thermal expansion coefficients were so vastly different between stainless steel and the columbium inner liner it was believed that a bond would not be affected between the liner and shell, due to the gap resulting at the imposed bonding temperature. This problem was eliminated when columbium was also selected for the outer structural shell.

b. Shell Material for the Hastelloy X Inner Liner Design

Hastelloy X was selected on the basis of excellent strength at the imposed temperature and chemical compatibility. Methods of joining the shell to the inner liner are discussed in the Fabrication Analysis section.

c. Shell Material for the TD Nickel Inner Liner Design

Two materials were considered, Hastelloy X and nickel (electrodeposited).

Both materials were considered excellent choices for meeting the design requirements and program objectives. The electrodeposited nickel was believed to be superior from an overall economical standpoint and is discussed in detail in the Fabrication Analysis section.

VII. FABRICATION ANALYSIS

A. DISCUSSION

1. Original Design Concept

From the inital preliminary design stage, applicable fabrication methods were analyzed by manufacturing engineers and optimum processes selected to insure the integrity and performance of the finished thrust chambers.

The first design to be so analyzed contained a formed columbium inner liner, to the outside of which a fibrous nickel metal layer was attached. To which, in turn, a series of stainless steel tubes were attached to form coolant flow channels.

It was felt that the optimum means of joining the components was by high temperature brazing. Experiments were performed to establish a capability for brazing stainless steel alloy 347 and SCb-291 columbium alloy to fibrous (80%) nickel.

It was found possible to braze the fibrous nickel to columbium with no stopoff material, obviating extensive soak-out operations, achieving sound joints with little capillary flow of braze metal into the fibrous nickel.

Following detailed analysis of heat transfer and coolant pressure drop, etc., the above construction concept was eliminated.

2. Second Design Configuration

The second design concept reviewed consisted of an inner liner of either tantalum/10% tungsten or SCb-291 columbium with flow passages machined in the liner and an outer shell of either stainless steel, nickel, or Hastelloy X fabricated in two halves and joined/attached to the liner by high temperature braze.

At this time, two methods of forming the inner liner were evaluated; (a) spinning and (b) high energy rate forming (HERF). Of these, spinning was selected since no HERF equipment currently available was suitable for this component and the spinning process would result in an equally sound part.

The widely differing coefficients of linear expansion of the liner and shell materials would have resulted in gaps between shell and liner during the brazing operation with subsequent failure to make an effective joint. So the design concept was changed once more to incorporate an outer shell of identical material (Ta/10% W or SCb-291 columbium alloy).

In order to permit the use of the design materials, means had to be found to prevent hydrogen embrittlement occurring in the interior of the flow channels. The only suitable coating which was compatible with subsequent fabrication operations was tungsten. Very limited work had been performed in the field of application of tungsten to other metals for this purpose and an extensive development program would have been necessary with high risk to the program.

3. Third Design Configuration

Accordingly, the design concept was again reviewed to permit the use of either Hastelloy X or TD nickel for the liner material.

Analyses of heat transfer, etc., revealed that Hastelloy X would require manufacturing tolerances to be held far closer than was practical to prevent structural failure by local overheating. For this reason, TD nickel was selected as the optimum liner material, its heat transfer characteristics permitting manufacturing tolerances of a more readily attainable level being applied without detriment to the performance of the finished thrust chamber, reduced the overall program risk.

The final overall process selection justification follows.

4. Final Design Configuration

Following the engineering decision to use TD nickel for the inner liner materials, studies were initiated to determine the optimum construction methods, joining techniques, and outer shell construction concepts.

Construction methods examined for the liner were:

(a) Segmental construction with three longitudinal joints, segments rough formed on drop hammer, sized between hot ceramic dies and trimmed to close tolerances mechanically.

(b) Combination of drop hammered segments and spun sections with combination of longitudinal and circumferential joints.

(c) One or two part spun construction with a maximum of one circumferential joint.

The use of high energy rate forming in place of drop hammer was discounted due to the energy levels required, in excess of those available along with no improvement in the mechanical properties of the material.

The use of HERF to form the chamber from a tube was also rejected due to the uncontrolled elongation likely to occur locally.

Joining techniques examined were:

(a) High temperature braze,

(b) Diffusion bonding,

(c) TIG welding,

(d) Explosive welding, and

(e) Electron beam welding

The construction methods considered for the outer shell were:

(a) Drop hammer shaped halves of nickel, accurately trimmed to contact all of the lands on the inner liner and either high temperature brazed or diffusion bonded in place.

(b) Strips, TIG welded longitudinally to bridge one passage each, the weld fillet to join adjacent strips and join them both to a land on the inner liner.

(c) Halves of the liner as in (a) to be dimpled, the dimples to be joined to a plain inner liner, thus avoiding machining of channels in the liner wall.

(d) Electroformed outer shell of pure nickel deposited over an inner liner with machined channels masked-off or alternatively a plain inner liner of thin wall construction with channel areas masked to electroform the lands also.

(e) Also considered was a scheme to build the chamber from coaxially assembled rings of different diameters with passages predrilled axially through the ring thickness, the rings to be diffusion bonded together.

The studies of joining techniques revealed that in order to obtain the strength at elevated temperatures required, together with absence of contamination,a welded or diffusion bonded joint was required. Diffusion bonding at its present state-of-the-art requires elaborate setup and equipment, close matched, finely finished parts, and is not considered sufficiently repeatable for this application. The explosive welding technique is apparently subject to porosity, using electron beam welding requiring extremely accurate mating edges and using no filler wire, which would melt the parent metal, which is most detrimental to the physical characteristics in the case of TD nickel.

Of the welding techniques investigated, vendors of wide experience in welding TD nickel strongly recommend TIG welding with a very minimum of melting of the parent metal and use of a filler wire such as Hastelloy W or similar.

Even the best of TIG welded joints in TD nickel suffers from a large reduction in physical properties at elevated temperatures (50% at 2000°F). This fact dictated the use of one, or at most, a two-part construction of the inner liner with a maximum of one circumferential TIG weld.

Initially it was hoped to form the entire inner liner, complete with end flanges, from a single sheet of material by shear spinning. However, nonavailability of wide enough sheet stock together with spinning vendor's opinions that configuration tolerances would be more readily obtained from two-part construction led to the decision to use two-part construction.

For strength reasons the decision was made to form the chamber from material thick enough to machine the cooling passages and lands integrally.

For machining the passages, the electrodischarge machining process was selected since the complex configuration required can be readily generated with electrodes machined from simple templates, also the low residual surface stress resulting from correct application of this process should further enhance the maintenance of tolerances throughout the entire piece.

By contrast, to machine the passages by conventional milling would require a complex setup due to the constantly varying cross-section, and the level of residual stress resulting would make the chamber liner subject to distortion.

Due to the difficulty of obtaining a reliable bond to the liner material brought on by the intricate fit-up required, the decision was made to electroform the outer case and manifolds over the liner, thus insuring the integrity of the passages and manifolds. Electroforming the nickel onto TD nickel indicated an excellent bond in preliminary experiments.

B. DETAILED ANALYSIS FOR FABRICATION OF INNER LINER

1. Methods Considered

Five methods were given serious consideration for fabrication of the inner liner once the design had been stablized to be of TD nickel with integral machined coolant passages.

The first approach considered was to rough form 120° segmental sections by drop hammer, finish size between hot ceramic dies and trim to close tolerances followed by assembly with three longitudinal welds. This method has the disadvantage, however, in that the weld joints are oriented in the wrong plane for maximum structural integrity.

Also considered was a combination of drop hammer formed, hot die sized segments and a spun or deep drawn section. This too was rejected due to undesirable weld joint orientation.

The third approach was to form the liner in one piece from a tubular blank by High Energy Rate Forming (HERF). However, capacitor discharge equipment with the level of power required is not available and explosive forming was not considered sufficiently repeatable for this project. Also grounds for rejection of this process was the uncontrolled elongation which occurs locally in this process. This would aggravate distortion tendencies in subsequent operations, necessitating machining the inside disc of the liner in addition to the outside.

The fourth approach was to form the liner from sheet, by shear spinning, in one piece if possible, or two parts with one circumferential weld. This has the advantages of controlled elongation, correct weld joint orientation for maximum structural integrity, availability of equipment and obviates the necessity to machine the inside diameter.

Also considered was to form the liner by a series of deep drawing operations. No equipment available has the necessary power/stroke, however, so this process was not pursued due to the cost of scaling up equipment.

From the above, it was decided that the liner should be spun of one or two parts with a maximum of one circumferential weld joint.

2. Justification of Selection (See Table 13)

The shear spinning process is already widely used for the production of many widely varying components, including various types and sizes of rocket engine thrust chambers.

It offers the following advantageous characteristics:

(a) Elongation is controlled and repeatable leading to a minimum of distortion on subsequent operations.

(b) Physical characteristics of the base metals are generally improved by the degree of cold working involved.

(c) Springback is controllable, obviating many subsequent machining operations.

(d) Minimizing of weld joints gives good structural integrity.

(e) Suitable equipment is available at a vendor with no scale-up required.

Some relative disadvantages (but not necessarily restrictive for this program) of shear spinning include:

(a) Fairly lengthy operation time necessitated by intermediate heat treatment of material. This, however, is largely offset by the relatively simple tooling required and the availability of a vendor source with equipment capable of performing such work.

(b) For certain configurations, a preform must be developed in order to control the flow of metal during spinning.

In view of the foregoing, the shear spinning process was selected by this contractor because it offers a combination of minimum welded joints, correctly oriented for maximum strength together with controlled elongation, improved physical properties of the metal, and minimizes the number of post-spinning maching operations.

C. DETAILED ANALYSIS FOR DIFFUSION BONDING

Diffusion bonding was investigated extensively as a means of joining the inner TD nickel liner to the outer Hastelloy X, or other superalloy, shell.

Of the two methods considered feasible, i.e., gas pressure bonding and the newer Thermo-Vac process, the latter method offered the greatest potential.

TABLE 13

OVERALL FABRICATION PROCESS SELECTION JUSTIFICATION CHART

Fabrication of Inner Liner	Structural Integrity	Cost	Time	Equipment In-House	Availability Outside	Residual Stress	Tolerance Control	Comments
1. Spun from sheet, one or two part construction with maximum of one circumferential joint.	Good	Medium	Medium	No	Yes			Best overall process available.
2. Drop hammer formed segmental sections with three longitudinal joints.	Poor	Medium	Short	Yes	Yes			Joints poorly oriented.
3. Combination of drop hammer formed segments and spun section with combination of longitudinal and circumferential joints.	Poor	Medium	Medium	No	Yes			Too many joints, some poorly oriented.
4. Formed in one part from tube by HERF.	Good	Medium	Short	No	No			Uncontrolled elongation, no equipment suitable or available.
5. Deep drawn in one piece	Good	Medium	Medium	No	No			No equipment available at this time.
Joining of Inner Liner								
1. TIG weld with filler wire	Accept	Medium	Medium	Yes	Yes			Recommended by authorities as best method.
2. Electron beam weld	Poor	Medium	Long	Yes	Yes			Melting of base metal undesirable.
Production of Flow Channels								
1. Electrical Discharge Machining (EDM)	Not Appl.	Low	Medium	Yes	Yes	Low	Medium	Equipment available in-house, electrodes simply made little other tooling required, short process development time most suitable overall.
2. Conventional machining	Not Appl.	High	Long	Yes	Yes	High	Fair	Complex setup to produce channels as designed, high residual stress promotes distortion.
3. Chemical mill	Not Appl	Medium	Medium	Yes	Yes	Lowest	Medium	Uncontrolled etching of sidewalls of channels, straight sides unobtainable. Varying depths a problem.
4. Electrochemical machining (ECM)	Not Appl	Medium	Short	No	Yes	Low	Good	No equipment in-house, extensive electrode/tool device required, electrolyte development may be required.
Construction of Outer Shell								
1. Electro-form	Good	Low	Short	Yes	Yes			Best overall process, no fit-up problem, short development cycle, possible to form outer shell and manifolds integral with good bond and material characteristics.
2. Form two pieces and braze	Poor	Medium	Medium	Yes	Yes			Difficult to ensure continuous sound joints.
3. Form two pieces and diffusion bond	Good	High	Long	No	Yes			No equipment in-house, local, would need extensive tooling, develop, cycle, possible explosive sizing to ensure fit-up.
4. Form two pieces and explosive weld	Good	High	Long	No	Yes			Extensive tooling/developing required, some reports of porosity in TD nickel explosive welds.
5. Form two pieces and EB weld	Medium	High	Long	Yes	Yes			Difficult to guarantee fit-up, inspection of welds difficult.

In gas pressure bonding, the work is fixtured, placed in a thin walled can and the can evacuated. The can is then sealed off and placed inside a furnace which is enclosed in, but insulated from, an autoclave. Bonding is accomplished by heating to approximately 2000°F.

In this bonding method, pressure is developed by pressurizing the autoclave to 10,000 psi, the pressure being transmitted to the work through the can. While gas pressure bonding is well suited for small, complex structures, the process is size limited and has several inherent disadvantages which render it unsuitable for the thrust chamber application. Foremost among these is the expendible tooling required to support internal passages during bonding. Preferred material for this tooling is Armco iron as it does not contaminate the joint and can be readily leached from the parts after bonding.

In the thrust chamber application each channel would have to be filled with an expendable mandrel. Not only would these mandrels be expensive to fabricate, as the channels vary in height, width, and depth, but they would be difficult to leach out,as the exposed surface at each end of the chamber is exceedingly small.

Fit-up is important in diffusion bonding. While the high pressures developed in gas pressure bonding provide the intimate contact necessary for the process, the cylindrical design of our chamber would necessitate a fit-up of ±0.005 inch between the inner and outer shells to insure bonding over the entire surface. It was felt that this tolerance might be achieved by explosive sizing.

From the practical standpoint, gas pressure bonding method is size limited because of technical problems with the design and operation of furnaces under the high pressures required in the process. The largest furnace available, and one representing a major breakthrough in furance technology, is approximately 14 inches in diameter. One solution to this problem is to lower the temperature required for bonding. A reduction from 2000°F to 1600°F reduces the magnitude of technical problems associated with the design and operation of the furnace, making it feasible to fabricate a furnace to accommodate our chamber. Diffusion bonding at this lower temperature would, however, necessitate the use of so-called diffusion aids; i.e., intermediate material placed in the joint to effect diffusion at a lower temperature. While diffusion aids seriously reduce joint strength at high temperatures, they could possibly be used in our application where the temperature does not exceed 1000°F. Candidate materials discussed included molybdenum and copper.

To sum up, gas pressure bonding would require the fabrication of intricate tooling, the design and construction of a suitable furnace, and a development program to qualify an intermediate material. Construction of a larger furnace in turn creates a new set of problems with the autoclave which, in effect, is the limiting factor in scaling up gas pressure bonding.

The Thermo-Vac process, on the other hand, appears well suited to the thrust chamber application and has the required scale-up potential. Thermo-Vac was developed for the fabrication of thin walled, hollow structures without the need for internal tooling. In the thrust chamber application, the outer shell would be placed over the ribbed inner shell and a vacuum pulled between the two shells to create a pressure differential of

approximately one atmosphere. Manifolding at each end of the chamber would be required; however, should this provide impractical, the unit could be canned as done in gas pressure bonding and the pressure differential created by evacuation of the can to some low pressure level and partially backfilling with inert gas.

While the pressure developed in the Thermo-Vac process is not high, the total load applied to the surface of the shells is transmitted to ribs, resulting in relatively high pressures across the rib interface. Conventional furnaces can be used for the Thermo-Vac process. Typical thermal cycle is 2000°F for one to two hours.

Aside from manifolding, the problems with the Thermo-Vac process are minimal. As the furnace is not pressurized, furnace size is not a problem and no autoclave is required. Part geometry, however, is critical as the width of the ribs and spacing between must be balanced to prevent the ribs from buckling and minimize dimpling of the outer shell. As in gas pressure bonding, fit-up between the inner and outer shells should be held to ±0.005 inch on the diameters. Test samples would be required for determining bonding parameters and for evaluation of joints so formed. The use of full size cylindrical specimens would be required instead of conventional flat specimens because such specimens would more closely represent problems in sizing and fit-up.

There is a current problem of obtaining TD nickel in sufficient thickness to allow machining the channels in the inner liner. In the Thermo-Vac process, the ribs could be made separately and diffusion bonded between the inner and outer shells. While some tooling would be required to position the ribs, it would not have to be elaborate. The ribs would be held together in several places with Armco iron spacers, "egg crate" fashion. These spacers would be spot welded to the TD nickel ribs and leached out after bonding. The Thermo-Vac process appears to offer a practical method for the joining of TD nickel and one worth serious future consideration.

D. DETAILED ANALYSIS FOR EXPLOSIVE WELDING

Explosive welding is effective in joining large surfaces and joints can be affected between a wide range of materials not considered weldable by conventional fusion techniques. No molten metal is formed in an explosively welded joint and explosive welding has excellent scale up potential. An interesting feature of explosive welding is the characteristic wave front at the joint interface and the cold working evident along the weld. An important parameter for explosive welding is the gap width between the parts to be welded. Parts in intimate contact cannot be explosively welded. Conversely, parts too far apart will not weld properly. A properly made explosive weld will exhibit parent metal strength in most metals. Explosively welded TD nickel joints must not be exposed to temperatures above 2300°F. Evidence exists of recrystallization and subsequent degradation of properties above 2300°F. Since the design wall temperature of the thrust chamber is 2150 to 2200°F the recrystallization problem would not occur but is mentioned to indicate the restriction to this process.

It was felt that the design of the chamber readily lent itself to explosive welding. While in its simplest form this involved welding the outer cover to the inner liner, it was felt that there was no technical reason why the ribs themselves couldn't be explosively welded to the inner liner and the outer cover subsequently explosively welded to the ribs.

Explosive welding offers a tremendous potential for joining large, complex parts, however, here again, tooling becomes a problem when internal channels have to be supported. While such tooling does not have to withstand high temperatures or meet the precise fit-up required in gas pressure bonding, the need for tooling places explosive welding somewhat below the Thermo-Vac diffusion bonding process in order of preference for this application.

E. DETAILED ANALYSIS FOR CONVENTIONAL WELDING OF TD NICKEL

Two companies, General Electric of Evandale, Ohio, and Pratt & Whitney of East Hartford, Connecticut, experienced in welding TD nickel, were consulted in order to obtain a better understanding of the joining problems associated with this material.

General Electric found that fusion welding TD nickel to itself without the use of filler metal produced inferior properties and severe porosity in the joint. It was found that TIG welding, using Hastelloy X as a filler metal produced good results. Further experiments indicated that excellent ductility in the weld joint resulted when a gap width between 0.060 and 0.080 inch was maintained, a large Hastelloy X rod was used and the heat input kept low. This latter process minimized the melting and dilution of the TD nickel.

General Electric also has considerable experience in joining TD nickel by resistance spot welding and by resistance diffusion bonding and feels both processes are suitable for applications involving moderate temperatures. The drawbacks to these methods are that such joints are difficult to evaluate and the electrodes have to be dressed after each joint has been made.

Pratt & Whitney was consulted and was in agreement with General Electric from the standpoint of using a filler metal in the TIG process. Pratt & Whitney, however, favored melting the TD nickel on both sides of the joint and subsequent dilution with the filler material.

Typical filler alloys include Hastelloy X, Inco 718, Hastelloy W, Waspalloy and Nichrome 5. Filler metal does not appear to influence the strength of the joint to any appreciable extent. At room temperature, failure is through the parent metal while at 2000°F failure invariably occurs through the weld. The solid solution filler alloys are favored over the precipitation hardening alloys as it is felt that overaging of the latter influences the ductility of the joint. Preferred is Waspalloy and Nichrome 5 as these alloys are the most stable at temperature above 2000°F and their low carbon content is beneficial in minimizing delamination.

Delamination in TD nickel has been traced to carbon. Where carbon pick-up in pure nickel occurs along equiaxed grain boundaries exposed to the surface, carbon penetrates TD nickel along the long, highly oriented, grain boundaries running parallel to the surface resulting in delamination. To minimize problems with carbon, the specification limits have been reduced for TD nickel from 200 ppm to 100 ppm. Care must be taken in welding TD nickel to insure that the carbon content of the filler metal is kept as low or lower than that of the parent metal.

Weld joint configuration and preparation is important in the welding of TD nickel, as joint geometry influences thoria agglomeration.

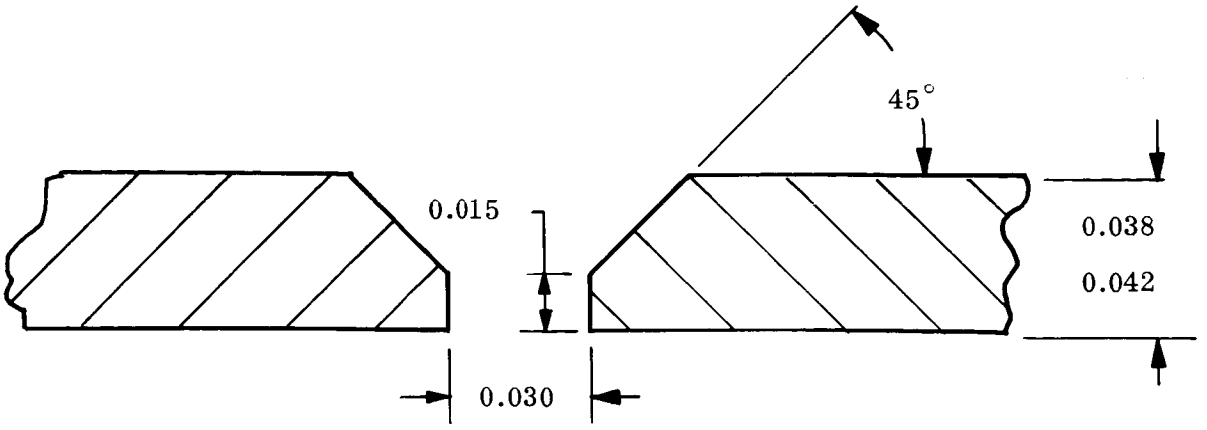

With the proper joint design, as in above sketch, agglomerated thoria is lightly dispersed on both sides of the filler metal resulting in good joint ductility. Without suitable preparation, heavy agglomeration is concentrated at the joint resulting in a corresponding decrease in joint ductility.

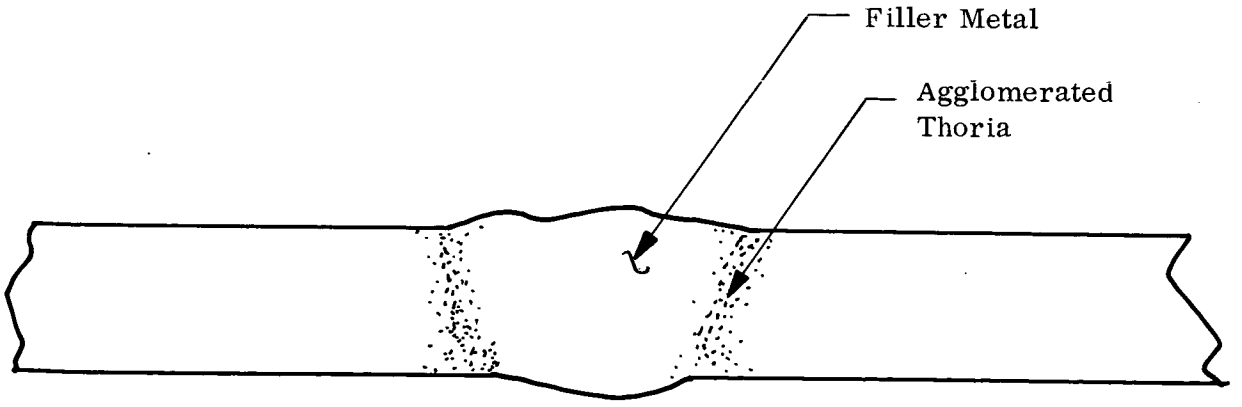

Optimum current for welding 0.038/0.042 inch TD nickel sheet is between 45-55 amps. All welding is done by hand. It was found necessary to train and qualify welders for welding TD nickel as the material has unusual welding characteristics and good joints are dependent upon the skill of the operator. Joints can be readily inspected by X-ray; however, interpretation is difficult as the thoria agglomeration often resembles cracks and other internal defects. After welding, TD nickel parts are stress relieved at 2000°F in argon or hydrogen. Typical properties of 0.038/0.042 inch TD nickel sheet, welded with Nichrome 5 filler wire were as follows:

Temperature of Test	UTS (ksi)	% Elongation
Room Temp	61	16.5
	60	16.5
	60	14.0
	61	11.0
2000°F	9.8	1.4
	9.7	1.3
	8.9	1.3
	7.9	1.4

Justification: Tungsten Inert Gas Welding

This method of joining was selected for the following reasons:

(1) The predominate amount of joining of TD nickel has been accomplished with this method.

(2) Considerable data on mechanical properties, physical properties and metallurgical phenomena are available on Tungsten Inert Gas Welding with filler metal.

(3) Tungsten Inert Gas Welding equipment is readily available and can be scaled up to any size required to meet future requirements. The minimum mechanical properties of the welded joints of TD nickel can further be improved by use of the, "hot wire" Tungsten Inert Gas Welding method. This equipment is available and will be used for this program. It is anticipated that a sound weld joint with considerably less thoria agglomeration will be accomplished. This will definitely improve the mechanical properties of the weld joint.

F. DETAILED ANALYSIS FOR GENERATION OF COOLANT FLOW PASSAGES

1. Methods Considered

Four methods were given serious consideration for generation of the coolant passages in the wall of the liner.

Conventional machining is capable of generating the passage configuration, however, the widely differing cross section of the passages would have required a complex setup using multiple templates to take a series of cuts using a narrow milling cutter. Numerically controlled, (N/C), machining, while possible, was not selected since in order to maintain wall thickness at the inside of the passages, i.e., within drawing tolerances, it is essential that a template be produced from the actual spun parts. The coolant passages would then be machined in the spun part accordingly, rather than to a nominal dimension by N/C. Removal of so large a percentage of the total wall thickness by conventional machining was considered inadvisable due to the high residual stresses likely to occur.

Chemical milling (etching) was considered as being capable of removing metal at an acceptable rate with virtually no residual stresses resulting from the process. However, the tendency to undercut the masking and produce an undesirable cross section together with the difficulty of controlling the varying depth of the channels made this process unacceptable.

Electro-Chemical Machining (ECM) was considered as being capable of high rate of metal removal with very low residual stress resulting, offering sufficiently close dimensional control and little electrode wear. However,to produce a long groove of varying cross section with a smooth bottom,would require an extensive tool and electrode development effort. The latter would have been complicated by the lack of in-house equipment. It is possible also that development would be required to select an optimum electrolyte.

The Electrical Discharge Machining Process (EDM) offers a moderate rate of material removal with the ability to control dimensional tolerances to an acceptable figure using expendable electrodes simply produced from templates. The process is one with which Bell has conducted a number of company sponsored development programs in machining of difficult configurations in the refractory and superalloy materials. The general procedure involved is the sparking of a pulsed dc current from an electrode to the work material through a cooling dielectric. The frequency of the pulsating sparks and the level of current used determines the rate of metal removal and the surface finish. Properly applied, the level of residual stress is low.

The Electrical Discharge MachiningProcess has been selected as the manufacturing process for the generation of the coolant passages on this contract.

2. Justification of Selection

The Electrical Discharge MachiningProcess has been in use now for more than 15 years. Introduced primarily as a process for reproducing forging, moulding, and stamping dies, it has more recently proved of high value in machining of complex shapes in difficult to machine aerospace alloys. By careful control of process parameters, a high degree of accuracy can be achieved together with an excellent surface finish and a low degree of residual stress.

Selection of this process was based upon the weighing of its advantages and disadvantages in comparison with other methods.

The advantages may be summarized as follows:

(a) With relatively simple tooling, a suitable degree of accuracy is readily obtained.

(b) Expendable electrodes may be fabricated from simple templates ensuring close control of finished channel wall thickness.

(c) Surface finish obtainable is adequately smooth and repeatable, ensuring consistent flow between channels.

(d) By careful control of parameters, the residual stress is low, minimizing distortion.

(e) Combinations of different materials as at weld joints, etc., will machine at equal rates.

Some relative disadvantages (but not necessarily restrictive for this program) include:

(a) Sharp internal angles represent a problem due to erosion of the electrode. In the case of the coolant grooves to be produced in this part of the program, however, adequate radii have been specified to minimize this problem.

(b) Rate of metal removal using parameters to provide low residual stress and good finish is relatively slow. This can be overcome by a faster, roughing operation, followed by a slower finish operation to remove the stressed layer and provide good finish.

In view of the foregoing, the Electrical Discharge Machining Process was selected because:

(a) It should be less difficult than producing the coolant grooves by conventional means.

(b) Close dimensional tolerances can be held relative to the actual inside diameter of the liner.

(c) Low residual stress will enhance the overall maintenance of tolerances.

G. DETAILED ANALYSIS FOR FABRICATION OF OUTER SHELL

1. Methods Considered

The following fabricating methods were given serious consideration. Forming the outer shell in two halves and explosive bonding the halves to the liner and edge to edge was considered a practical method of bonding materials containing complex passages. However, these passages require physical support during the process with a substantial filler material, which is capable of withstanding the high energy rate stresses induced. The subsequent removal of this filler material is often difficult, time consuming and costly.

Hot isostatic-gas-pressure bonding also affords an attractive means of solid-state diffusion bonding from complex shapes; however, from a standpoint of fabricating large structures as anticipated in future regeneratively cooled rocket engine designs, scale-up of bonding facilities, which at present do not exist, would be extremely costly.

Thermal vacuum bonding has been successfully used in the development of diffusion bonded joints in complex, hollow walled, cylindrical chambers. However, this process also suffers from the difficulty of removing the substantial filler material together with the considerable cost of scaling up equipment if this became necessary.

Powdered metal compaction has been applied to produce composite shapes which were subsequently extruded to produce the desired configuration. Disadvantages exist with this method in that if extrusion is omitted by virtue of limitation in scale-up potential, expensive, heat resistant dies must be used and homogeneity in the compacted metal is difficult to control on a reproductive basis.

Electrolytic deposition has found widespread use in the production of items having complexities comparable to regeneratively cooled thrust chambers. The general procedure involved is the passing of a current through a solution of a metallic salt, which removes metal from an anode composed of the metal to be plated and deposits it on the article to be plated. With this process, the present state-of-the-art is such that there is a higher degree of assurance that the required structures can be produced with fewer problems and at less expense than can be reasonably predicted with the alternatives.

Electrolytic deposition from aqueous solutions has been selected as the primary fabrication technique. The selection was on the basis of its overall suitability including such factors as structural integrity, cost, time, equipment availability, and scale-up potential.

2. Justification of Selection

The electrolytic deposition process has been applied for more than twenty years to the manufacture of electro type printing plates and the preparation of phonograph record stamping dies. More recently its field of applications has been expanded to include many components difficult or impossible to manufacture in any other way; examples are: complex radar waveguides, pitch tubes, denture molds, heat sinks for missile nose cones and complex airfoil leading edge skins (having nonlinear draft angles).

Selection of this process was based on weighing the advantages and disadvantages in comparison with other methods. The beneficial potentials may be summarized as follows:

(a) Metallurgical and mechanical properties of an electrodeposited material can be controlled over a wide range by choice of a suitable metal and by adjusting the process parameters.

(b) An excellent intermolecular bond with the inner liner metal can be obtained, with no detrimental effect on the liner metal physical properties.

(c) A wide range of part sizes may be produced by this process. Foil 0.0001 inch thick and art statues thirty feet tall and weighing three tons have been so produced.

(d) Shapes impossible to fabricate by other methods may be readily produced by electrodeposition. The outer shell, manifolds and injector bolt flange will be formed as a one-part, integral structure.

(e) Consecutive layers of different metals may be built up in a prescribed laminar configuration.

(f) Electrodeposition is equally applicable to the manufacture of single pieces or large production runs.

Some disadvantages (but not necessarily restrictive to this program) are essentially:

(a) The cost is often high if only a few articles of a given configuration are to be produced. As applied to this contract, however, this cost is more than offset by the considerable capital equipment and machine setup costs which would be incurred by using other fabricating methods.

(b) The production rate of an individual piece is quite slow, often being measured in days. However, difficult machining operations by other fabrication processes may also take as long, during which time constant attendance of skilled workmen is required. Scale-up of electrodeposition facilities is relatively inexpensive as compared with machine tool equipment.

(c) Sharp angles can cause difficulty in electrodeposition. A review of the objects to be produced in this contract shows sufficient radii allowed to minimize this problem.

In view of the foregoing, electrolytic deposition was selected by this contractor because:

(a) Difficulty and cost of producing the parts by other applicable methods is unusually high.

(b) Physical properties required can be held uniform on the chambers.

(c) Close dimensional tolerances can be held on surfaces of irregular contour.

(d) Electrodeposition offers an opportunity to choose the physical properties desired in the deposited metal and vary these properties at different stages in the fabrication, even though only one metal may be employed to compose the entire structure. This is accomplished by choosing an appropriate bath, utilizing selected additives, and carefully controlling the parameters of temperature, current density, and concentration.

VIII. STRESS AND WEIGHT ANALYSIS

A. GENERAL

The detail structural analysis of the 8489 regeneratively cooled thrust chamber involved the determination of critical stress distributions arising from the relatively severe temperature gradients and high pressure loadings imposed during the steady-state operational cycle. Initially, several design concepts were investigated to determine the optimum structural configuration of the thrust chamber, i.e., integrated tube bundles and rectangular channels. A stress analysis was conducted on various tube bundle designs, e.g., nickel felt, innner liner, interconnected stainless steel tubes, etc. These concepts were eliminated due to thermal requirements.

For the rectangular channel construction several materials were considered; SCb-291 columbium alloy, Hastelloy X, and a nickel alloy composition. The columbium was dropped due to nonstructural reasons noted earlier in the report. The Hastelloy X design was stress analyzed at a typical chamber location and was determined to have an operational cyclic capability of 20 cycles. This material was then discarded because of the critical thermal and manufacturing limitations. In the final configuration it was determined that using the combination of a TD nickel inner liner and an electrodeposited nickel outer shell represented the optimum design for heat transfer, pressure drop, and manufacturing requirements.

The design criteria utilized in the analysis of the thrust chamber were:

(1) Factors of Safety

Yield strength - F.S.	= 1.50
Pressure - Ultimate strength - F.S.	= 2.0
Thermal - F.S.	= 1.0
Dynamic ultimate F.S.	= 1.25 x 1.25

(2) Pressure Loads

H_2 Coolant - variable, depending on longtitudinal station in thrust chamber (see thermal analysis)

Chamber P_c = 400 psia

P_{throat} = 228 psia

(3) Temperature

Variable, depending on longitudinal station in thrust chamber (see thermal analysis)

Initially the structure was analyzed for thickness requirements based on the coolant and chamber pressures with a specified liner temperature distribution. The TD and electrodeposited nickel strength properties used in the analysis are referenced in Figures 24 and 25 respectively. The method of loading utilized was:

(1) Hydrogen Coolant Pressure

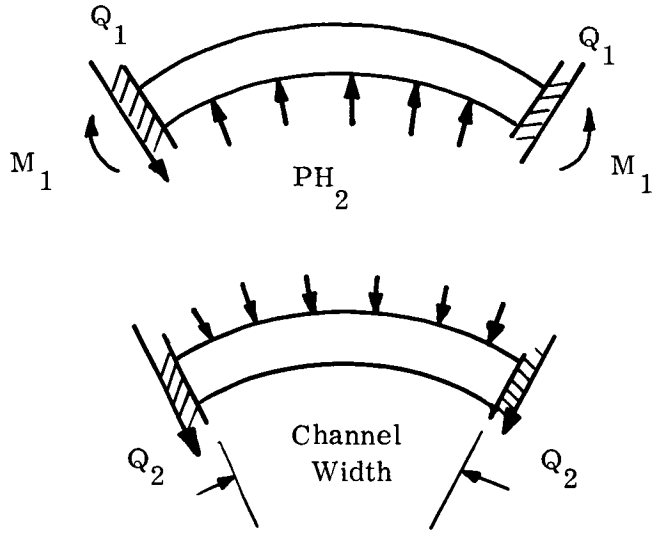

(2) Chamber Pressure

Outer nickel shell assumed to carry full chamber pressure in hoop stress

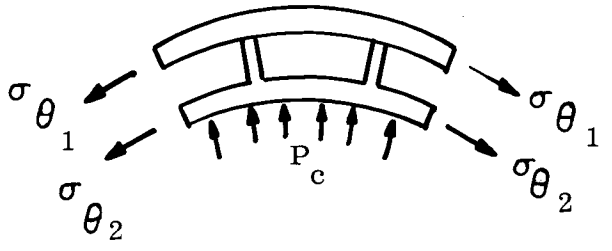

$$\sigma_{\theta_1} = P_c \frac{R_1}{t_1}$$

$$\sigma_{\theta_2} = 0$$

Several longitudinal stations were investigated in an effort to define the projected requirements throughout the thrust chamber. These thicknesses were then used for determination of the detailed temperature distributions.

The detailed structural analyses conducted on the regeneratively cooled thrust chamber and nozzle extension were as follows:

Ref.
"Mechanical - Property Evaluations of Newly Developed Structural Materials"
AFM-FR-66-155 April, 1966

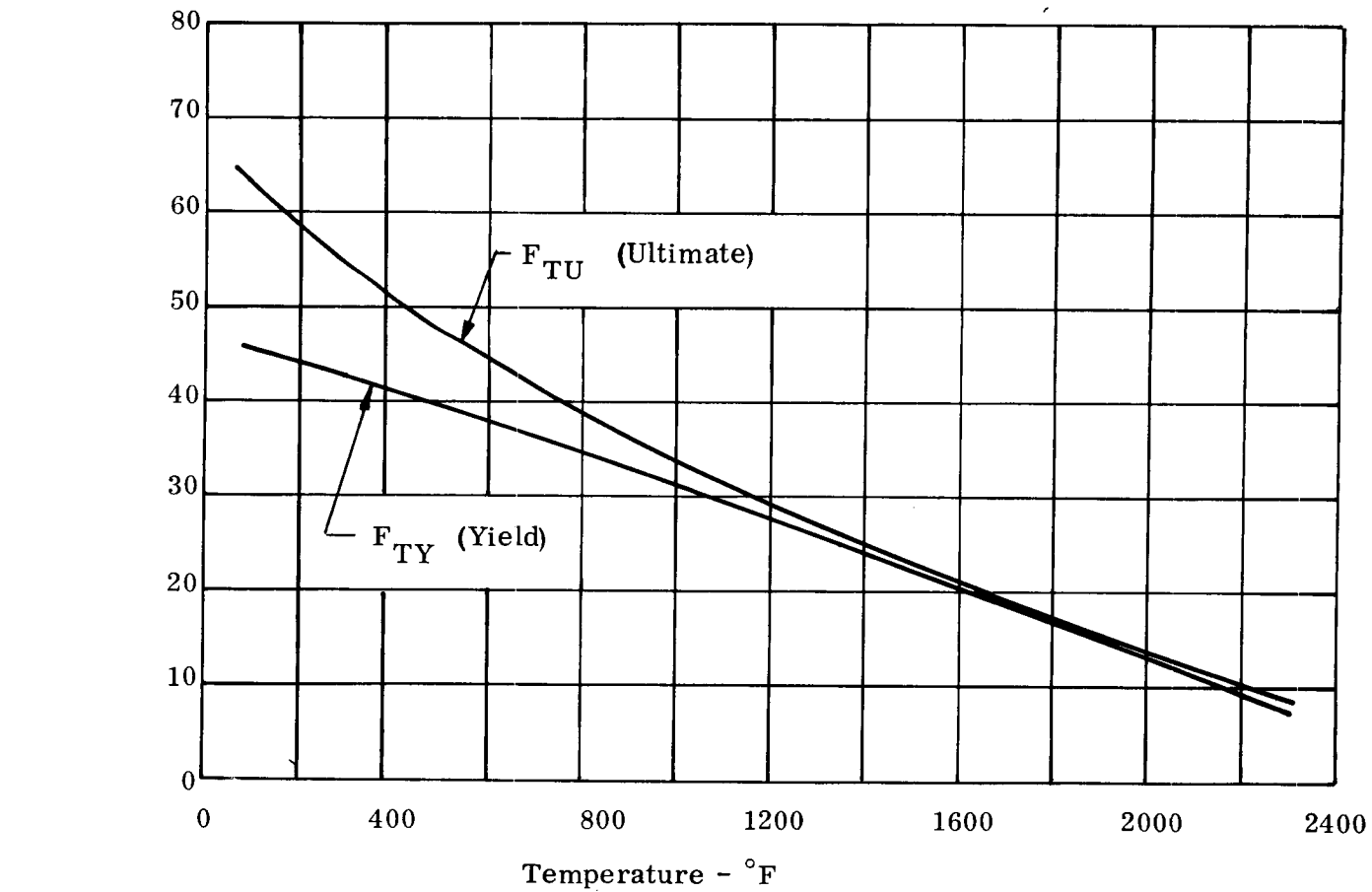

Figure 24. TD Nickel Tensile Strength versus Temperature

Ref.
"Engineering Properties of Nickel"
Inco Alloy Products
Technical Bulletin T-15
Feb. 1960

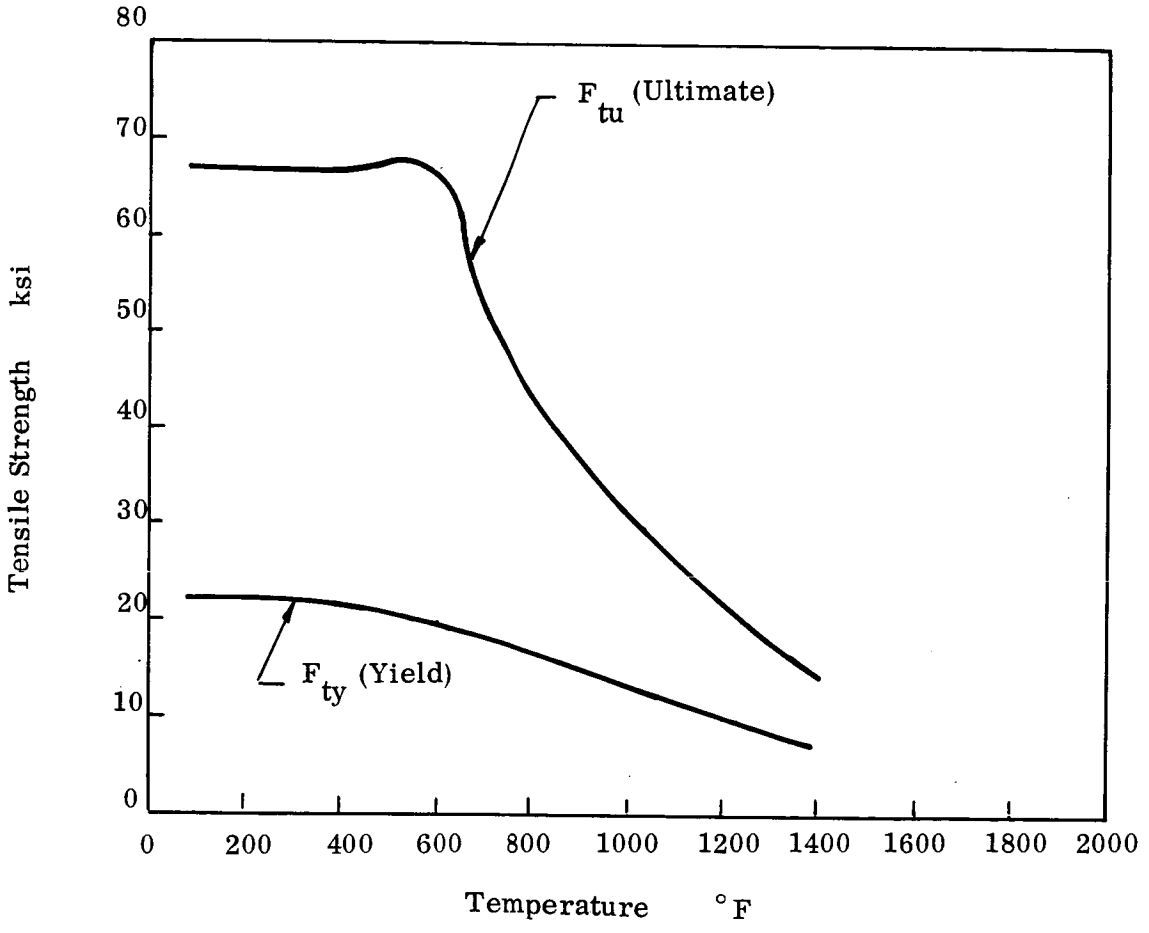

Figure 25. A Nickel Tensile Strength versus Temperature

(1) Thermal and pressure stress analysis of thermal nodes 3, 6 and 8.

(2) Analysis of inlet and outlet manifolds for pressure loading.

(3) General stability analysis in divergent section (operating and ambient conditions).

(4) Stress analysis of radiation nozzle.

Each of the above analyses is described in the following discussion along with a description of the structural analysis computer program. A summary of results is also included in which the operational limits of the thrust chamber are defined for the steady-state temperatures and external loads (pressure, thrust and vibration).

B. THERMAL AND PRESSURE STRESS ANALYSIS OF THERMAL NODES 3, 6 AND 8

Due to the operating environment imposed on the regeneratively cooled thrust chamber, relatively large temperature gradients are generated internally in the structure thereby developing a condition of thermal stress. In the thermal stress analysis of the thrust chamber, a computer program solution was utilized to determine the local stress distribution in the channel structure. The finite element method of programming is described in a separate section of this report. The basic assumptions in the analysis were that the pressure and temperature distributions were symmetrical in the circumferential direction, therefore only half of the channel was analyzed with appropriate boundary conditions. The boundary conditions stipulated were that the middle sections of the channel width and land were prevented from translation in the circumferential direction but were free to move radially (refer to Figure 26). Only a two-dimensional analysis was used (circumferential and radial) for the structure, therefore three longitudinal stations were investigated to define the complete critical design condition of the TD nickel liner. The material properties utilized in the analysis are shown in Figures 27 through 30.

Because of the relatively severe temperature gradients occurring in the structure, the predominant mode of thermal stress generally exceeds the pressure stresses by an order of magnitude. Therefore, the critical design mode was established as thermal fatigue resulting from the fact that part of the structure enters into a plastic state because of the above stresses. The method used in determining the cyclic capability based on thermal fatigue is given in Reference 1, where the relationship between the component of plastic strain and cyclic capability is:

$$\epsilon_{plastic} = MN_f$$

$$M \sim \text{Material constant} = 0.827\ D \left[1 - 82 \left(\frac{\bar{V}_u}{E} \right) \left(\frac{\bar{V}_f}{\bar{V}_u} \right)^{0.179} \right]^{-1/3}$$

$N_f \sim$ Cycles to failure

$$Z \sim \text{Materials constant} = -0.52 - 1/4 \log D + 1/3 \log \left[1 - 82 \left(\frac{\bar{V}_u}{E} \right) \left(\frac{\bar{V}_f}{\bar{V}_u} \right)^{0.179} \right]$$

$D \sim$ Ductility Factor - ln (1-R.A.)

R.A. = reduction of area

$\epsilon_p \sim$ Component of plastic strain

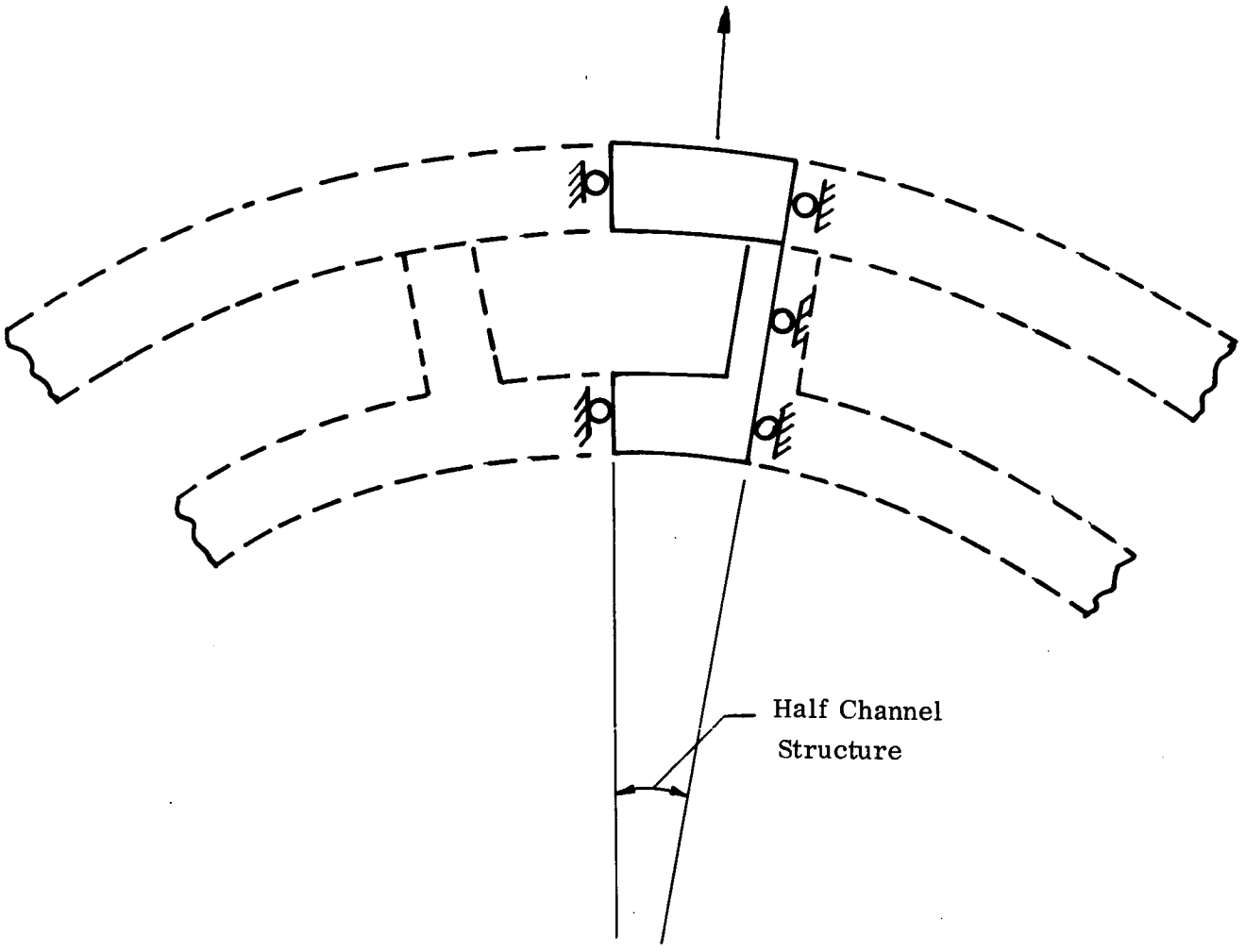

Figure 26. Regenerative Thrust Chamber Depicting a Typical Section Used in the Thermal Stress Analysis and Boundary Conditions

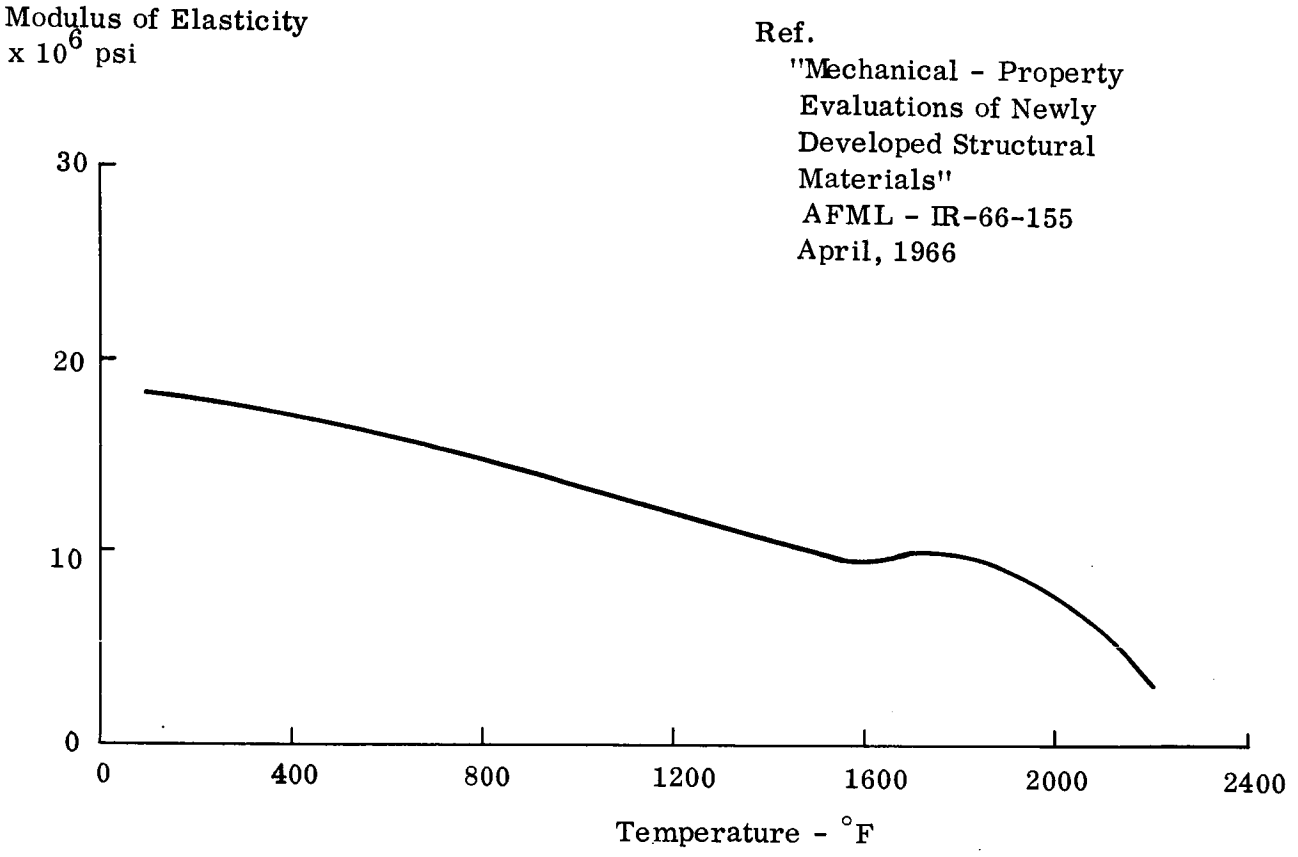

Figure 27. TD Nickel Modulus of Elasticity versus Temperature

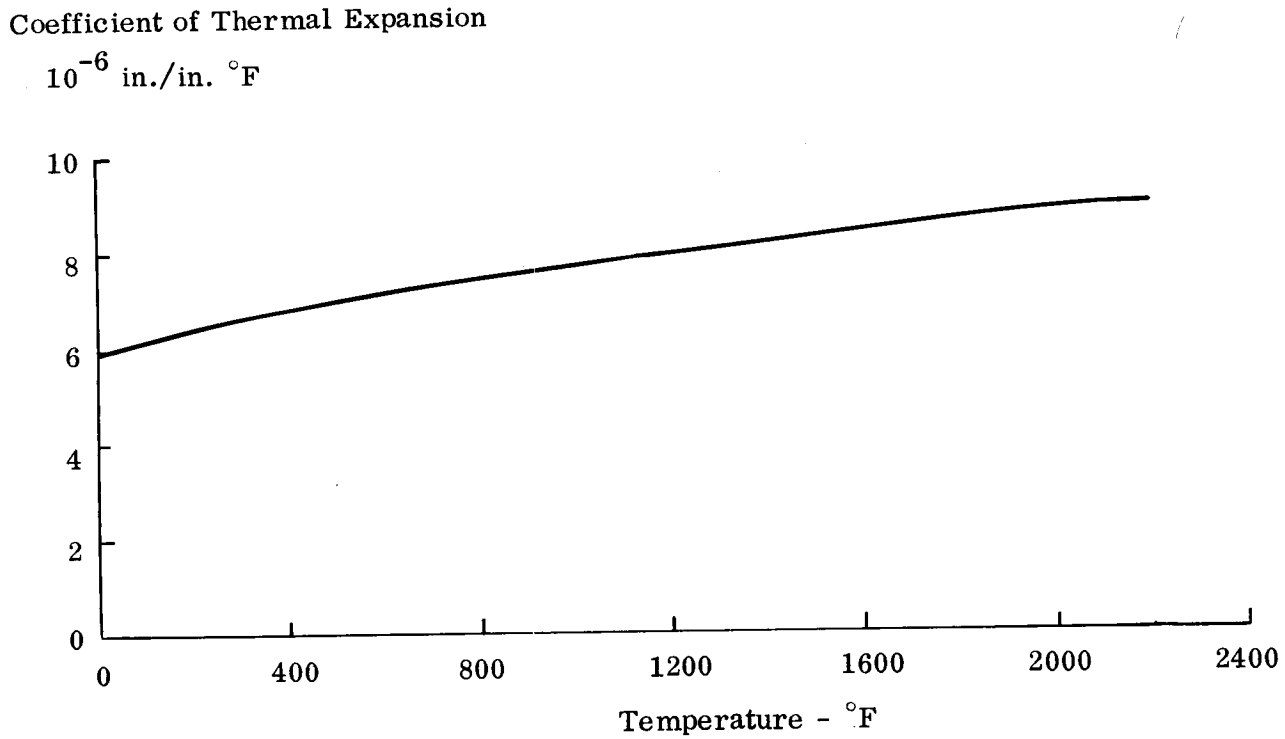

Figure 28. TD Nickel Coefficient of Thermal Expansion versus Temperature

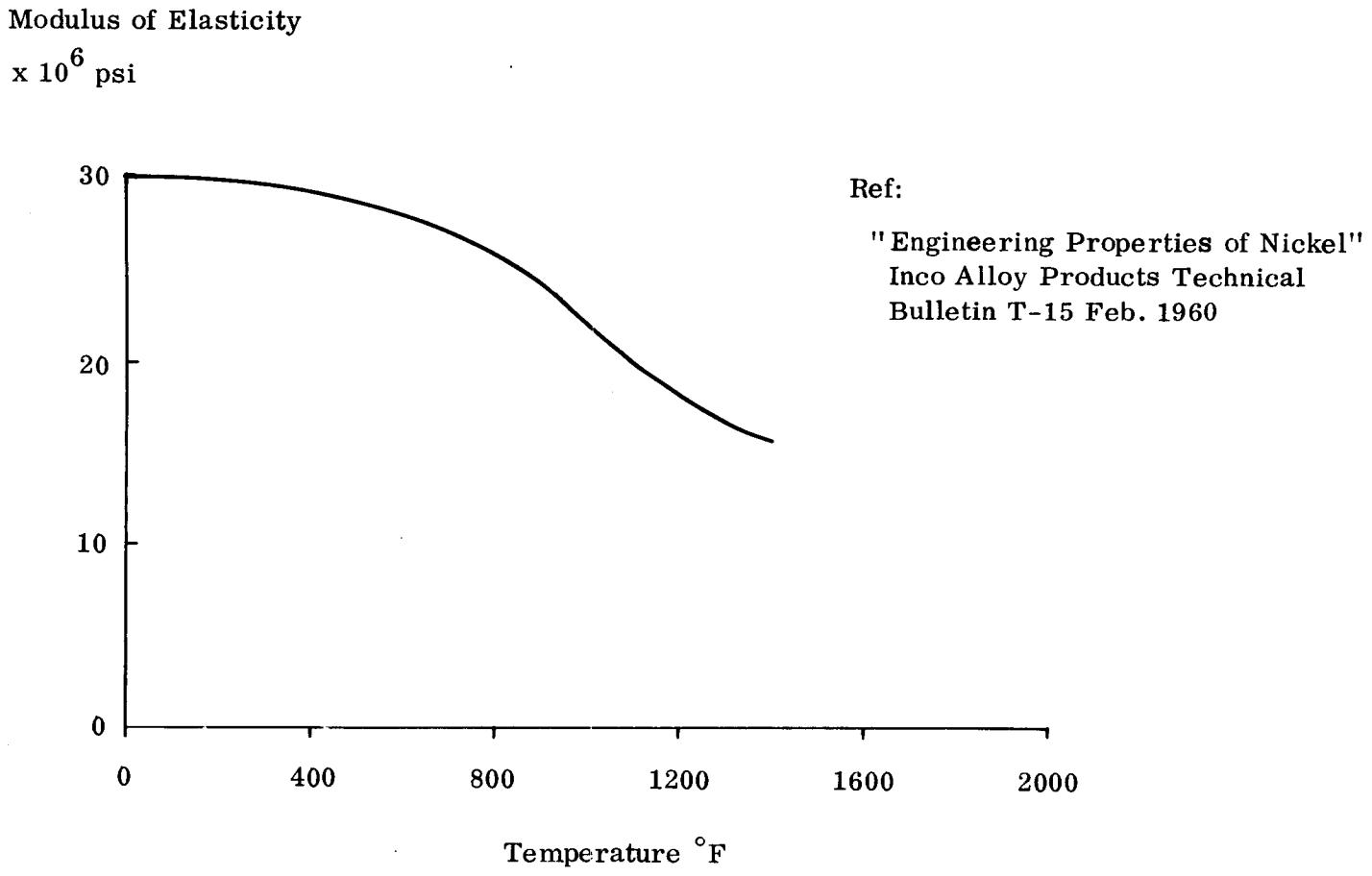

Figure 29. "A" Nickel Modulus of Elasticity versus Temperature

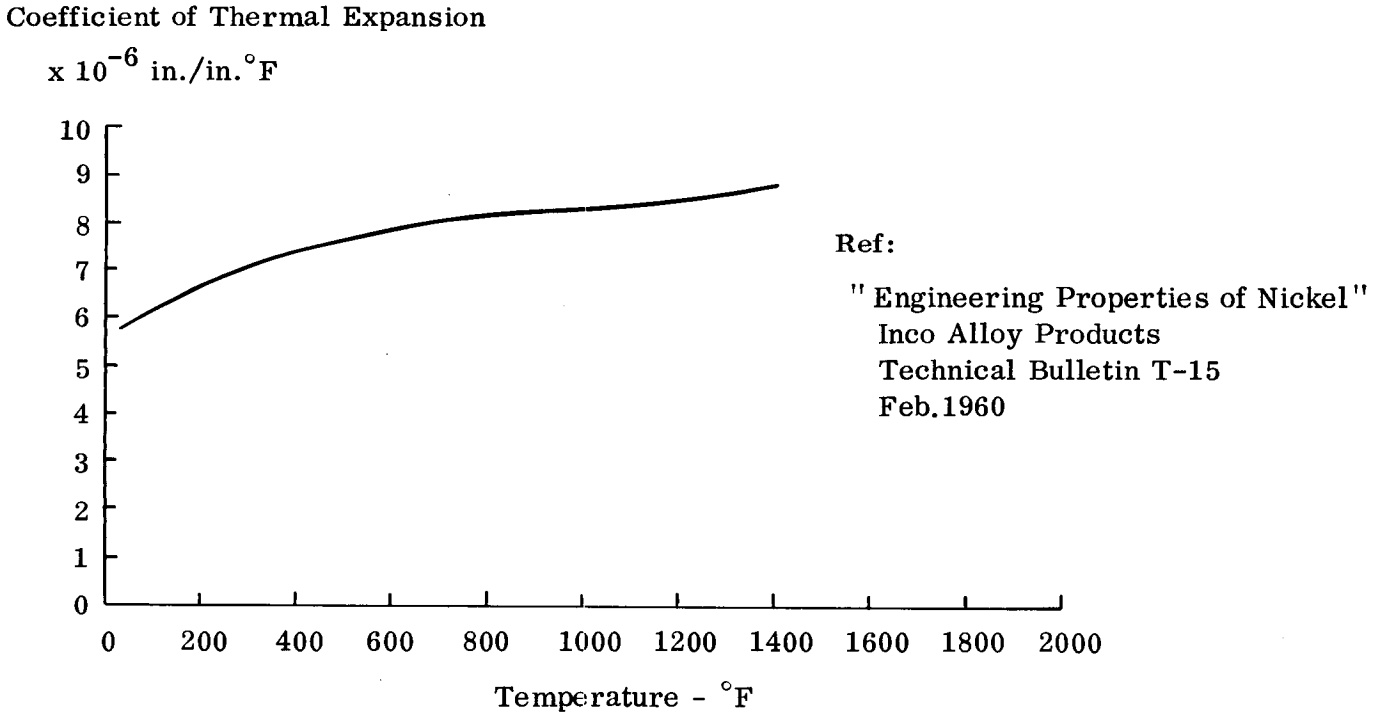

Figure 30. "A" Nickel Coefficient of Thermal Expansion versus Temperature

It should be noted that the stress analysis is primarily an elastic analysis which did not account for any plastic flow in the material. Therefore, many of the quoted stresses exceed the yield and ultimate strength (Figures 24 and 25). Figure 31 demonstrates the method used in determining the actual stress levels and the corresponding strain components for those stresses which exceed the elastic limit. Although TD nickel exhibits a relatively low tensile elongation at elevated temperatures, the predominant stress mode is compression which is a less severe loading condition for the material. But because of the reversal of stress during a cyclic operation, the one criteria used was that the calculated total strain did not exceed the actual strain capability of the material, based on the tensile elongation values.

The three stations investigated were designated as thermal nodes 3 (divergent), 6 (throat), and 8 (chamber). Figures 32, 33 and 34 illustrate the element mesh used in the initial elastic computer analysis along with the numbered structural nodes to which the stresses are referenced. The temperature distributions utilized in the analysis of the thermal nodes are shown in Figures 35, 36 and 37. The distribution of the elastic pressure and thermal stresses through the half channel structure are depicted in Figures 38 through 43. Tables 14, 15 and 16 reflect the total amount of strain associated with the resultant stresses developed at each of the structural nodes.

At the end of each table are the calculations for determination of the critical cyclic capability utilizing the equations noted previously. The resultant values are:

(1) Node 3 N_f = 320,000 cycles

(2) Node 6 N_f = 2280 cycles

(3) Node 8 N_f = 297 cycles

As can be seen from the above, the minimum cyclic mode (297) occurs in the chamber section which develops the most severe operating environment. Although the minimum calculated cycles to failure is 297, the design limit is established as 20 cycles because the analysis was conducted under symmetric loading and geometry which in all probability will not occur in the actual thrust chamber.

C. ANALYSIS OF INLET AND OUTLET MANIFOLDS FOR PRESSURE LOADING

The stress analysis of the inlet and outlet manifolds involved the determination of critical design thicknesses based on coolant and pressure loadings. Temperature gradients in the manifolds were not critical and therefore thermal stresses were excluded in the analysis. The effects of elevated temperatures on material strength properties were included as shown in Figures 24 and 25.

Because of the manifold toroidal configuration two separate analyses were conducted; one concerned with the inner contour and one with the outer (see Figure 44). The inner contours were analyzed as built-in thin shells subjected to an external pressure loading condition. For the inlet location an equivalent cylinder was used to determine the discontinuity loads induced because of the above boundary condition. The method of analysis is given in Reference 2.

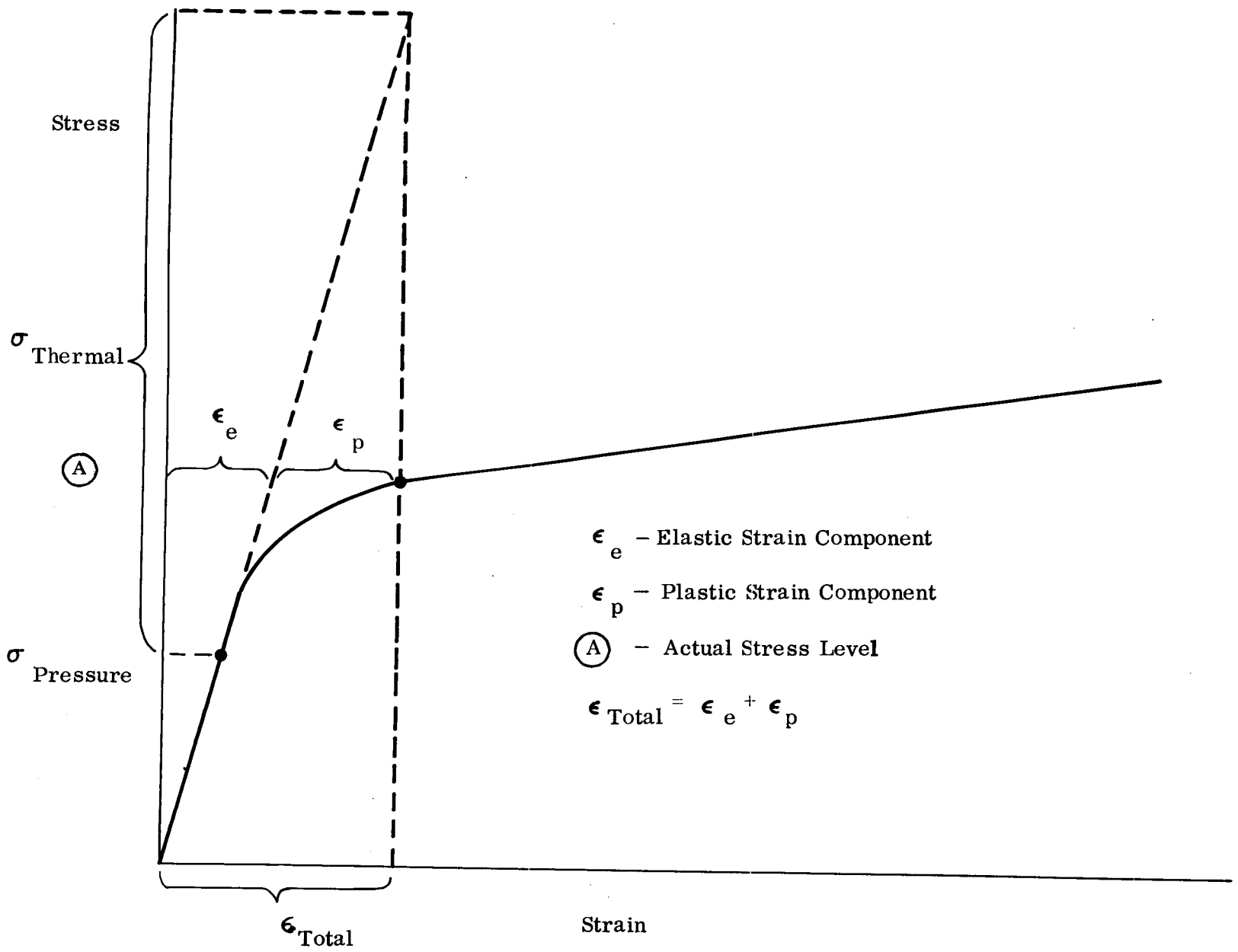

Figure 31. Determination of Actual Stress Levels and Strain Components (Typical)

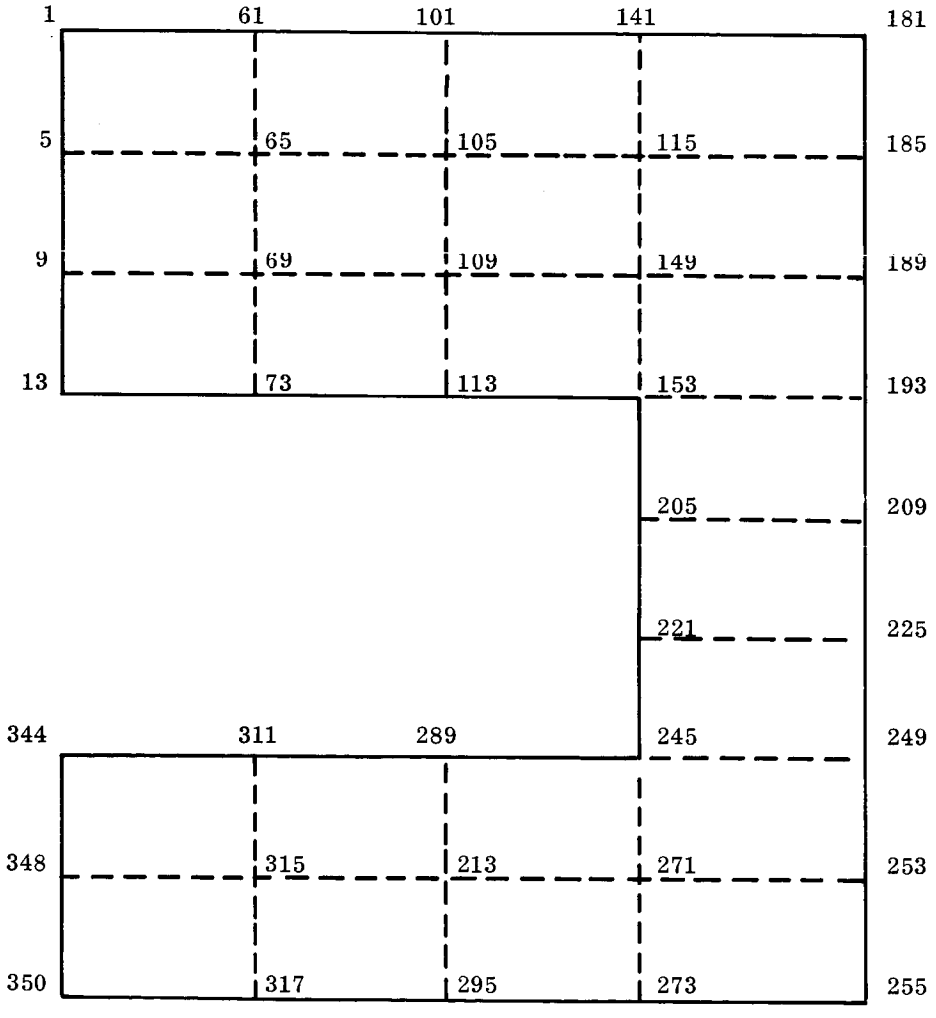

Figure 32. Half Channel (θ /2) Structure with Node Designation for Computer Stress Analysis (Thermal Node 3)

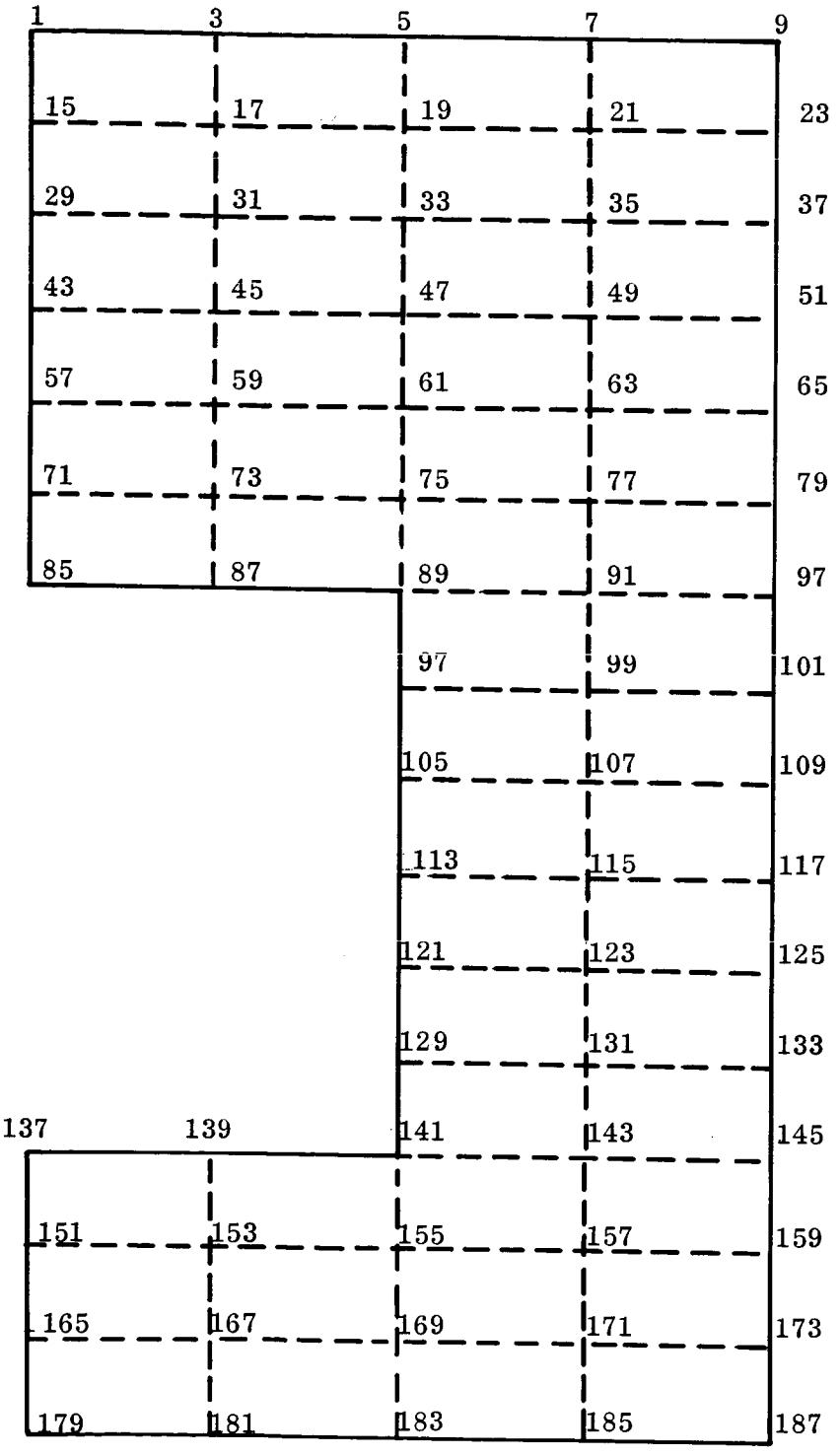

Figure 33. Half Channel (θ /2) Structure with Node Designation for Computer Stress Analysis (Thermal Node No. 6)

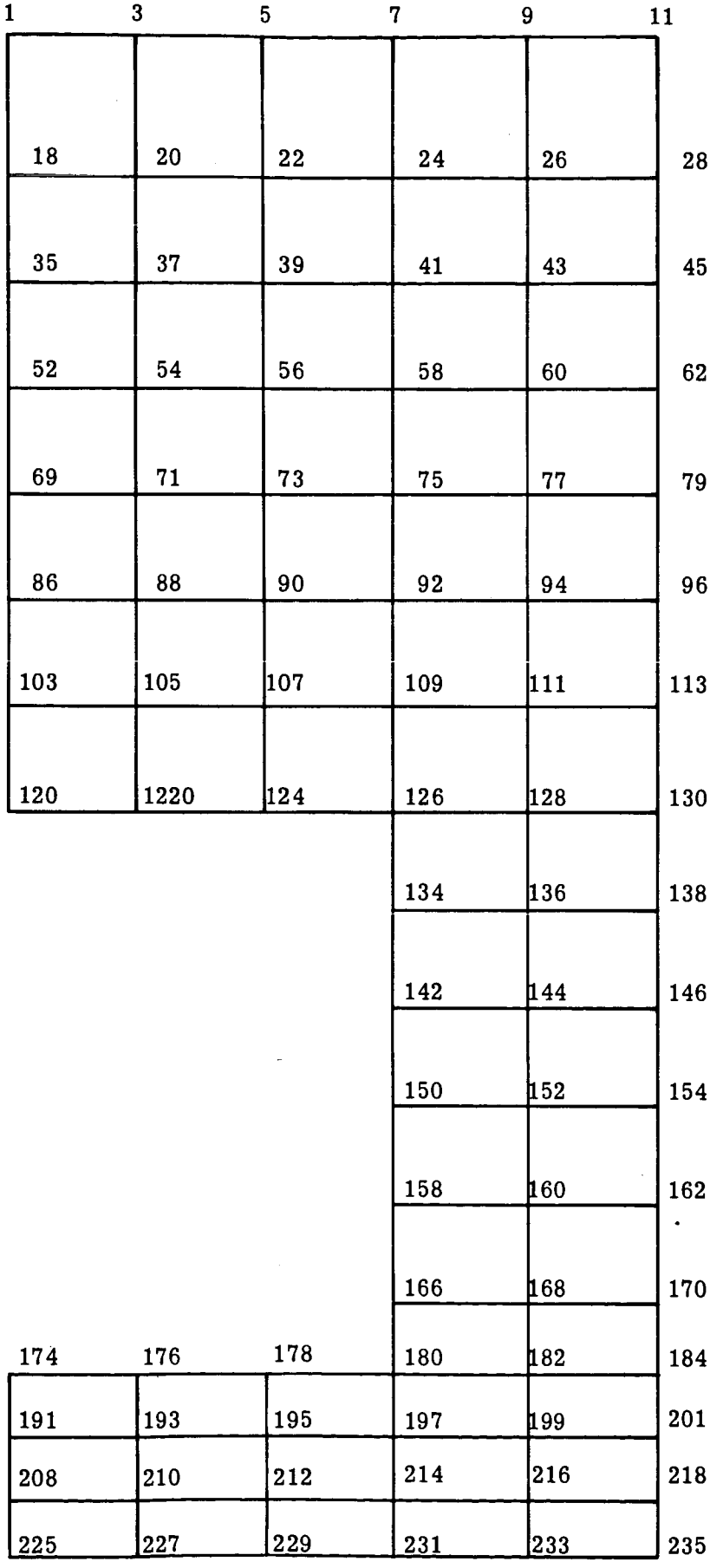

Figure 34. Element Mesh and Node Designations for Half Channel Structure Thermal Node No. 8

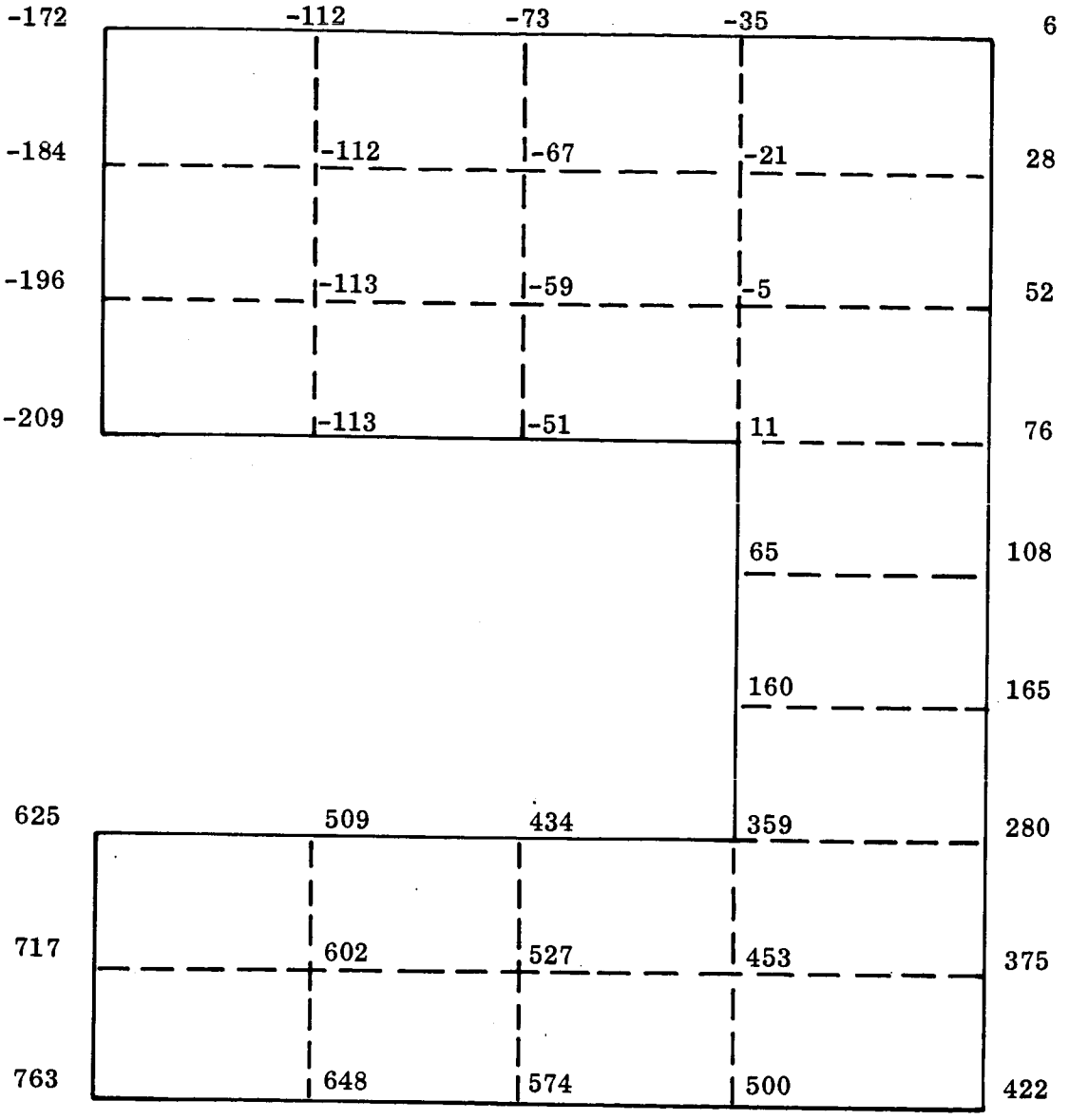

Figure 35. Temperature Distribution (°F) Used in Stress Analysis (Thermal Node 3)

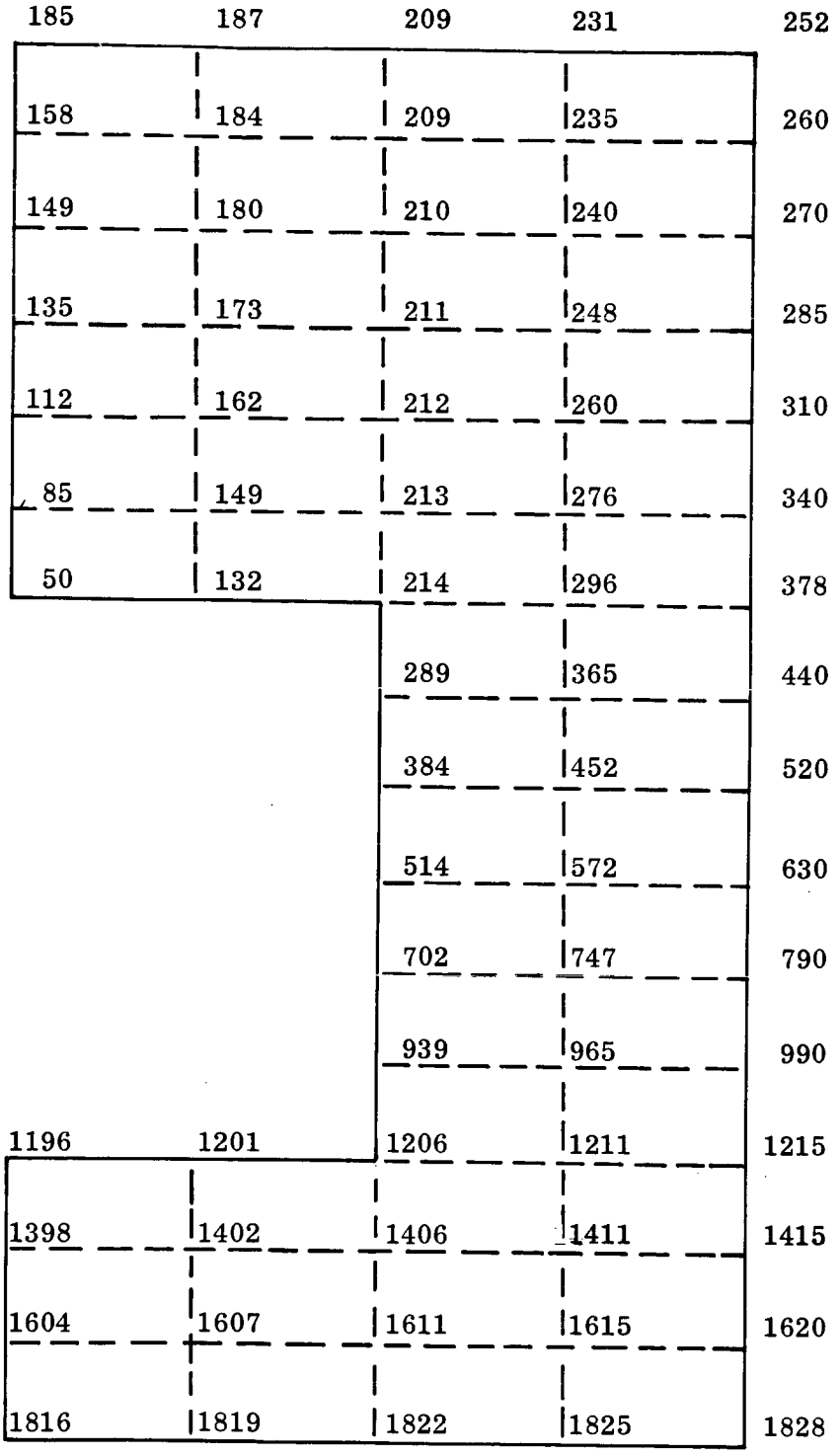

Figure 36. Temperature Distribution (°F) Used in Stress Analysis (Thermal Node 6)

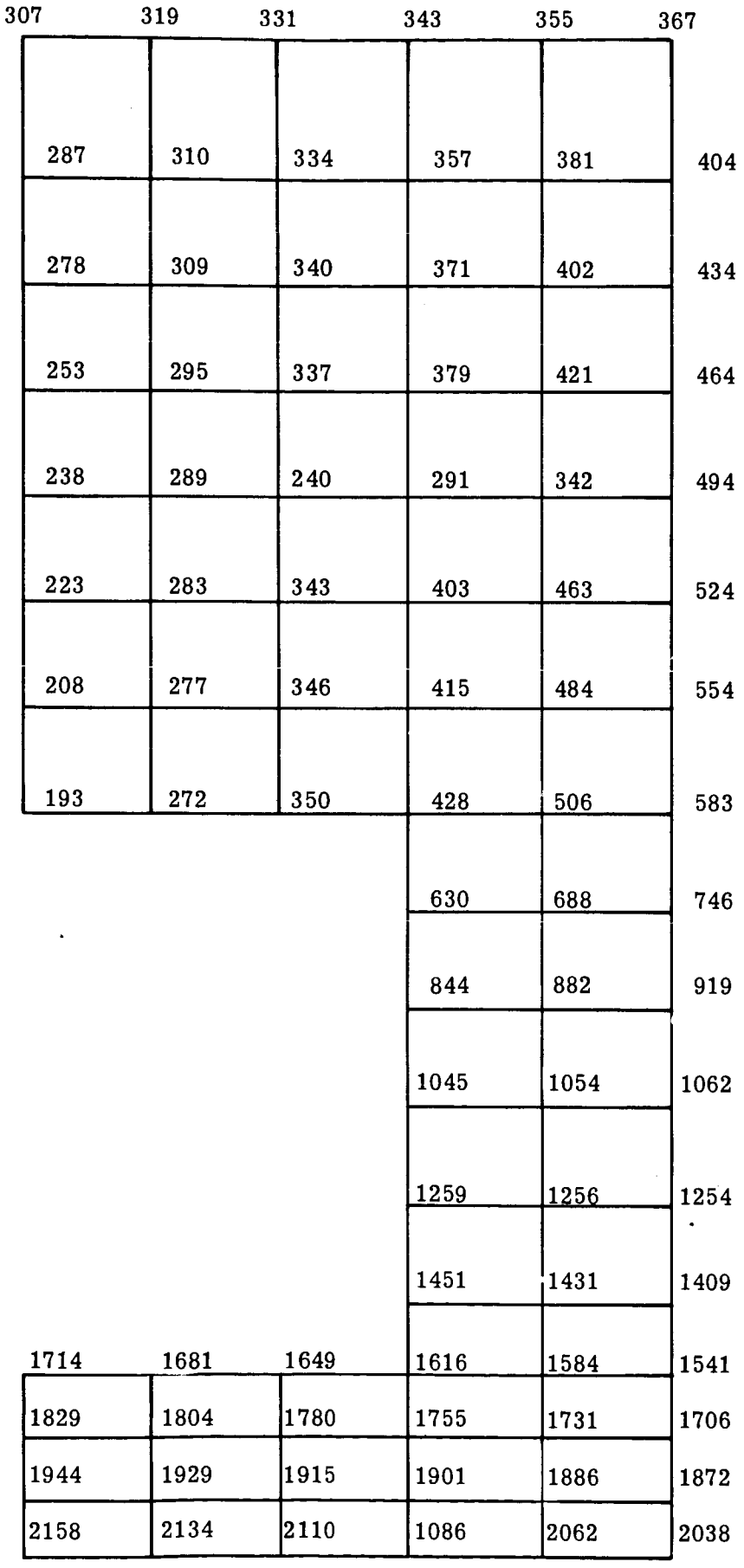

Figure 37. Temperature Distribution Used in the Stress Analysis Thermal Node No. 8

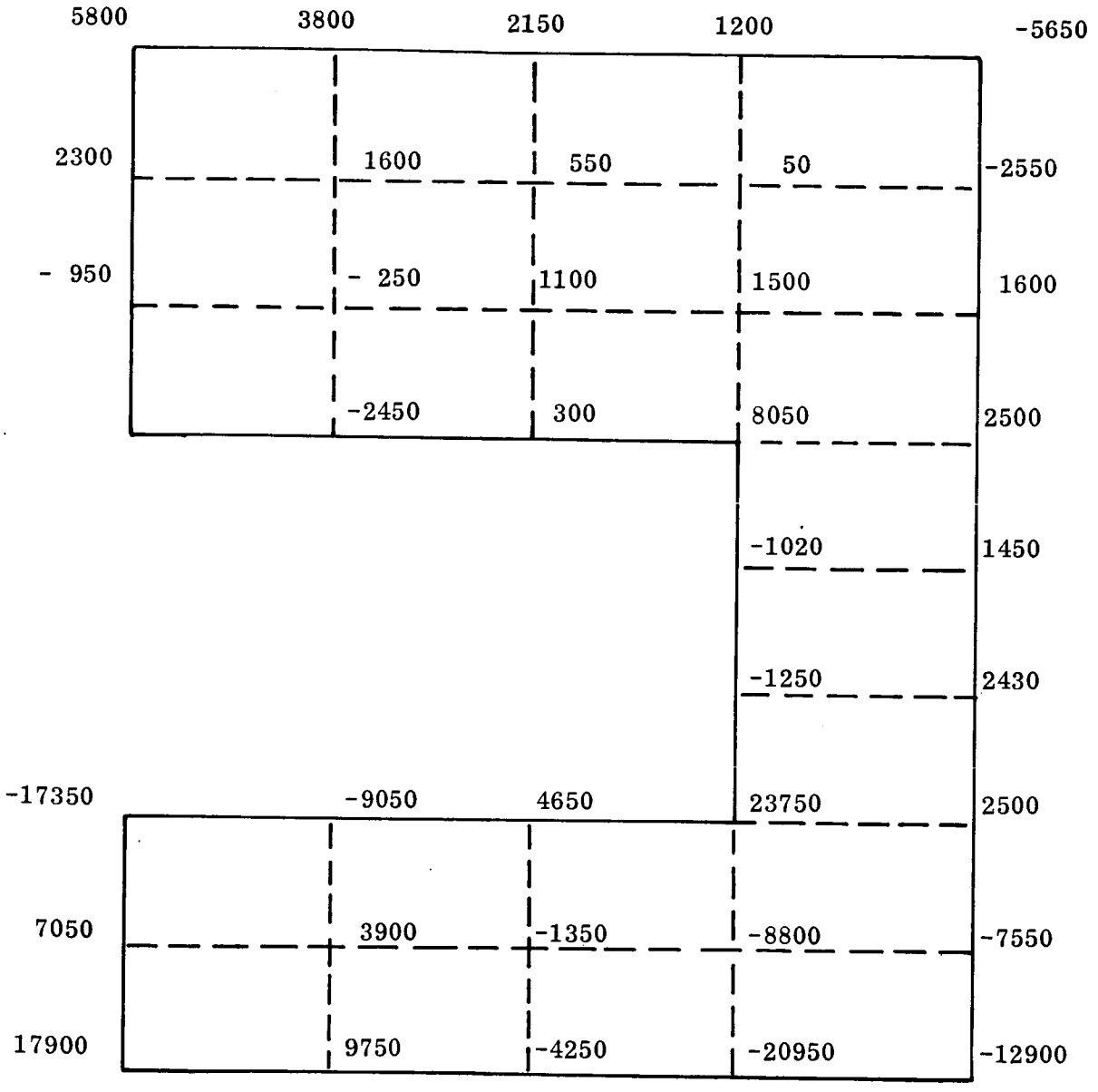

Figure 38. Tangential Pressure Stresses from Initial Existing Stress Analysis

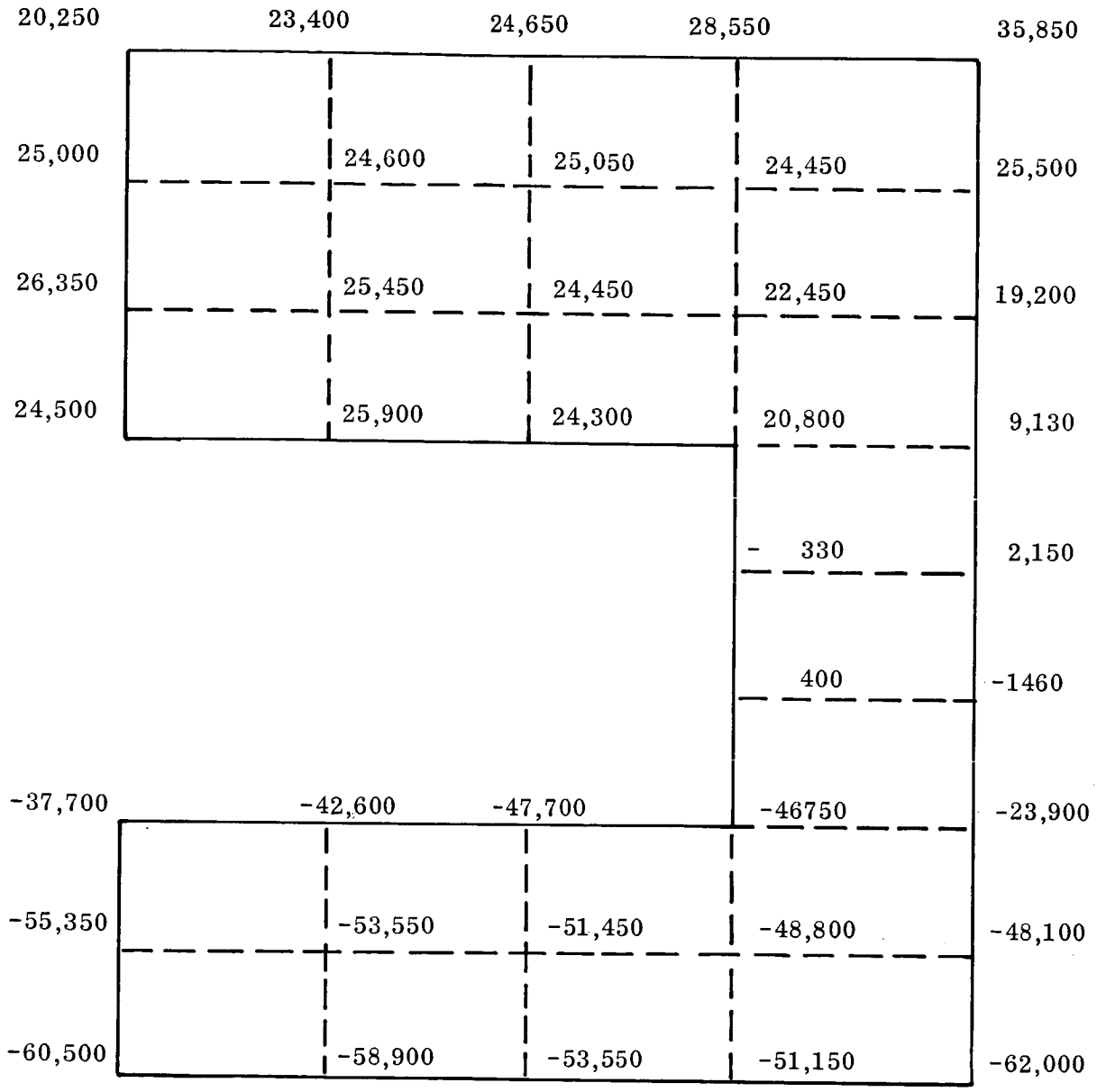

Figure 39. Tangential Thermal Stresses from Intial Elastic Stress Analysis

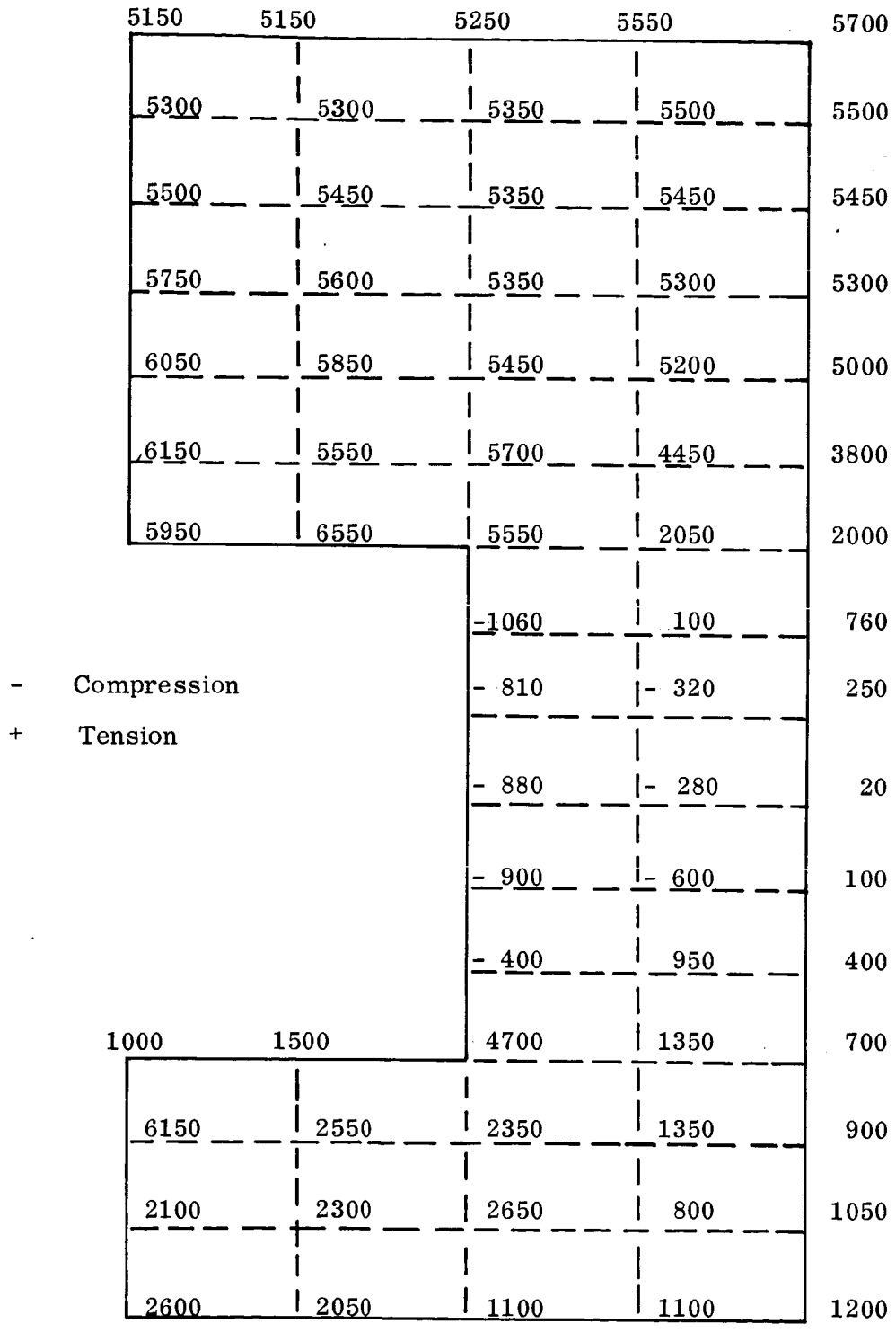

Figure 40. Tangential Pressure Stresses from Initial Elastic Stress Analysis (Thermal Node 6)

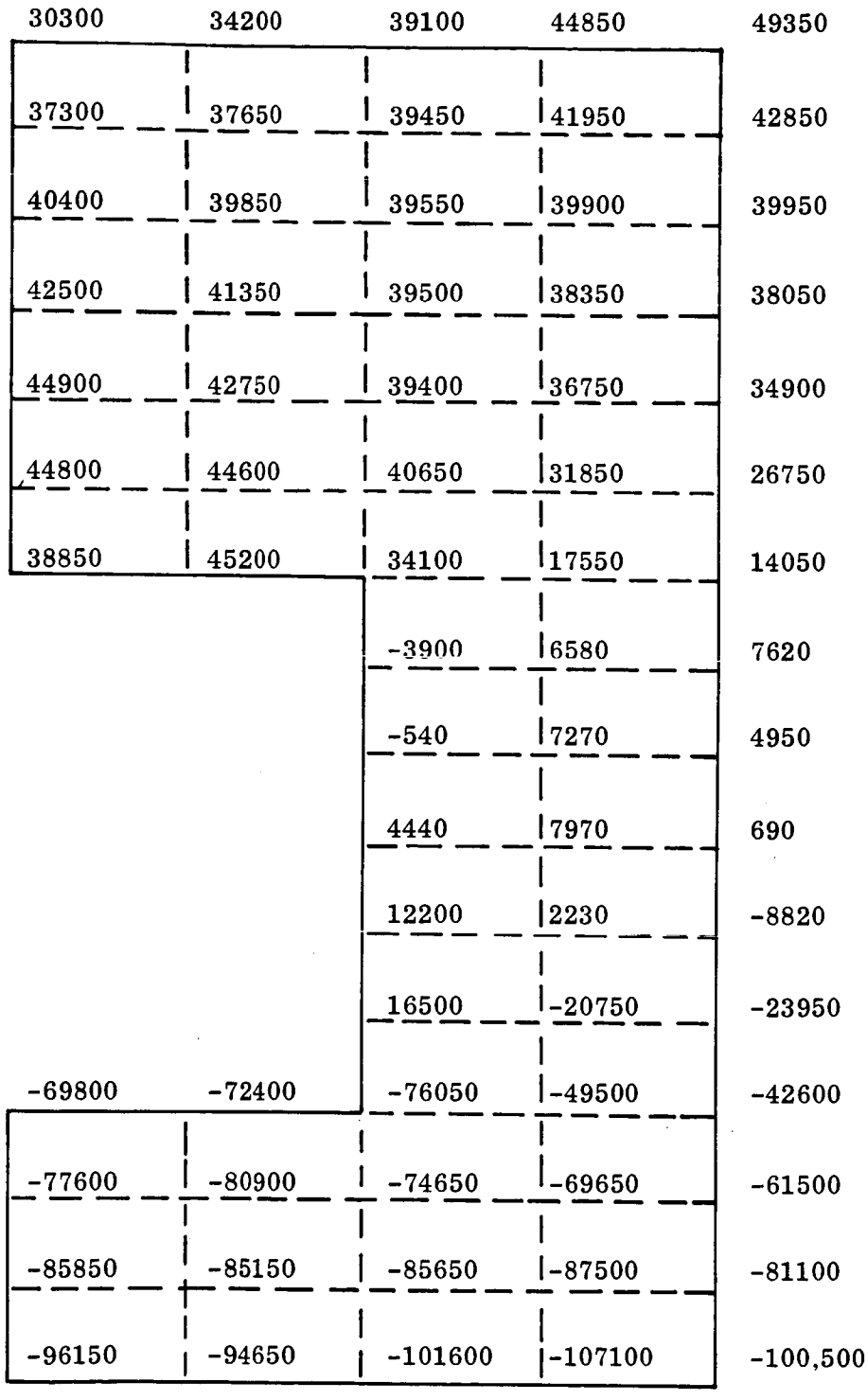

Figure 41. Tangential Thermal Stresses from Initial Elastic Stress Analysis (Thermal Node 6)

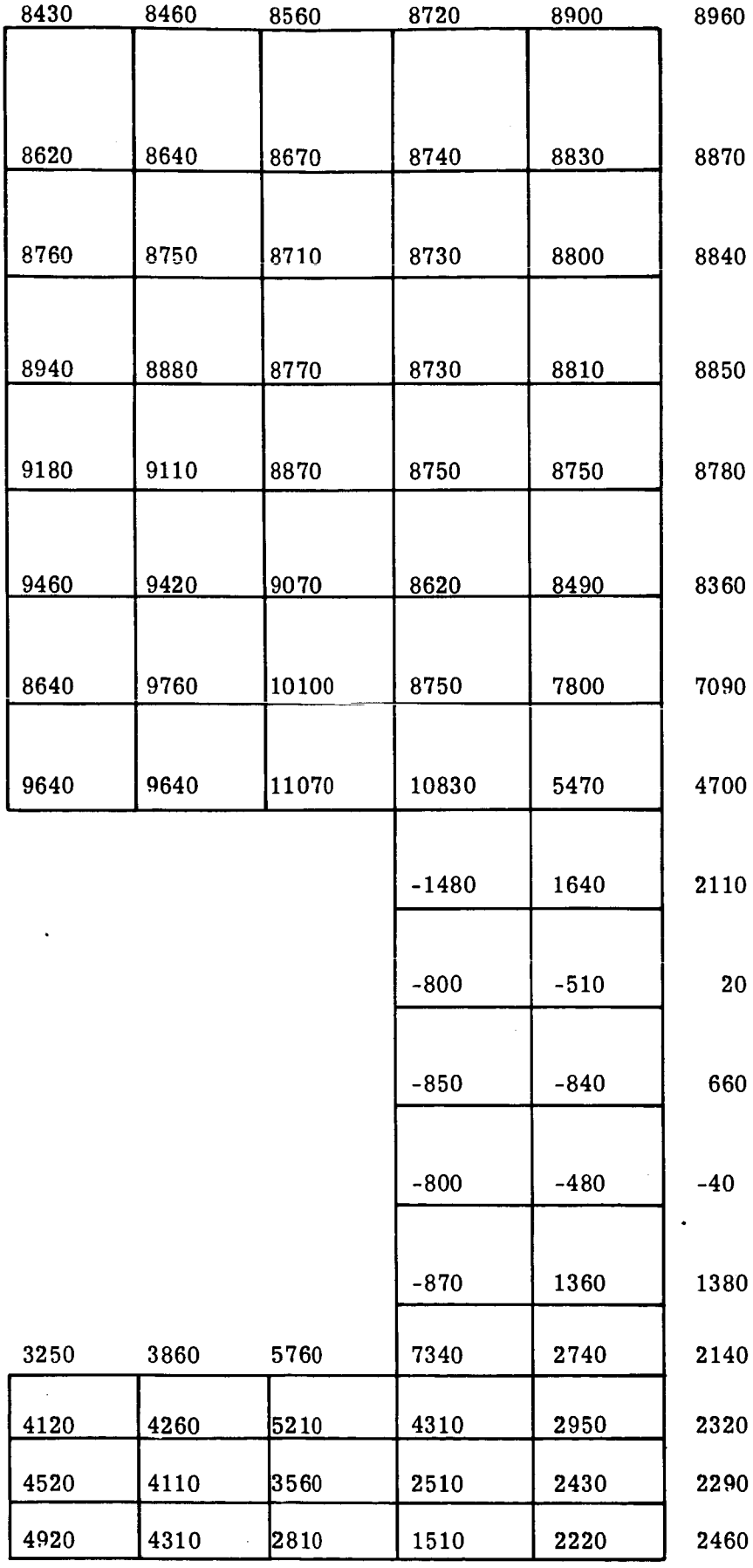

Figure 42. Tangential Pressure Stresses from Initial Elastic Stress Analysis Thermal Node No. 8

25190	29160	34880	40790	47780	52570
35750	35420	35650	36880	38150	38480
37560	36620	34460	32860	32690	33090
41620	41310	33160	31140	28100	34100
41190	40320	53320	50840	47730	30340
39180	38450	29730	27710	23830	29190
32100	30530	29350	28150	24890	24000
13440	19340	28760	28450	28410	30110
			-3250	8860	15150
			-620	1820	5250
			680	4430	5690
			2160	-5600	-18160
			8240	-44090	-57590
-179310	-182810	-190510	-155270	-96830	-92710
-163080	-164750	-170570	-158160	-124960	-114800
-143180	-126520	-140100	-139380	-133820	-126180
-137230	-143070	-133350	-144840	-152380	-144650

Figure 43. Tangential Thermal Stresses from Initial Elastic Stress Analysis Thermal Node No. 8

TABLE 14

TOTAL STRAINS ASSOCIATED WITH STRESSES OF FIGURES 38 AND 39 (THERMAL NODE 3)

Node	Temp (°F)	Total Strain x 10^{-6} in./in.	Node	Temp (°F)	Total Strain x 10^{-6} in./in.
1	-172	843	103	-70	828
3	-178	886	105	-67	842
5	-184	881	107	-63	850
7	-190	858	109	-59	857
9	-196	820	111	-55	853
11	-202	758	113	-51	826
13	-209	645	121	-54	782
21	-152	886	123	-49	812
23	-156	883	125	-44	824
25	-160	873	127	-38	830
27	-164	853	129	-32	859
29	-168	812	131	-26	934
31	-172	756	133	-20	913
33	-176	698	141	-35	807
41	-131	904	143	-28	816
43	-133	882	145	-21	808
45	-135	863	147	-13	791
47	-137	842	149	- 5	796
49	-139	813	151	3	856
51	-141	775	153	11	958
53	-144	714	161	-15	901
61	-112	889	163	- 6	848
63	-112	871	165	3	803
65	-112	856	167	13	769

TABLE 14 (CONT)

Node	Temp (°F)	Total Strain x 10^{-6} in./in.	Node	Temp (°F)	Total Strain x 10^{-6} in./in.
67	-112	840	169	23	743
69	-113	824	171	33	700
71	-113	797	173	43	490
73	-113	767	181	6	1000
81	- 93	853	183	17	856
83	- 92	856	185	28	797
85	- 90	851	187	40	757
87	- 88	846	189	52	710
89	- 86	837	191	64	630
91	- 84	820	193	76	388
93	- 82	797	197	31	- 78.0
101	- 73	846			
199	60	543	278	397	-2272
201	88	- 37.8	280	444	-2780
205	65	73.0	282	491	-3416
207	87	109	284	537	-4060
209	108	230	289	434	-2609
213	105	- 60.1	291	480	-2957
215	119	56.6	293	527	-3321
217	133	149	295	574	-3729
221	160	- 47.2	300	472	-2933
223	163	34.4	302	519	-3091
225	165	53.9	304	565	-3252
229	220	- 2.27	306	611	-3435
231	210	- 50.3	311	509	-3228
233	200	-184	313	555	-3196

TABLE 14 (CONT)

Node	Temp (°F)	x 10^{-6} in./in.	Node	Temp (°F)	Total Strain x 10^{-6} in./in.
237	286	- 82.8	315	602	-3224
239	262	- 409	317	648	-3255
241	238	- 614	322	546	-3465
245	359	-1402	324	593	-3341
247	320	-1190	326	639	-3215
249	280	-1230	328	685	-3117
251	328	-2199	333	586	-3594
253	375	-3330	335	632	-3447
255	422	-4539	337	678	-3200
260	367	-2299	339	724	-3045
262	414	-3455	344	625	-3646
*264	461	-4592	346	671	-3523
269	406	-2617	348	717	-3308
271	453	-3512	350	763	-2958
273	500	-4506			

* The maximum strain occurs at Node 264

$$\epsilon_{max} = 4592 \times 10^{-6} \text{ in./in.}$$

From Coffin's equation relating number of cycles to failure and strain we have:

$$N_f^{0.2948} = \frac{0.0911}{\Delta \epsilon_p} = \frac{0.0911}{0.00217} = 42$$

$$N_f = 320{,}700 \text{ cycles}$$

For Design and Operating Use $N_{CAPAB} = 32{,}000$ cycles

TABLE 15

TOTAL STRAINS ASSOCIATED
WITH STRESSES OF FIGURES 40 AND 41 (THERMAL NODE 6)

Node	Temp (°F)	Total Strain x 10^{-6} in./in.	Node	Temp (°F)	Total Strain x 10^{-6} in./in.
1	185	1194	85	50	1474
3	187	1325	87	132	1725
5	209	1498	89	214	1325
7	231	1714	91	296	670
9	252	1879	93	378	561
15	158	1430	97	289	-285
17	184	1446	99	365	393
19	209	1514	101	440	511
21	235	1614	105	384	-80
23	260	1650	107	452	424
29	149	1535	109	520	325
31	180	1525	113	514	223
33	210	1517	115	572	493
35	240	1543	117	630	46
37	270	1555	121	702	769
43	135	1608	123	747	228
45	173	1576	125	790	-614
47	211	1515	129	939	1220
49	248	1490	131	965	-1523
51	285	1485	133	990	-1854
57	112	1693	137	1196	-6035
59	162	1625	139	1201	-6219
61	212	1515	141	1206	-6323
63	260	1432	143	1211	-4261

TABLE 15 (CONT)

Node	Temp (°F)	Total Strain x 10^{-6} in./in.	Node	Temp (°F)	Total Strain x 10^{-6} in./in.
65	310	1376	145	1215	-3708
71	85	1687	151	1398	-7374
73	149	1711	153	1402	-7607
75	213	1566	155	1406	-7019
77	276	1243	157	1411	-6696
79	340	1061	179	1816	-9546
159	1415	-5941	181	1819	-9546
165	1604	-8816	183	1822	-10458
167	1607	-8721	*185	1825	-11042
169	1611	-8737	187	1828	-10344
171	1615	-9084			
173	1620	-8426			

*The maximum strain occurs at Node 185

$$\epsilon_{max} = -11042 \times 10^{-6} \text{ in./in.}$$

From Coffin's equation relating number of cycles to failure and strain we have:

$$N_f^{0.2948} = \frac{0.0911}{\epsilon_p} = \frac{0.0911}{0.00934}$$

$$N_f = 2280 \text{ cycles}$$

For design and operating use $N_{CAPAB} = 228$ cycles

TABLE 16

TABLE OF TOTAL STRAINS ASSOCIATED WITH THE THERMAL AND PRESSURE STRESSES
(THERMAL NODE 8)

Node	Temp (°F)	Stress psi	Strain in./in.	Node	Temp (°F)	Stress psi	Strain in./in.
1	307	33620	0.00111	103	208	41740	0.00136
3	319	37620	0.00124	105	277	40290	0.00133
5	331	43440	0.00144	107	346	39450	0.00131
7	343	49510	0.00165	109	415	36900	0.00123
9	355	56680	0.00189	111	484	32690	0.00110
11	367	61530	0.00205	113	554	31090	0.00106
18	287	44370	0.00142	120	193	23080	0.00075
20	310	44060	0.00145	122	272	28980	0.00095
22	334	44320	0.00147	124	350	39830	0.00132
24	357	45620	0.00152	126	428	39280	0.00131
26	381	46980	0.00157	128	506	33880	0.00115
28	404	47350	0.00158	130	583	34810	0.00119
35	278	46320	0.00152	134	630	-4730	-0.00016
37	309	45370	0.00150	136	688	10500	0.00037
39	340	43170	0.00143	138	746	17260	0.00061
41	371	41590	0.00139	142	844	-1420	-0.00005
43	402	41490	0.00138	144	882	1310	0.00005
45	434	41930	0.00140	146	919	5270	0.00019
52	253	50560	0.00166	150	1045	170	-0.00001
54	295	50190	0.00166	152	1054	3590	0.00014
56	337	41930	0.00139	154	1062	5030	0.00019
58	379	39870	0.00133	158	1259	1360	0.00006
60	421	36910	0.00123	160	1256	-6080	-0.00025
62	464	42950	0.00144	162	1254	-18200	-0.00075
69	238	50370	0.00165	166	1451	7370	0.00035
71	289	49430	0.00163	168	1431	-42730	-0.00197

TABLE 16 (CONT)

Node	Temp (°F)	Stress psi	Strain in./in.	Node	Temp (°F)	Stress psi	Strain in./in.
73	240	62190	0.00204	170	1409	-56210	-0.00256
75	291	59590	0.00196	174	1714	-176060	-0.01334
77	342	56480	0.00187	176	1681	-178950	-0.01278
79	494	39120	0.00132	178	1649	-184750	-0.01257
86	223	48640	0.00160	180	1616	-147930	-0.00942
88	283	47870	0.00158	182	1584	-94090	-0.00570
90	343	38800	0.00129	184	1541	-90570	-0.00503
92	403	36330	0.00121	191	1829	-158960	-0.01445
94	463	32320	0.00109	193	1804	-160490	-0.01408
96	524	37550	0.00127	195	1780	-165360	-0.01378
197	1755	-153850	-0.01241				
199	1731	-122010	-0.00953				
201	1706	-112480	-0.00839				
208	1944	-138660	-0.01475				
210	1929	-122410	-0.01275				
212	1915	-136540	-0.01408				
214	1901	-136870	-0.01369				
216	1886	-131390	-0.00993				
218	1872	-123890	-0.01191				
225	2158	-132310	-0.01813				
227	2134	-138760	-0.01850				
229	2110	-130540	-0.01695				
231	2086	-143330	-0.01814				
233	2062	-150160	-0.01854 *				
235	2038	-142190	-0.01693				

* Maximum Strain

Cyclic life - by a modified Coffin Equation

Temp = 2062°F

Reduction in area RA = 10%

$$\epsilon_{el} + \epsilon_p = \frac{G}{E} N_f^{\gamma} + MN_f^{z}$$

The elastic strain is small compared to the plastic strain.

$$\epsilon_p = MN_f^{z}$$

$$M = 0.827\ D \left[1 - 82 \left(\frac{\sigma_u}{E}\right)\left(\frac{\sigma_f}{\sigma_u}\right)^{0.179}\right]^{-1/3}$$

$$Z = -0.52 - 1/4 \log D + 1/3 \log \left[1 - 82 \left(\frac{\sigma_u}{E}\right)\left(\frac{\sigma_f}{\sigma_u}\right)^{0.179}\right]$$

$$D = -\ln\ (1 - RA) = \ln\ (9) = 0.1054$$

$$Z = -0.52 - 1/4 \log (0.1054) + 1/3 \log \left[1 - 82\left(\frac{12 \times 10^3}{8.1 \times 10^6}\right)\left(\frac{10}{9}\right)^{0.179}\right]$$

$$Z = -0.2948$$

$$M = 0.827\ (0.1054) \left[1 - 82\left(\frac{12 \times 10^3}{8.1 \times 10^6}\right)\left(\frac{10}{9}\right)^{0.179}\right]^{-1/3}$$

$$M = 0.0911$$

$$0.017 = 0.0911\ N^{-0.2948}$$

$$N = 297 \text{ Cycles}$$

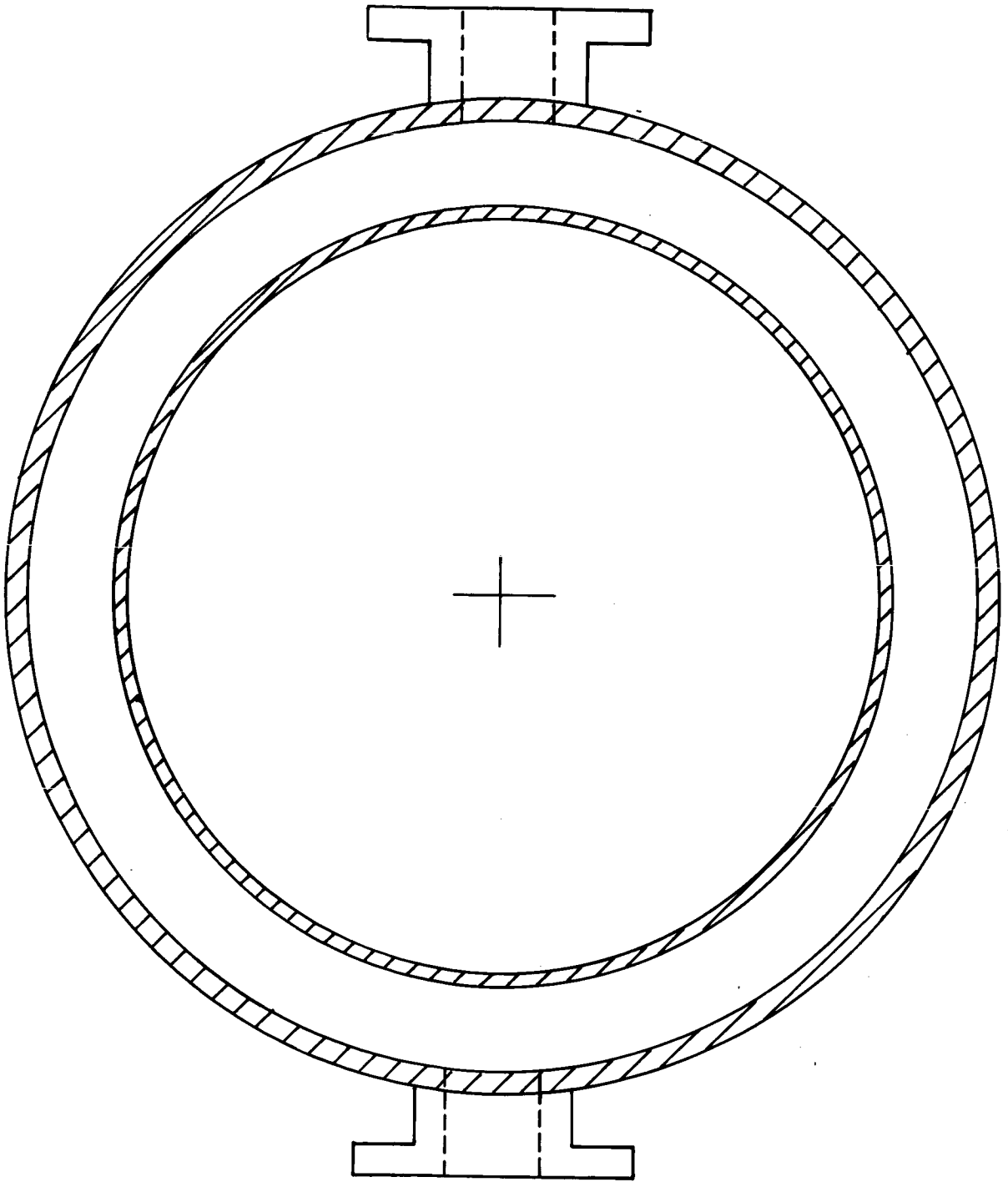

Figure 44. Longitudinal View of a Typical Manifold Configuration

The loading environment and discontinuity loads were considered as:

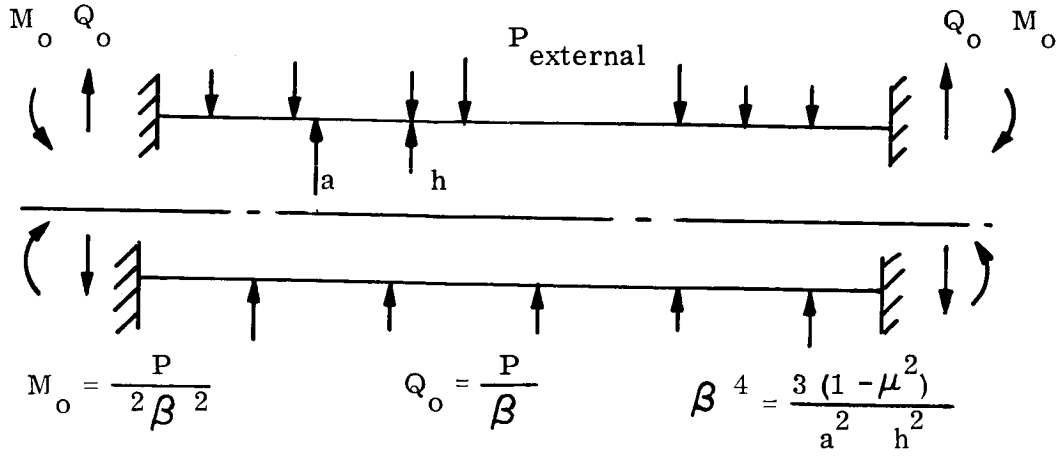

where

$$M_o = \frac{P}{2\beta^2} \qquad Q_o = \frac{P}{\beta} \qquad \beta^4 = \frac{3(1-\mu^2)}{a^2 h^2}$$

The β term is defined from a calculated equivalent thin shell based on the typical channel configuration.

Figure 45 depicts the corresponding inner shell contours and pressures at the inlet and outlet manifold locations. Once the applied moment distribution was established, the built-in design configuration was determined based on the tensile properties of the electro-deposited nickel (Figure 25). For the inlet manifold the required rib height to sustain the imposed loads, (see Figure 50), was 0.55 in. , for the outlet the required height was 0.40 in.

For the inlet manifold the outer structural contour was analyzed as a continuous arc. The method of analysis is given in Reference (3). The arc was symmetric therefore only one-half of the structure was necessary for the analysis. The equivalent load structure was:

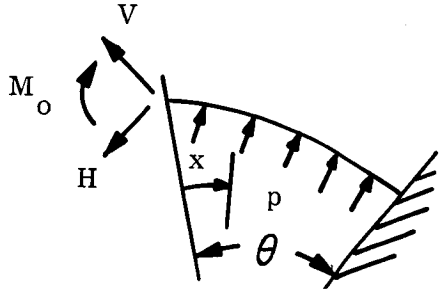

The governing equations were:

Moment: $M = M_o + HR\left[\sin(\theta - X) - \sin\theta\right] + VR\left[\cos(\theta - X) - \cos\theta\right] + pR^2(1-\cos X)$

Vertical Deflection $= \frac{1}{E1}\left[M_o R^2(\sin\theta - \theta\cos\theta) + VR^3\left(\frac{1}{2}\theta + \theta\cos^2\theta - \frac{3}{2}\sin\theta\cos\theta\right) + HR^3\left(\frac{1}{2} - \cos\theta + \theta\sin\theta\cos\theta + \frac{1}{2}\cos^2\theta - \sin^2\theta\right) + pR^4\left(\sin\theta + \sin\theta\cos\theta - \frac{3}{2}\theta\cos\theta - \frac{1}{2}\sin^3\theta - \frac{1}{2}\sin\theta\cos^2\theta\right)\right.$

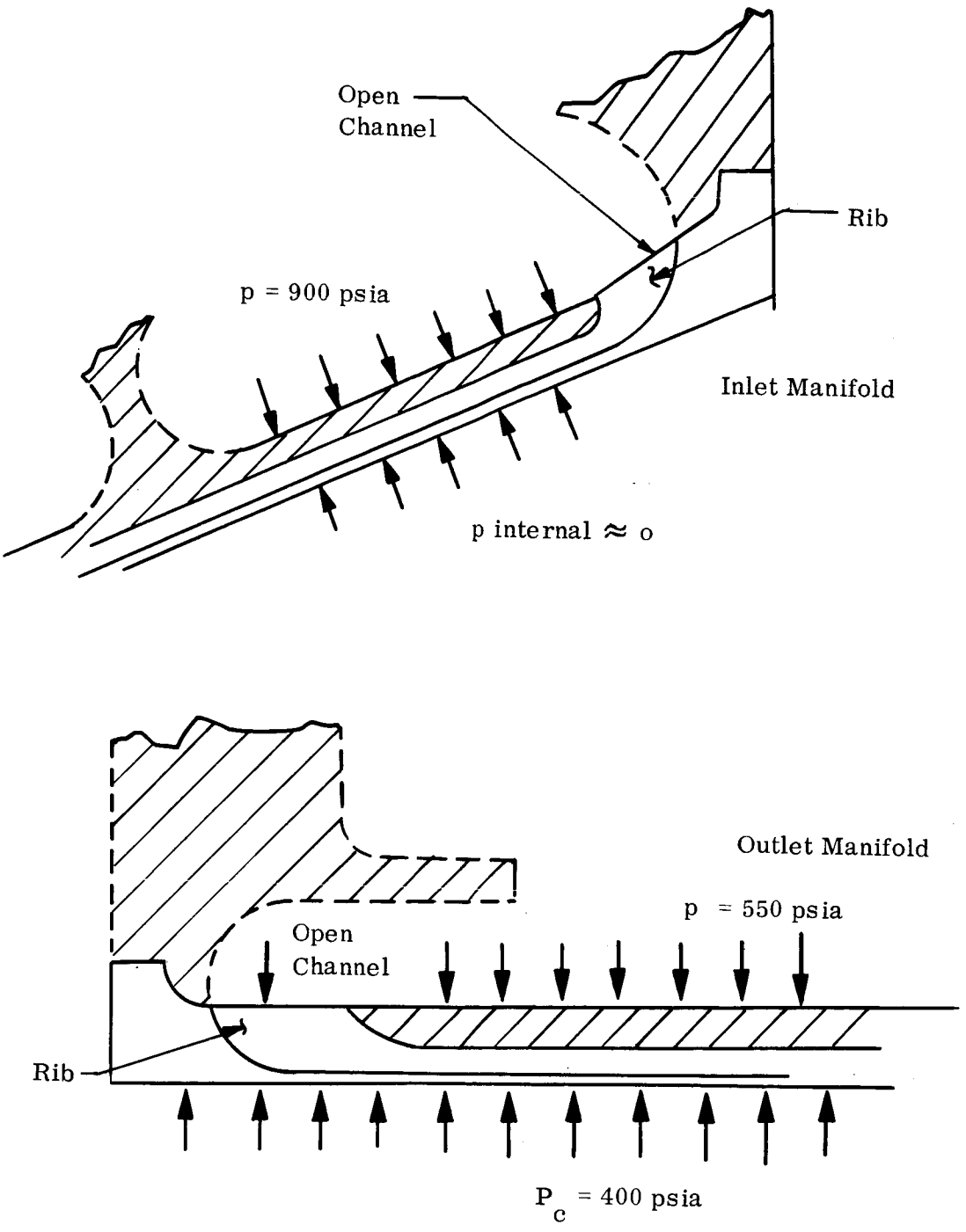

Figure 45. Inner Shell Contours and Pressures at Inlet and Outlet Manifold Locations

$$\text{Horizontal Deflection} = \frac{1}{EI}\left[M_o R^2 (1 - \theta \sin\theta - \cos\theta) + VR^3 \left(\frac{1}{2} - \cos\theta + \theta \sin\theta \cos\theta + \frac{1}{2}\cos^2\theta - \sin^2\theta\right) + HR^3 (-2\sin\theta + \theta \sin^2\theta + \frac{1}{2}\theta + \frac{3}{2}\sin\theta\cos\theta) + pR^4 \left(\frac{1-3}{2}\theta \sin\theta + \sin^2\theta - \cos\theta\right)\right]$$

$$\text{Rotation} = \frac{1}{EI}\left[M_o R\theta + VR^2 (\sin\theta - \theta\cos\theta) + HR^2 (1 - 0\ \sin\theta - \cos\theta) + pR^3 (\theta - \sin\theta)\right]$$

Because of symmetry the boundary conditions are:

(1) Vertical shear at midspan = 0

(2) Rotation at midspan = 0

(3) Horizontal deflection at midspan = 0

Solving the above equations for the three unknowns (M_o, H and V) constitutes a solution for the built-in arc structure. Then utilizing this method and the strength properties of Figure 25, the required thickness was established as 0.130 in.

The outer shall structure of the outlet manifold is similar to that of the inlet except that a thin cylindrical shell-to-arc joint is utilized in place of one of the built-in edges. This results in a less severe loading environment in the arc, therefore the same arc thickness (0.130 in.) was used. The juncture of the thin cylindrical shell to injector flange was analyzed similarly to that used in the analysis of the inner structural shell. The required thickness for this shell was calculated to be 0.11 in.

The above results were used to determine the critical design thicknesses of the manifold configurations based on the steady-state operating temperatures and pressures. These analyses all utilized an elastic solution with appropriate factors of safety to establish that the critical stress mode was that of the thermal stress condition. This latter criterion was discussed in a previous section.

D. DYNAMIC - STABILITY ANALYSIS IN DIVERGENT SECTION (OPERATING AND AMBIENT CONDITIONS)

A stress analysis was conducted on the divergent section of the regeneratively cooled thrust chamber at operating conditions to define the ultimate loading factor for a lateral vibration environment. The total load occurring in this section is the result of:

(1) Thrust load

(2) Moment due to lateral vibration

A schematic of the loading is:

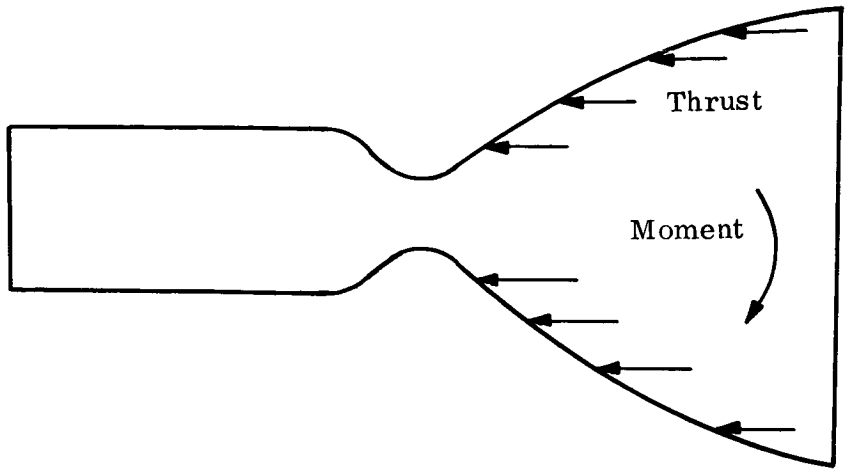

The thrust load distribution was determined from the integration of the internal pressure over the longitudinal projection of the divergent area (See Figure 46).

It was ascertained that the critical stress mode was compressive yielding in the electro-deposited nickel outer shell. It was also assumed that the compressive and tensile yield strength for the nickel were identical, therefore the strength curve of Figure 25 was utilized in determining yield versus temperature. The method of analysis was:

$$\text{Margin of Safety} = \frac{\sigma_{cy}}{\sigma_{thrust} + M} - 1 = 0$$

σ_{cy} compressive yield strength at temperature

σ_{thrust} compressive stress due to thrust

σ_{M} bending moment stress

solving the above margin of safety equation for σ_M determines the maximum allowable bending system. Once σ_M was calculated the allowable moment was determined from:

$$M = \sigma_M \frac{I}{C} = \frac{(d^2 + d_1^2)\ tR}{4\ d}$$

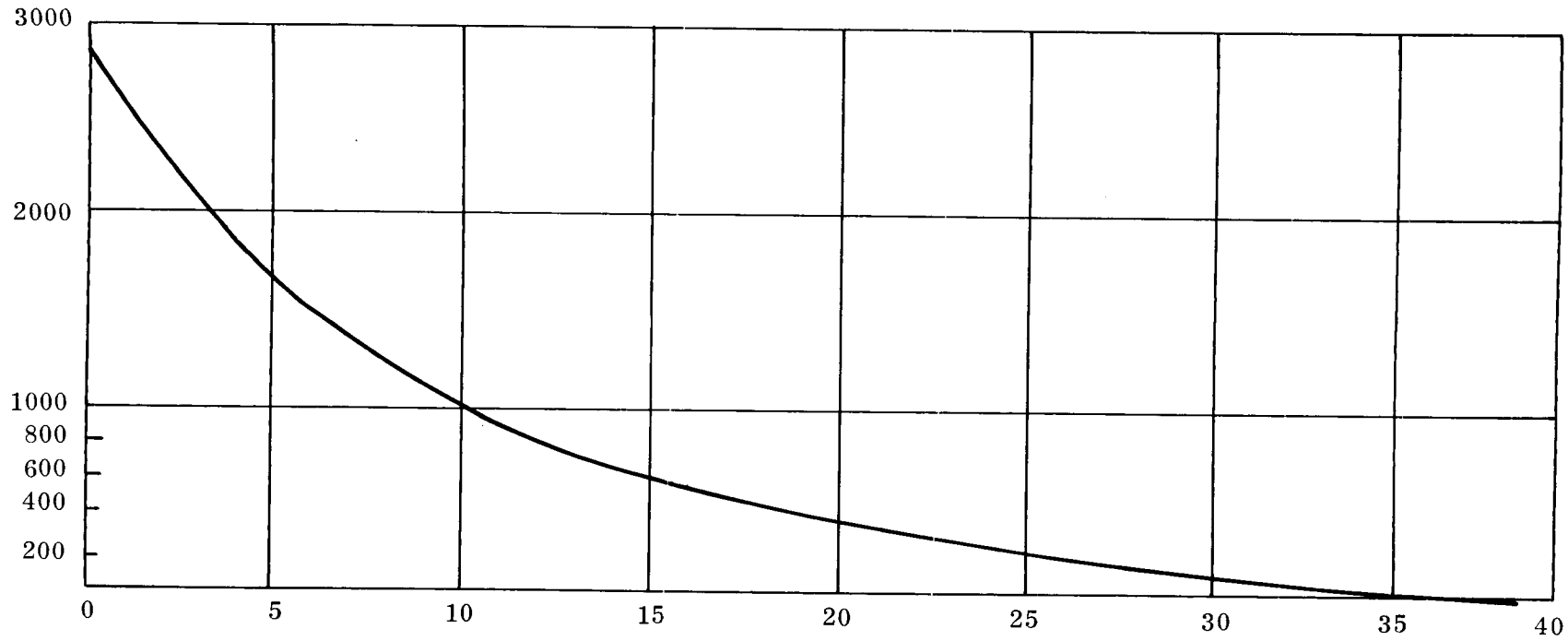

Figure 46. Accumulated Thrust versus Longitudinal Distance

d ~ outer diameter

d_1 ~ inner diameter

R ~ mean radius

t ~ thickness

M ~ allowable moment

C = distance from neutral axis to extreme fiber

The ultimate loading factor is then given by:

$$ULF = \frac{M}{(1.25 \times 1.25)\ (W)\ (e)}$$

(1.25 x 1.25) Ultimate factor of safety

W ~ Weight of divergent section and radiation nozzle

e ~ Moment arm to centroid of above

The resulting minimum loading factor for the thrust chamber occurred in the throat area because of the minimum cross-sectional geometry and relatively large bending moment. This minimum value was calculated to be ULF = 11 g with the elevated operating temperatures. General stability was not critical because of the high modulus of elasticity for the outer nickel shell, the critical buckling stress being about 300,000 psi.

For the stress analysis of the divergent section for ambient lateral vibrational conditions, the method described previously was used with the exception that there is no thrust loading.

Since the outer nickel shall has a higher modulus of elasticity than the inner TD nickel liner, only the outer shall was assumed in carrying this load. In actuality some portion of the load will be carried by the inner liner so the resulting load factor is on the conservative side.

Again, the critical region was the throat area because of the geometry and large moment. The derived ultimate loading factor was ULF = 14 g based on the tension yield of the electro-deposited nickel.

It should be noted that the circumferential weld in the inner TD nickel liner was not critical because the analysis utilized primarily the outer nickel cover as the critical structure.

E. STRESS ANALYSIS OF RADIATION NOZZLE.

In the stress analysis of the radiation nozzle a general stability criteria was utilized based on the thrust loading and lateral vibration condition. This distribution of the accumulated thrust in the divergent section of the thrust chamber is shown in Figure 46. The ultimate loading factor for lateral vibration was established as 11g from the dynamic capability analysis of the throat area.

The material selected was a columbium alloy, SCb-291 which exhibits good strength and stability characteristics for the operating temperature range of the nozzle. Figure 47 shows the variation of the modulus of elasticity versus temperature for the SCb-291 material. The expected maximum operating temperature distribution in the nozzle is shown in Figure 48.

The method of analysis used is given in References 4, 5 and 6. The stabilizing effect of internal pressure on the buckling strength of the nozzle extension is accounted for by an increase in the buckling coefficient. Theoretical studies show that the effect of internal pressure on the buckling of thin walled circular cylinders under axial compression depends on the dimensionless parameter $\bar{p} = \frac{P}{E}\left(\frac{R}{t}\right)^2$ where p is the internal pressure, E the modulus of elasticity, R the cylinder radius, and t the wall thickness of the cylinder. For a cone, the radius of curvature is equal to $R/\cos\alpha$, where α is the semivertex angle of the cone. The net buckling coefficient has been calculated from the equations for cylindrical shells. Experimental data shows that cones have a higher buckling coefficient than cylinders, making this analysis quite conservative. The critical load for a cone or cylinder under axial compression may be determined from the following equation (Reference 1):

$$P_{cr} = 2 \times CEt^2 \cos^2 \alpha$$

Where:

C = buckling coefficient

E = modulus of elasticity

t = shell wall thickness

α = semivertex angle of cone

The effect of cone length on the critical load is only vaguely known at this time, and is ignored as a parameter. Experimental data shows the buckling coefficient for cylinders under axial compression is lower than that for a cone, and is determined from the following equation (Reference 1):

$$C_c = 0.606 - 0.546 \quad 1\text{-}e^{-\frac{1}{16}\sqrt{\frac{R}{t \cos\theta}}}$$

The buckling coefficient correction factor for internal pressure is added to C_c to give a net effective buckling coefficient. A conservative design curve for the incremental

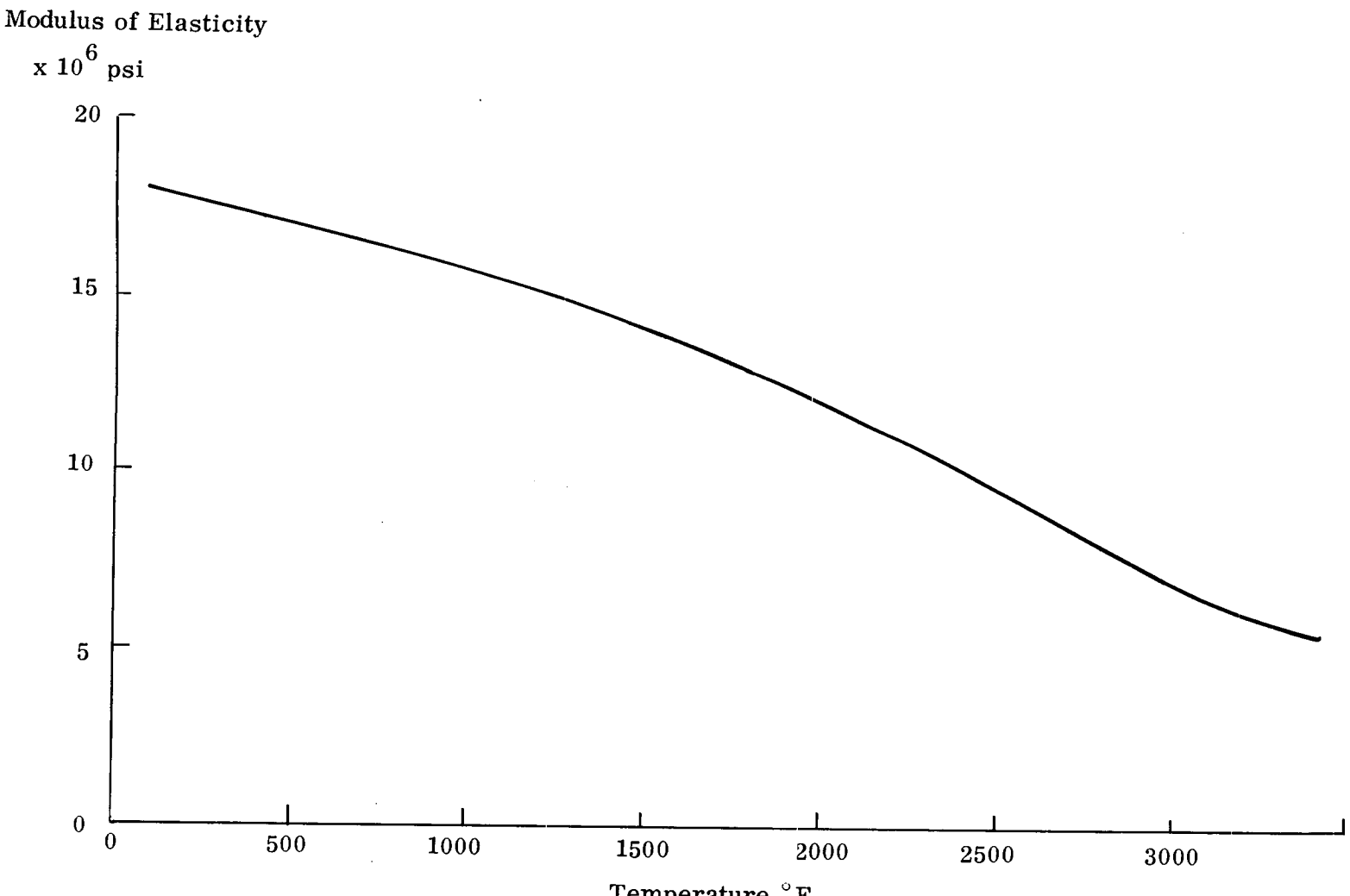

Figure 47. SCb - 291 Modulus of Elasticity versus Temperature

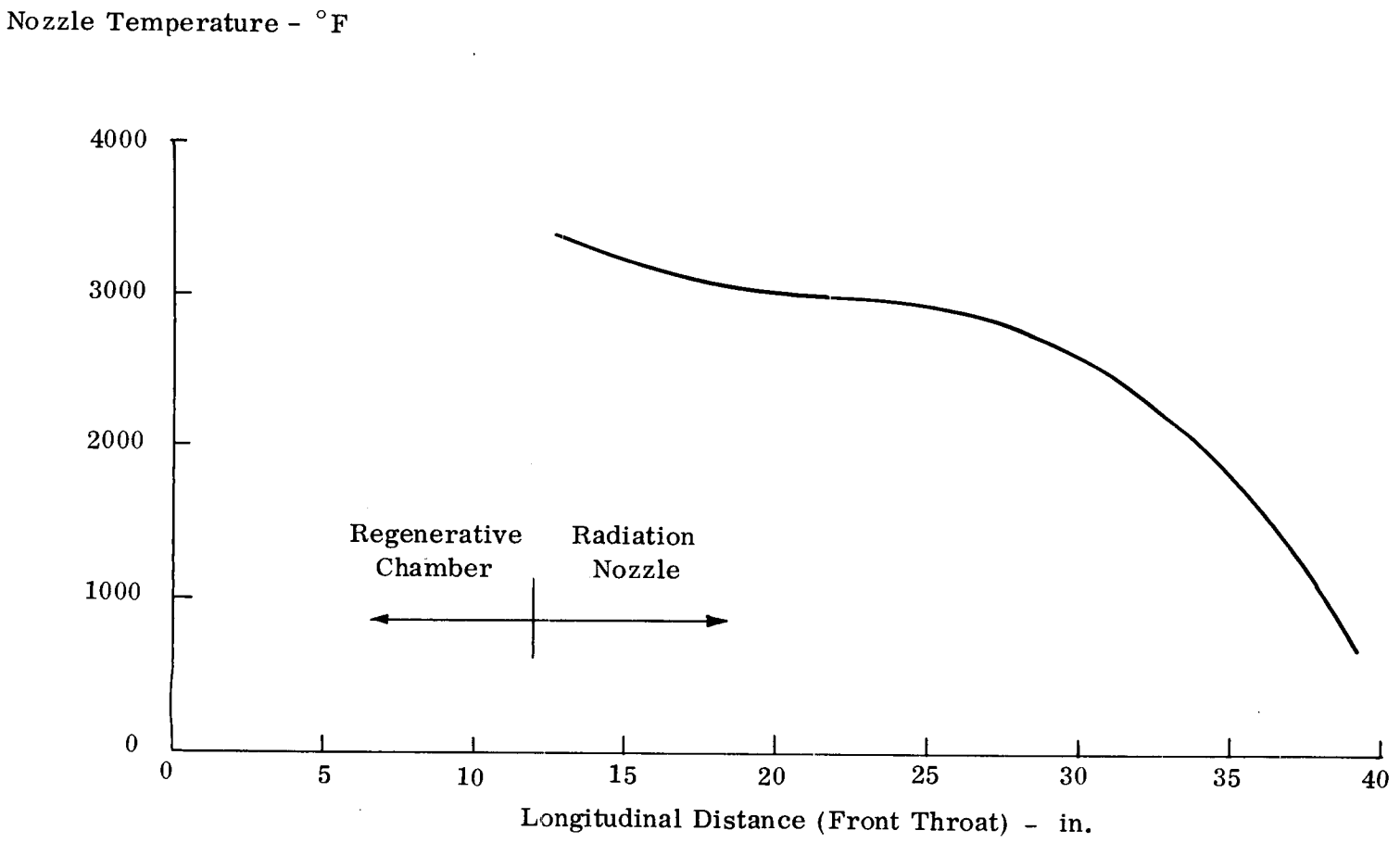

Figure 48. Nozzle Temperature versus Longitudinal Station

buckling stress due to pressure is given in (Reference 5). This buckling coefficient can be determined from the following equations:

$$C_p = 0.229 \quad \frac{\bar{p}}{1.2} \quad \text{for } 0 \ \bar{p} \ 1.2$$

$$C_p = 0.229 \quad \text{constant for } p \ 1.2$$

Where: $\bar{p} = \frac{P}{E} \left(\frac{R}{t \cos} \right)^2$ as defined above.

The critical elastic buckling load was determined at several stations in the shell by assuming that each station could be treated as an equivalent cylinder based on the local radius and slope.

The most critical station is where the attachment flange tapers to create a smooth transition with the nozzle shell. The analysis established a shell thickness of 0.030 in. at that transition point. Theoretically, the wall thickness could be gradually decreased as the nozzle increases in diameter due to decreasing temperatures and higher moment of inertia. The thickness of 0.030 in. was maintained for the entire nozzle, however, to facilitate fabrication and subsequent handling.

F. SUMMARY OF RESULTS

Based on the results of the previous analyses, the maximum operating environment for the regeneratively cooled thrust chamber is:

(1) Restart capability

N = 20 cycles

(2) Lateral vibrational loading factor

a. Operational
ULF = ±11 g

b. Ambient
ULF = ±14 g

The above summarizes the loading capabilities of the chamber for the steady-state loads and temperatures.

G. STRUCTURAL ANALYSIS COMPUTER PROGRAM

For the stress analysis of the channel cross-sectional structure a Bell Aerosystems General Purpose Computer Program for structural analysis was utilized (Reference 7). This program was developed by Bell Aerosystems to accommodate the analyst with a tool to handle complex structures with various loading conditions. The sub-routine used for the regenerative thrust chamber was a quadralateral thin shell element with thermal and pressure loading. The method of analysis employed is the discrete element stiffness technique based on the selection of specified displacement modes.

The shape of the general quadrilateral element is defined by the coordinates of the four corners and has a zero radius of curvature, i. e. ,

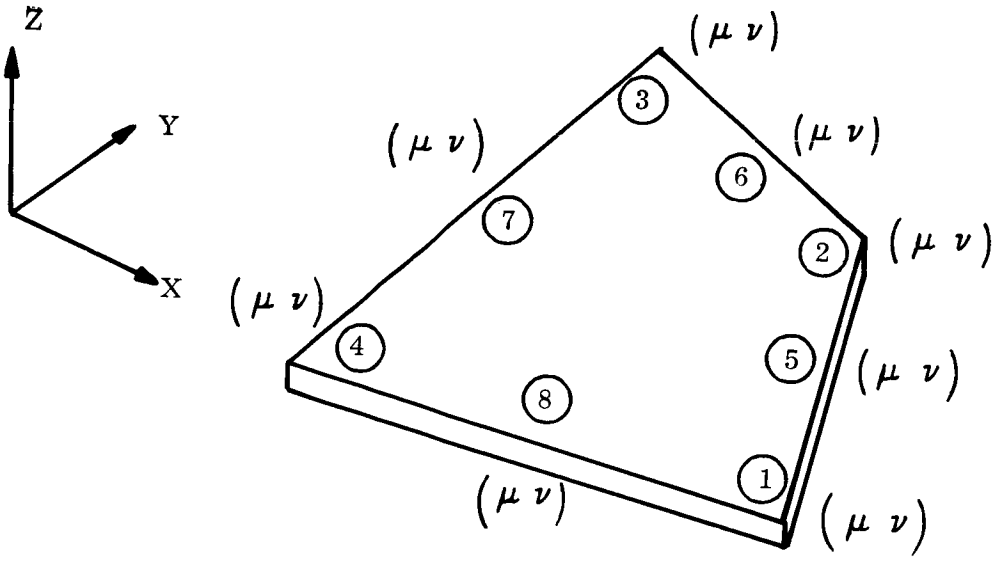

The plane of the element is determined by the first three corner point coordinates. For the analysis, only membrane action was considered because of the manner in which the channel structure was idealized.

Under normal circumstances, the four corner points and mid-side points participate in establishing continuous connection of the thin shell element with adjacent elements. An option is provided to suppress the mid-side nodes individually if associated complexities arise in grid refinement or non-standard connections with adjacent elements. Invoking this suppression option causes linear variation to be imposed on the specified mid-side variables. A linear generalized Hook's Law is employed for determination of the equations of state. Two options are provided, namely, conventional plane stress or strain.

The element formulation is discretized by the construction of node shapes. Membrane displacement within the subject element is approximated by quadratic polynominals. Transverse displacement is represented by cubic polynominals. A linear variation is provided for midplane and gradient variations in thermal loading. Other element loadings such as pressure are assumed constant over the element and are derived as work equivalent loads. Deformation behavior of the quadrilateral thin shell element is taken to be described by the displacement degrees-of-freedom associated with the grid-points which it connects.

The variation in strain within the element which is permitted by the assumed displacement functions leads to similar stress variation. Advantage is taken of this by exhibiting predicted stress resultants at the four corners as well as at the center of the element. Inplane and normal direct, and shear stress resultants are included. The display of stresses implies a set of axes of reference which are specified from the initial input data.

H. WEIGHT ANALYSIS

The weights of each individual components were calculated and are summarized below. The weight of the regenerative part of the thrust chamber was calculated to be 62.0 lb and that of the radiation cooled nozzle extension to be 46.1 lb.

WEIGHT ESTIMATE BREAKDOWN		lb
Chamber and Nozzle Extension Total =		108.1
Inside Shell TD Nickel 0.322 lb/in^3		15.6
Outside Shell A Nickel 0.343 lb/in^3	(27.2 lb)	
Flange Injector Attachment		8.4
Inlet Ports (2)		3.6
Outside Shell		15.2
Manifold Assy-bolt-on version for nozzle attachment (scroll type) Nickel A		19.2
Divergent Nozzle Extension	(46.1 lb)	
Shell - 030 SCb-291		22.1
Coating - outside silicide		1.4
- inside tungsten and aluminide		7.7
Flange - SCb-291		11.3
Exit Ring - SCb-291		2.1
Nuts, bolts, gasket to attached nozzle		1.5

SYMBOLS

a	Radius
c	Distance from neutral axis to extreme fiber
C	Buckling coefficient
C_c	Buckling coefficient for cylinders
C_p	Buckling coefficient due to pressure
d	Outer diameter
d_1	Inner diameter
D	Ductility factor
e	Moment arm to centroid
E	Modulus of elasticity
F. S.	Factor of safety
F_{tu}	Ultimate tensile strength
F_{ty}	Tensile yield strength
h	Thickness
H	Horizontal force
I	Moment of inertia
M	Bending moment, Material constant
M_o	Moment reaction
M. S.	Margin of safety
N_f	Cycles to failure
P	Pressure
P_c	Chamber pressure
P_{cr}	Critical buckling load
P_{H2}	Hydrogen pressure
P_{throat}	Pressure at the throat

SYMBOLS (Cont'd)

Q	Shear force
R	Mean radius
R. A.	Reduction of area
t	Thickness
U	Deflection in X direction
U. L. F.	Ultimate loading factor
v	Deflection in Y direction
V	Vertical force
W	Weight
Z	Material constant
α	Slope angle of nozzle shell
β	Thin shell stiffness parameter
ϵ	Strain
ϵ_e	Elastic component of strain
$\epsilon_{Plastic}$	Plastic component of strain
μ	Poisson's ratio
σ_{cy}	Compressive yield strength at temperature
σ_f	Fracture stress
σ_M	Bending moment stress
σ	Circumferential (hoop) stress
σ_{Thrust}	Compressive stress due to thrust
σ_u	Ultimate tensile stress
	Semi-angle of arc

IX. INSTRUMENTATION

A. THERMOCOUPLE LOCATIONS

Figure 49 shows locations for thermocouples to measure wall temperature of the TD nickel and coolant temperature of the hydrogen at local stations.

The stations located by Sections B-B and E-E were determined to be the most critical during the heat transfer analysis for this thrust chamber. The station located by Section H-H though for less critical would verify the calculated reduction in heat flux and wall temperature.

As can be seen from Figure 49 the wall temperatures (approximately 0.015 in. from the surface) are measured at sections B-B, P-P, E-E, R-R and H-H. Then at specified distances on either side of the wall temperature measurement locations the coolant temperature is measured; which is shown by Sections A-A, C-C, D-D, F-F, G-G and J-J.

B. INFORMATION TO BE DERIVED FROM THERMOCOUPLE DATA

Figure 50 shows a detailed theoretical temperature distribution in the form of isotherms for a representative case of a hydrogen passage cross section. Such data can be determined for any cross section knowing the thermal boundary conditions of hydrogen bulk temperature, passage geometry, heat flux and coolant heat transfer coefficients compatible with coolant wall to hydrogen temperature ratios. It can be seen that the heat flow under the channel flows directly to the hydrogen and the heat flow under the land is gradually removed from the lands as in the case of a fin. By locating thermocouples in a flow passage at two axial locations (e.g. Section A-A and Section C-C) the heat added (per unit length of the engine) can be determined by a simple heat balance.

$$\dot{Q} = \dot{W} \dot{C}_p \Delta T$$

where

$\dot{Q}$ is heat added between the thermocouple stations BTU/sec
$\dot{W}$ is total hydrogen flow rate - lb/sec
C_p is specific heat at average hydrogen bulk temperature BTU/lb°F
ΔT is measured temperature difference between the thermocouple stations.

The pairs of thermocouples are located 120° apart on the circumference to average out any maldistribution of heating rates, geometry and hydrogen flow/channel. Thus, having determined the heating rate and dividing by the heated wall area the heat flux at the thermocouple locations is now known.

Figure 51 represents the thermal path resistances through a passage cross section under the channel with representative temperatures. The diagram (a) is based on the theoretical analysis using the McCarthy-Wolf expression for coolant heat transfer coefficient.

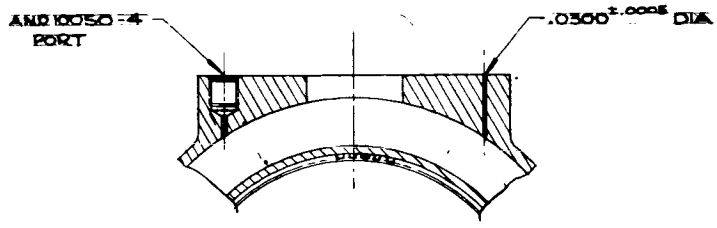

SECTION **M-M**
(TYPICAL 2 PLACES
180° APART)

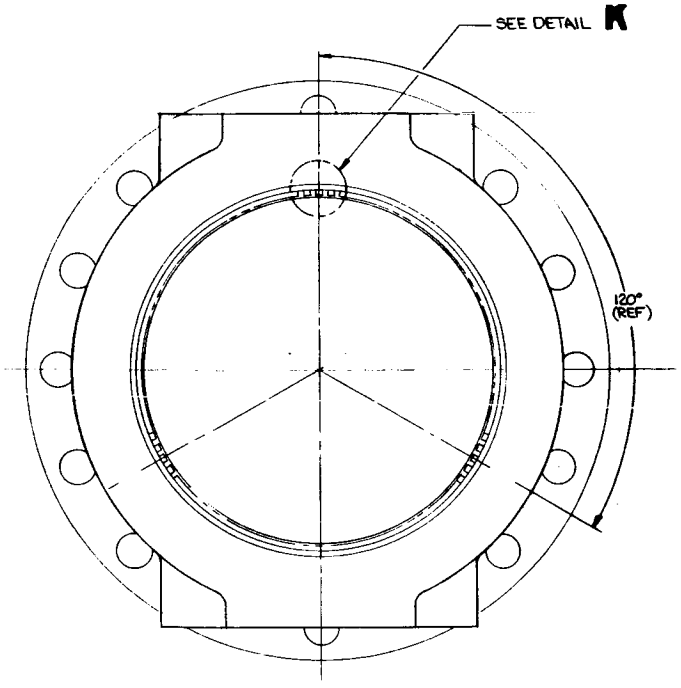

TYPICAL SECTIONS **A-A** & **C-C**

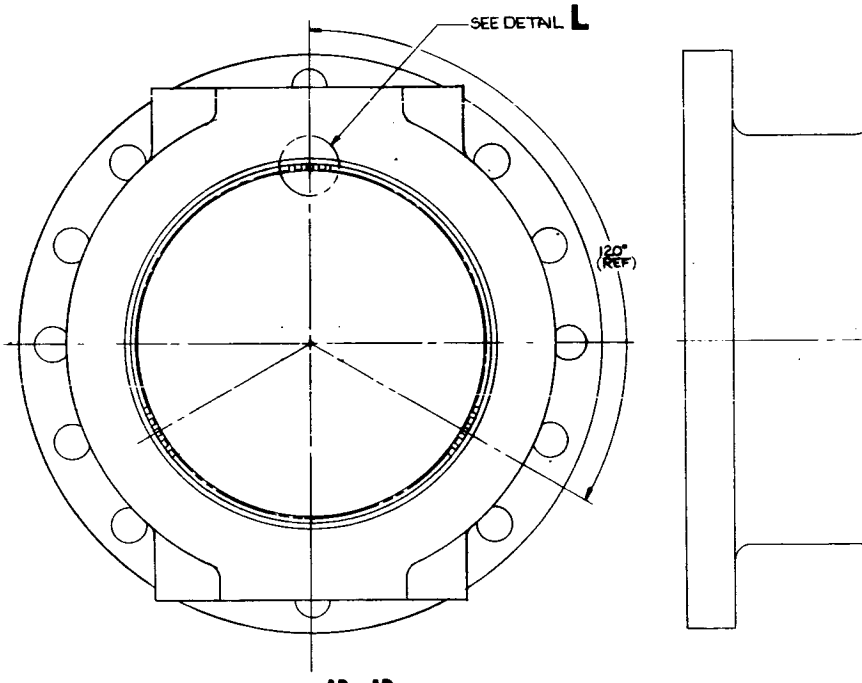

SECTION **B-B**

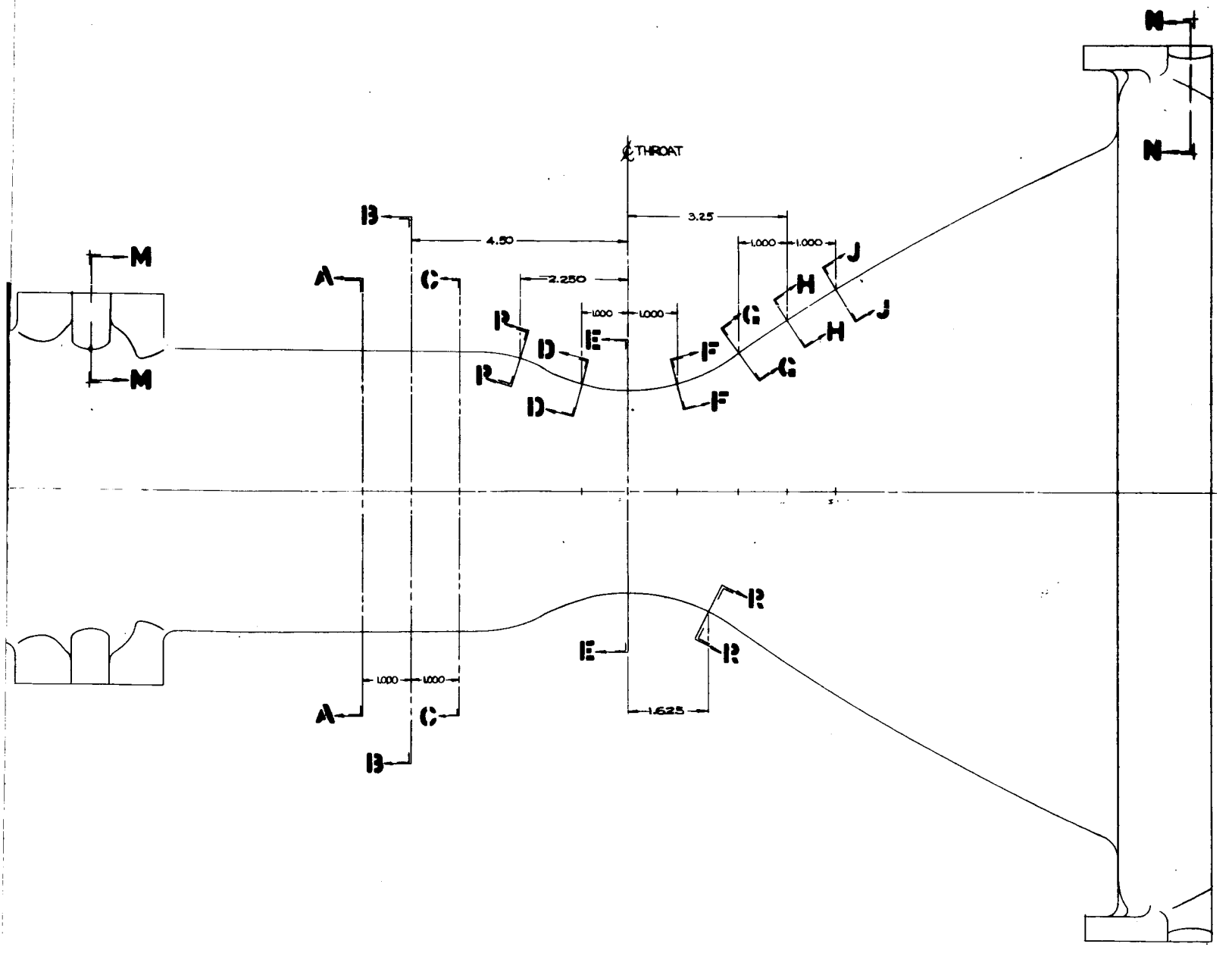

Figure 49. Layout of Chamber Instrumentation

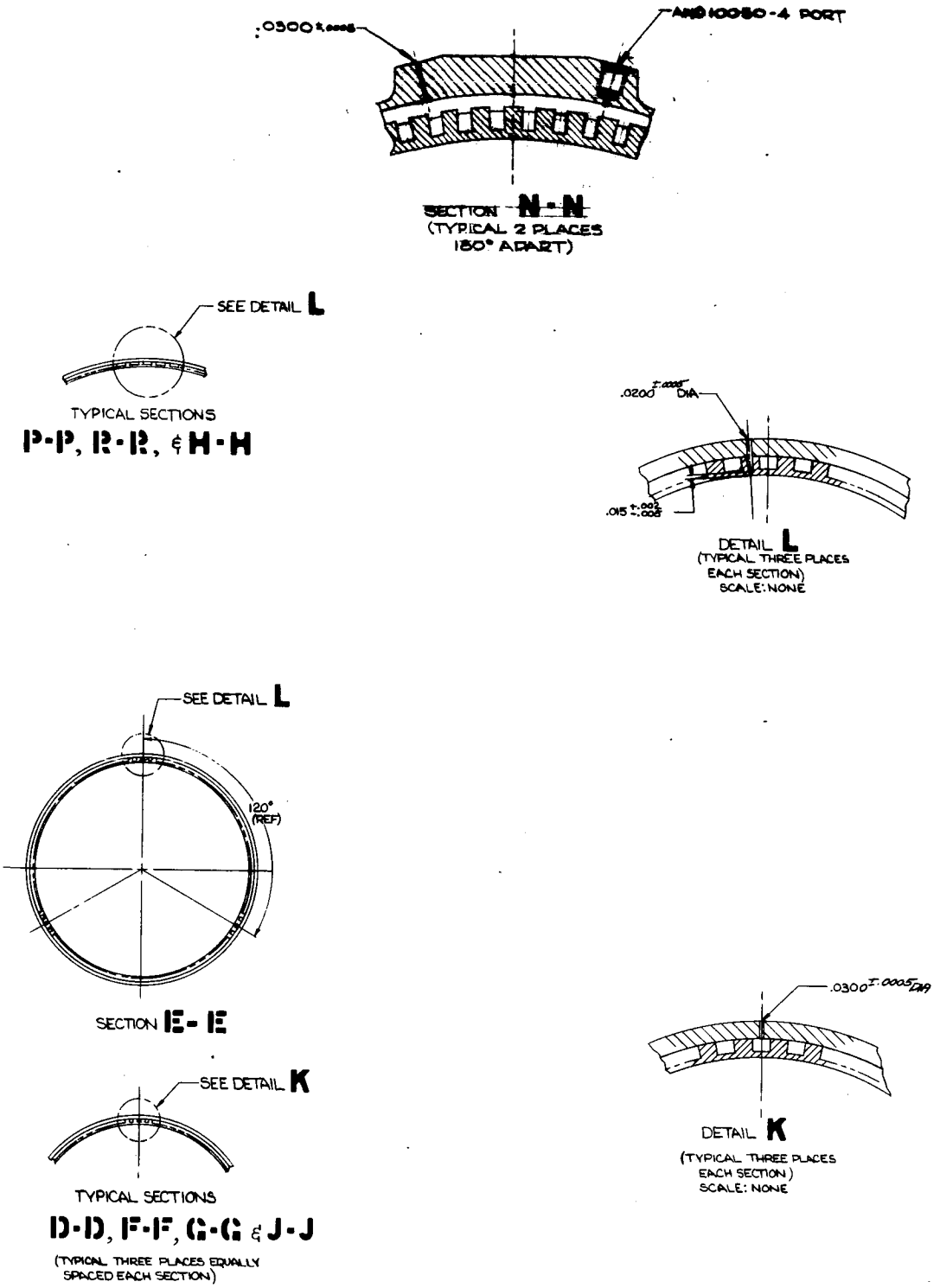

Figure 49. Layout of Chamber Instrumentation (Cont)

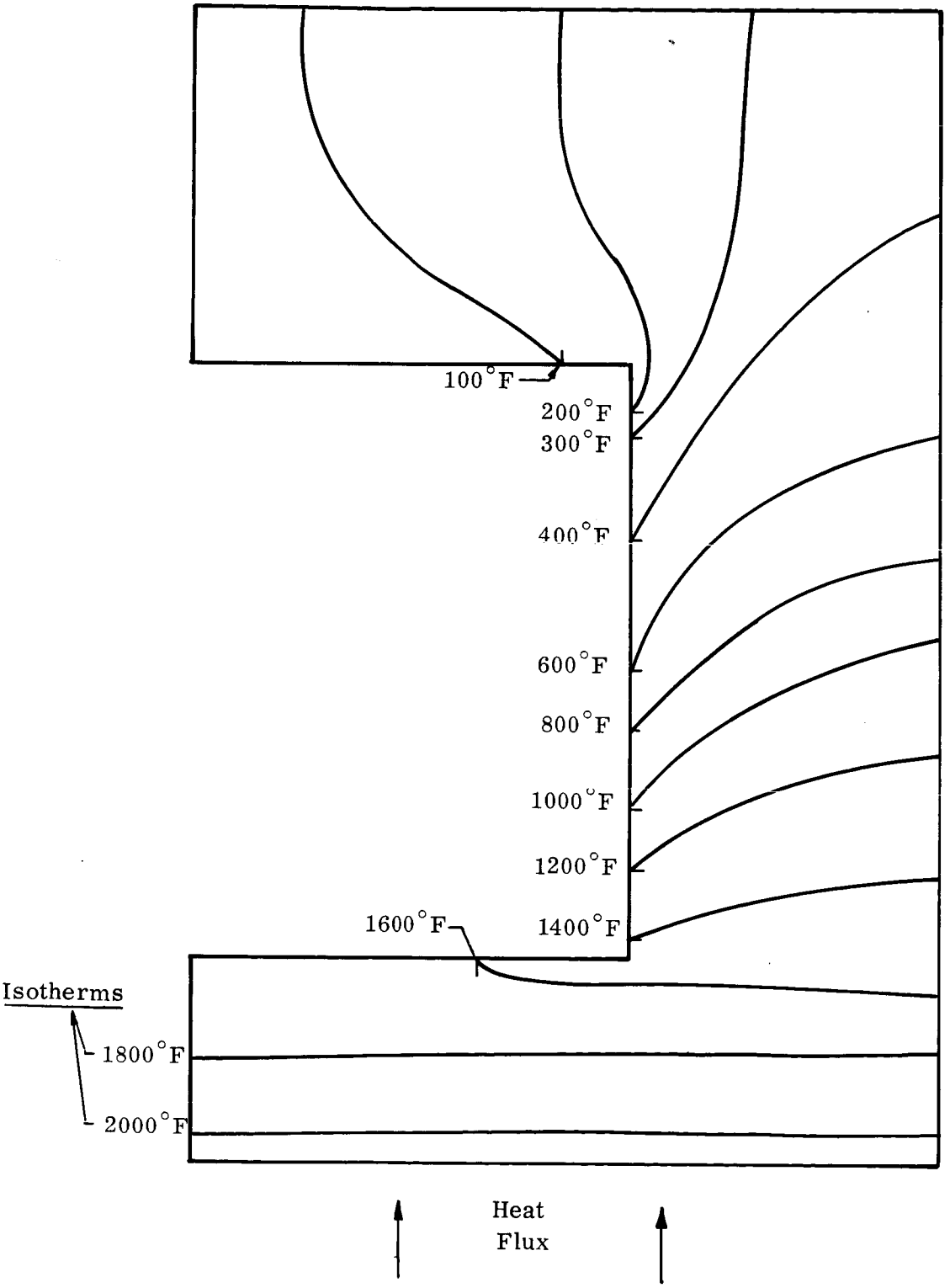

Figure 50. Diagram of Isotherms

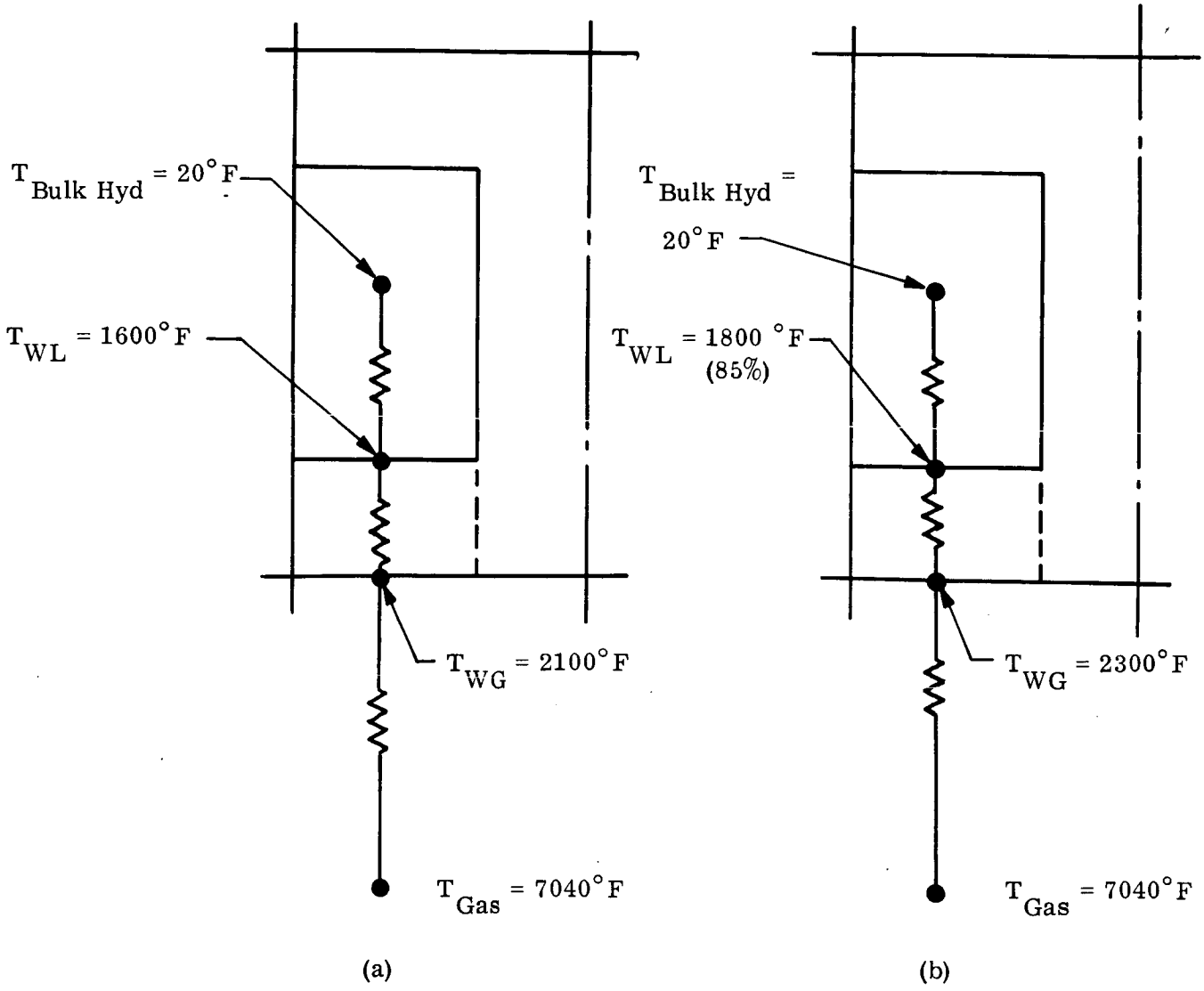

Figure 51. Diagram of Thermal Path Resistances

The value of h is represented by the temperature difference of $(T_{WL} - T_{Bulk}) = 1580^\circ F$. Should the actual heat transfer coefficient be 85% of the theoretical value, the coolant sidewall temperature will increase from $1600^\circ F$ (theoretical) to $1800^\circ F$ (actual) and the gas sidewall temperature will also increase from $2100^\circ F$ (theoretical) to $2300^\circ F$ (actual) based on the measured heat flux. It can be seen, therefore, that for a specific heat flux that the wall temperature distribution is very dependent on the coolant heat transfer coefficient h. If it is therefore apparent that in order to compare the experimental values (temperatures and heat transfer coefficients) with the theoretical values a thermocouple must be located within the wall between each pair of hydrogen bulk thermocouples.

C. ADDITIONAL THERMOCOUPLES

Additional thermocouples as well as pressure taps shown on the inlet and outlet coolant manifolds will monitor the entrance and exit conditions of the hydrogen coolant.

X. CONCLUSIONS

The results of the heat transfer analysis indicated a severe thermal environment for this engine which dictated a high temperature material for the liner. Considering the mechanical properties, chemical compatibility and fabrication characteristics of the materials investigated, it was concluded that TD nickel, a dispersion hardened alloy, was the best material choice for meeting the overall objectives of this program. The machined channel (flow passage) configuration appeared to offer the greatest potential in reducing fabrication cost, time and flexibility in design change relative to a conventional formed and tapered tube bundle. An electroformed nickel outer shell was determined to be the most economical and reliable method of obtaining an enclosure for the flow passages as well as structural reinforcement to the inner liner.

Though the original design goal of 125 psi pressure drop could not be met,the resulting pressure drop of 300 psi is believed to be reasonable for the design requirements imposed, considering todays state-of-the-art on materials and processes.

The pressure drop attributed to loss due to frictional resistance could be further reduced by decreasing the chamber length upstream of the throat. The same chamber volume could be maintained by increasing the chamber diameter. The decreased chamber length would also simplify fabrication and reduce costs in that the amount of metal extruded in the spinning process is considerably decreased and the time and tooling required to produce flow channels is lessened.

REFERENCES

1. Knudsen, J. G., and Katz, D. L., "Fluid Dynamics and Heat Transfer," McGraw-Hill, 1958.

2. "The Heat Transfer Characteristics of Gaseous Hydrogen and Helium," Report No. RR60-12 (NP-10572), North American Aviation Inc., December 1960.

3. "A Study of Forced Convention Heat Transfer to Supercritical Hydrogen," Paper 63-WA-205, ASME, 1963.

4. Geery, E. L., and Thompson, W. R., "Heat Transfer Characteristics of Cryogenic Hydrogen at High Heat Fluxes and Pressures from 800 to 1200 psia, "AIAA Paper No. 66-581, Presented at Colorado Springs, Colorado, June 13-17, 1966.

5. Shaffer, A., and Rousseau, J., "Thermodynamic Properties of 20, 4°K Equilibrium Hydrogen, " Air Research Mfg. Company, ASD Technical Report 61-360, October 1961.

6. Rogers, J. D., Zeigler, R. K., and McWilliams, P., "Hydrogen Transport Property Calculations," LASL Report LA-2527, 17 September 1962.

7. Rogers, J. D., Zeigler, R. K., and McWilliams, P., "Hydrogen Transport Property Calculations," LASL Report LA-2719, 17 September 1962.

8. Harry, D. P., III, "Formulation and Digital Coding of Approximate Hydrogen Properties for Application to Heat-Transfer and Fluid-Flow Computations," NASA Report TND-1664, Lewis Research Center, Cleveland, Ohio.

9. Lezberg, Erwin A., and Franciscus, Leo C., "Effects of Exhaust Nozzle Recombination of Hypersonic Ramjet Performance," NASA, Lewis Research Center, Cleveland, Ohio, AIAA Journal, September 1963.

10. Eckert, R. G., "Survey of Boundary-Layer Heat Transfer at High Velocities and High Temperatures," WADC Tech. Report 59-624, April 1960.

11. Seide, Weingarten, and Morgan, "Final Report on the Development of Design Criteria for Elastic Stability of Thin Shell Structure," STL/TR-60-000-19425, 31 December 1960.

12. Fung, and Sechler, "Buckling of Thin-Walled Circular Cylinders Under Axial Compression and Internal Pressure," JAS Journal, May 1957.

13. Weingarten, Morgan, and Seide, "Elastic Stability of Thin-Walled Cylindrical and Conical Shells under Combined Internal Pressure and Axial Compression," AIAA Journal, Vol. 3, No. 6, June 1965.

14. Manson, S. S., "Thermal Stress and Low-Cycle Fatigue," McGraw-Hill, 1966.

15. Timosheko and Woinowsky-Krieger, "Theory of Plates and Shells," Second Edition, Page 475, McGraw-Hill, 1959.

16. Roark, R. J., "Formulas for Stress and Strain," Fourth Edition, Page 180, Case 35, McGraw-Hill, 1965.

17. Mallett, R. H., "Bell Operational Program for Structural Analysis," (Part I-General Description), Technical Report No. 9500941016, June 1967.

XI. APPENDIXES

APPENDIX A

COMPUTER PROGRAM NO. 068B (1965)
COMPUTER PROGRAM FOR CALCULATING PROPERTIES OF GAS MIXTURES

Presented is a description of a computer program for calculating thermodynamic and transport properties for gas mixtures under various conditions. Frozen and equilibrium properties for equilibrium gas mixtures are computed by the program. Properties are also obtained for a gas mixture whose concentrations have been frozen at a particular temperature. The computer program can calculate properties for shifting and frozen isentropic expansions and for conditions of constant pressure, variable temperature. The equilibrium gas concentrations are determined using the Bell Theoretical propellant performance program, which employs JANAF Thermochemical Data (Ref. 1). All transport property calculations are based upon the Lennard-Jones (6-12) model of the intermolecular potential.

COEFFICIENT OF VISCOSITY

The following equation is used to calculate the first approximation to the coefficient of viscosity for a multi-component gas mixture (Reference 2):

$$\mu_{vis},\ g/m\ sec = - \frac{\begin{vmatrix} F_{11} & F_{12} & \cdots & F_{1n} & x_1 \\ F_{12} & F_{22} & \cdots & F_{2n} & x_2 \\ \vdots & \vdots & & \vdots & \vdots \\ F_{1n} & F_{2n} & \cdots & F_{nn} & x_n \\ x_1 & x_2 & & x_n & o \end{vmatrix}}{\begin{vmatrix} F_{11} & F_{12} & \cdots & F_{1n} \\ F_{12} & F_{22} & \cdots & F_{2n} \\ \vdots & \vdots & & \vdots \\ F_{1n} & F_{2n} & & F_{nn} \end{vmatrix}} \qquad (1)$$

The elements F_{ii} and F_{ij} are given by:

$$F_{ii} = \frac{x_i^2}{\mu_{vis\ i}} + \sum_{\substack{k=1 \\ k \neq i}}^{n} \frac{2x_i x_k}{(M_i + M_k)} \left[\frac{R_2 T}{P \mathcal{D}_{ik}} 1 + 0.6 \frac{M_k}{M_i} A_{ik}^* \right] \quad (2)$$

$$F_{ij} = \frac{-2x_i x_j}{(M_i + M_j)} \frac{R_2 T}{P \mathcal{D}_{ij}} \left[1 - 0.6\ A_{ij}^* \right] \text{ for } i = j \quad (3)$$

where $\mu_{vis\ i}$ = first approximation to the coefficient of viscosity for component i as a pure gas, g/cm sec.

$\mathcal{D}_{ik}$ = first approximation to the coefficient of diffusion of a binary mixture of i and k, cm^2/sec.

A_{ik}^* = function to be defined later

x_i, M_i = mole fraction and molecular weight of component i,

T = temperature, °K

P = pressure, atm and

R_2 = gas constant, 82.0561 cc atm/g-mole °K

The equations for $\mu_{vis\ i}$ and $\mathcal{D}_{ik}$ are as follows:

$$\mu_{vis\ i},\ g/cm\ sec = 266.93 \times 10^{-7} \times \left[\frac{\sqrt{M_i T}}{\sigma_i^2 \Omega_i^{(2,2)}} \right] \quad (4)$$

$$\mathcal{D}_{ik},\ cm^2/sec = 0.0026280 \times \left[\frac{\sqrt{T3\ (M_i + M_k)\ /(2M_i\ M_k)}}{P \sigma_{ik}^2 \Omega_{ik}^{(1,1)}} \right] \quad (5)$$

where T is in °K, P is in atm, and σ is in A.

The variables A*, σ, $\Omega^{(2,2)*}$, and $\Omega^{(1,1)*}$ will be discussed in a later section.

FROZEN THERMAL CONDUCTIVITY

The frozen thermal conductivity is the conductivity which ignores contributions due to chemical reaction. The first approximation to the frozen thermal conductivity of a gas mixture is given by the following Equation (Ref. 2):

$$K_{frozen}, \text{ cal/cm sec } ^\circ K = K'_{mix} - \frac{1}{2} R_1 \sum_{i=1}^{n} \sum_{\substack{j=1 \\ j=i}}^{n} \frac{R_2 T \, x_i \, x_j}{P \mathcal{D}_{ij}} \left[\frac{D_i^T}{x_i M_i} - \frac{D_j^T}{x_j M_j} \right]^2 \quad (6)$$

where D_i^T = first approximation to the coefficient of thermal diffusion in a multicomponent gas mixture,

R_1 = gas constant, 1.98717 cal/g-mole $^\circ K$,

R_2 = gas constant, 82.0561 cc atm/g-mole $^\circ K$,

$\mathcal{D}_{ij}$ = is in cm^2/sec and is given by Equation 5,

T = is in $^\circ K$, and P is in atm.

The terms K'_{mix} and D_k^T are given by the following equations:

$$k'_{mix}, \text{ cal/cm sec } ^\circ K = 4 \frac{\begin{vmatrix} L_{11}^{00} & \cdots & L_{1n}^{00} & L_{11}^{01} & \cdots & L_{1n}^{01} & 0 \\ \vdots & & \vdots & \vdots & & \vdots & \vdots \\ L_{n1}^{00} & \cdots & L_{nn}^{00} & L_{n1}^{01} & \cdots & L_{nn}^{01} & 0 \\ L_{11}^{10} & \cdots & L_{1n}^{10} & L_{11}^{11} & \cdots & L_{1n}^{11} & x_1 \\ \vdots & & \vdots & \vdots & & \vdots & \vdots \\ L_{n1}^{10} & \cdots & L_{nn}^{10} & L_{n1}^{11} & \cdots & L_{nn}^{11} & x_n \\ 0 & \cdots & 0 & x_1 & \cdots & x_n & 0 \end{vmatrix}}{\begin{vmatrix} L_{11}^{00} & \cdots & L_{1n}^{00} & L_{11}^{01} & \cdots & L_{1n}^{01} \\ \vdots & & \vdots & \vdots & & \vdots \\ L_{n1}^{00} & \cdots & L_{nn}^{00} & L_{n1}^{01} & \cdots & L_{nn}^{01} \\ L_{11}^{10} & \cdots & L_{1n}^{10} & L_{11}^{11} & \cdots & L_{1n}^{11} \\ \vdots & & \vdots & \vdots & & \vdots \\ L_{n1}^{10} & \cdots & L_{nn}^{10} & L_{n1}^{10} & \cdots & L_{nn}^{10} \end{vmatrix}} \quad (7)$$

$$D_k^T = -\frac{8M_k}{5R_1} \times \frac{\begin{vmatrix} L_{11}^{00} \cdots L_{1n}^{00} & L_{11}^{01} \cdots L_{1n}^{01} & 0 \\ \vdots \quad\quad \vdots & \vdots \quad\quad \vdots & \vdots \\ L_{n1}^{00} \cdots L_{nn}^{00} & L_{n1}^{01} \cdots L_{nn}^{01} & 0 \\ L_{11}^{10} \cdots L_{1n}^{10} & L_{11}^{11} \cdots L_{1n}^{11} & x_1 \\ \vdots \quad\quad \vdots & \vdots \quad\quad \vdots & \vdots \\ L_{n1}^{10} \cdots L_{nn}^{10} & L_{n1}^{11} \cdots L_{nn}^{11} & x_n \\ x_1 \mathcal{O}_{1k} \cdots x_n \mathcal{O}_{nk} & 0 \cdots 0 & 0 \end{vmatrix}}{\begin{vmatrix} L_{11}^{00} \cdots L_{1n}^{00} & L_{11}^{01} \cdots L_{1n}^{01} \\ \vdots \quad\quad \vdots & \vdots \quad\quad \vdots \\ L_{n1}^{00} \cdots L_{nn}^{00} & L_{n1}^{01} \cdots L_{nn}^{01} \\ L_{11}^{10} \cdots L_{1n}^{10} & L_{11}^{11} \cdots L_{1n}^{11} \\ \vdots \quad\quad \vdots & \vdots \quad\quad \vdots \\ L_{n1}^{10} \cdots L_{nn}^{10} & L_{n1}^{11} \cdots L_{nn}^{11} \end{vmatrix}} \qquad (8)$$

If $\ell = k, \mathcal{O}_{\ell 1k} = 1$; if $\ell \neq k, \mathcal{O}_{1k} = 0$.

A value of 1.98717 cal/g-mole °K is used for the gas constants in Equation 8. The $L_{ij}^{mm'}$ terms are defined as follows:

$$L_{ii}^{00} = 0. \qquad (9)$$

$$L_{ii}^{01} = 1.6 \times \text{constant} \times \frac{T}{P} \sum_{\substack{k=1 \\ k \neq i}}^{n} \frac{x_i x_k M_k \ (1.2\, C_{ik}^* - 1)}{(M_i + M_k)\, \Omega_{ik}} \qquad (10)$$

$$L_{ii}^{10} = L_{ii}^{10} \qquad (11)$$

$$L_{ii}^{11} = -\frac{4x_i^2}{K_i} - 0.64 \times \text{constant} \times \frac{T}{P} \times$$

$$\sum_{\substack{k=1 \\ k\neq i}}^{n} \frac{x_i x_k (7.5M_i^2 + 6.25M_k^2 - 3M_k^2 B_{ik}^* + 4M_i M_k A_{ik}^*)}{(M_i + M_k)^2 \mathcal{D}_{ik}} \tag{12}$$

$$L_{ij}^{00} = 0.64 \times \text{constant} \times \frac{T}{P} \left[\frac{x_i x_j}{\mathcal{D}_{ij}} + \sum_{\substack{K=1 \\ k\neq i}}^{n} \frac{x_j x_k M_j}{M_i \mathcal{D}_{ik}} \right] \quad \text{for } i\neq j \tag{13}$$

$$L_{ij}^{01} = 1.6 \times \text{constant} \times \frac{T}{P} \times \frac{x_i x_j M_i (1.2 C_{ij}^* - 1)}{(M_i + M_j)\mathcal{D}_{ij}} \quad \text{for } i\neq j \tag{14}$$

$$L_{ij}^{10} = \frac{M_j}{M_i} L_{ij}^{01} \quad \text{for } i\neq j \tag{15}$$

$$L_{ij}^{11} = 0.64 \times \text{constant} \times \frac{T}{P} \times \frac{x_i x_j M_i M_j}{(M_i + M_j)^2 \mathcal{D}_{ij}} \times \left[13.75 - 3B_{ij}^* - 4A_{ij}^* \right] \quad \text{for } i\neq j \tag{16}$$

where K_i = first approximation to the coefficient of thermal conductivity for component i as a pure gas, cal/cm sec °K,

A_{ij}^*, B_{ij}^*, C_{ij}^* = functions to be defined later,

$\mathcal{D}_{ij}$ is in cm^2/sec and is given by Equation 5,

T is in °K and P is in atm, and
constant = 41.293 cm^3 atm/cal (conversion factor required to make units work out).

The following equation, which was derived from Equation 8.2-33 of Ref. 2, yields values for K_i:

$$K_i, \text{ cal/cm sec } °K = \frac{\mu_{\text{vis i}}}{M_1} (C_{p\ i} + 1.25\ R_1) \tag{17}$$

where $C_{p\ i}$ = heat capacity at constant pressure for component i, cal/g-mole °K,

R_1 = gas constant, 1.98717 cal/g-mole °K, and

$\mu_{\text{vis i}}$ is in g/cm sec and is given by Equation 4.

EQUILIBRIUM THERMAL CONDUCTIVITY

The equilibrium thermal conductivity for a mixture of gases is given by:

$$K_{equilibrium}, \text{ cal/cm sec } ^\circ K = K_{frozen} + K_{reaction}$$

where K_{frozen} is the chemical reaction contribution, cal/cm sec $^\circ K$

The thermal conductivity due to chemical reaction is given by the following Equation (Ref. 4):

$$K_{reaction}, \text{ cal/cm sec } ^\circ K = -\frac{1}{R_1 T^2} \times \frac{\begin{vmatrix} A_{11} & A_{12} & \cdots & A_{1_\upsilon} & \Delta H_1 \\ A_{12} & A_{22} & \cdots & A_{2_\upsilon} & \Delta H_2 \\ 1 & \vdots & & \vdots & \vdots \\ A_{1_\upsilon} & A_{2_\upsilon} & \cdots & A_{\upsilon\upsilon} & \Delta H_\upsilon \\ \Delta H_{1_\upsilon} & \Delta H_2 & \cdots & \Delta H_\upsilon & 0 \end{vmatrix}}{\begin{vmatrix} A_{11} & A_{12} & \cdots & A_{1_\upsilon} \\ A_{12} & A_{22} & \cdots & A_{2_\upsilon} \\ \vdots & \vdots & & \vdots \\ A_{1_\upsilon} & A_{2_\upsilon} & & A_{\upsilon\upsilon} \end{vmatrix}} \qquad (18)$$

where ΔH_j = heat of reaction of reaction j, cal/g-mole, (Note: It is necessary to describe the system by a set of independent chemical reactions.)

R_1 = gas constant, 1.98717 cal/g-mole $^\circ K$, and

T is in $^\circ K$

The elements A_{ij} are given by:

$$A_{ij} = A_{ji} = \sum_{k=1}^{n-1} \sum_{=k+1}^{n} \left[\frac{R_2 T x_k x_\ell}{\mathscr{D}_{k_\ell} P}\right] \left[\frac{a_{ik}}{x_k} \quad \frac{a_{i\ell}}{x_\ell}\right] \left[\frac{a_{jk}}{x_k} - \frac{a_{j\ell}}{x_\ell}\right] \qquad (19)$$

where a_{ik} = stoichiometric coefficient for chemical species k in reaction i,

R_2 = gas constant, 82.0561 cc atm/g-mole °K,

D_k is in cm^2/sec and is given by Equation 5

p is in atm, and T is in °K.

PARAMETERS USED IN CALCULATING TRANSPORT PROPERTIES

The parameters A*, B*, and C* used in calculating the previously described transport properties are defined as follows:

$$A^* = \Omega^{(2,2)*} / \Omega^{(1,1)*} \tag{20}$$

$$B^* = \left[\frac{5\Omega^{(1,2)*} - 4\Omega^{(1,3)*}}{\Omega^{(1,2)*} / \Omega^{(1,1)*}} \right] / \Omega^{(1,1)*} \tag{21}$$

$$C^* = \tag{22}$$

The $\Omega^{(i,j)*}$ terms are integrals for calculating the transport coefficients for the Lennard-Jones (6-12) potential. Tables of $\Omega^{(i,j)*}$ as a function of reduced temperature are given on pages 1126-1127 of Reference 2. The reduced temperature T* is given by:

$$T^* = T / \left[\epsilon / k \right] \tag{23}$$

where T = temperature, °K, and

$\left[\epsilon/k\right]$ = a potential parameter in the Lennard-Jones (6-12) potential, °K.

The other parameter in the Lennard-Jones (6-12) potential is the collision diameter σ. The collision diameter is used in calculating μ_{vis_i} and σ_{ik} (See Equation 4 and Equation 5). For interactions of molecules with themselves, values of the potential parameters are obtained from the literature. The parameters used in calculating combustion-product transport properties for the F_2/H_2 propellant are listed below (Reference 3).

Interaction	$\left[\epsilon/k\right]$ °K	σ, Å
F-F	112.6	2.968
F_2-F_2	112.6	3.357
H-H	37.0	2.708
HF-HF	330.0	3.148
H_2-H_2	59.7	2.827

For interactions of two different molecules, the potential parameters are obtained using the following combining rules (Reference 2, page 567):

$$\epsilon_{ij} = \sqrt{\epsilon_i \times \epsilon_j} \tag{24}$$

$$\sigma_{ij} = \frac{1}{2} (\sigma_i + \sigma_j) \tag{25}$$

where i indicates the interaction between two molecules of i,

j indicates the interaction between two molecules of j, and

ij indicates the interaction between a molecule of i and a molecule of j.

Other Properties

The equations employed in the calculation of frozen and equilibrium heat capacity of an ideal gas mixture are given below:

$$C_{p\ \text{frozen}},\ \text{cal/g}\ ^{\circ}\text{K} = \left[\sum_{j=1}^{n} x_j\ C_{p\ j} \right] / M_g \qquad (26)$$

where

$C_{p\ j}$ = heat capacity at constant pressure for gaseous species j, cal/g-mole °K, and

M_g = molecular weight of gas mixture (= $\sum_{i=1}^{n} x_i M_i$).

$$C_{p\ \text{equilibrium}},\ \text{cal/g}\ ^{\circ}\text{K} = C_{p\ \text{frozen}} +$$

$$\sum_{j=1}^{N_n} \left[\frac{H_j}{M_g} - \left(\sum_{i=1}^{n} x_i\ H_i \right) \frac{M_j}{(M_g)^2} \right] \left(\frac{\partial x_j}{\partial T} \right)_P \qquad (27)$$

where $H_j = \Delta H_f^{\circ}\ 298\ j + \int_{298}^{T} C_{p\ j}\ dT$

$\Delta H_f^{\circ}\ 298\ j$ being the heat of formation of gaseous species j at 298 °K

(H_j and $\Delta H_{f\ 298\ j}$ are in cal/g-mole)

The partial derivatives of the mole fractions $\left[\left(\frac{\partial\ x_j}{\partial\ T} \right)_P \right]$ are determined by using the equilibrium mole fractions and thermochemical data for each gaseous species. The frozen and equilibrium Prandtl numbers are obtained as follows:

$$Pr_{\text{frozen}} = \frac{\mu \text{vis}\ C_{p\ \text{frozen}}}{K\ \text{frozen}} \qquad (28)$$

$$Pr_{\text{equilibrium}} = \frac{\mu \text{vis}\ C_{p\ \text{equilibrium}}}{K\ \text{equilibrium}} \qquad (29)$$

where

μ_{vis} is in g/cm sec,

C_p is in cal/g °K, and

K is in cal/cm sec °K.

The equations used by the program for computing the enthalpy H (referred to the elements in their thermodynamic standard state at 298°K) and the entropy S of an ideal gas mixture are:

$$H, \text{ cal/g} = \left[\sum_{j=1}^{n} x_j H_j \right] / M_g \qquad (30)$$

where H_j is in cal/g-mole.

$$S, \text{ cal/g °K} = \left[\sum_{j=1}^{n} x_j S_j - R_1 \sum_{j=1}^{n} x_j \ln p_j \right] / M_g \qquad (31)$$

where

S_j = absolute entropy of gaseous species j at one atm pressure, cal/g-mole °K,

P_j = partial pressure of gaseous species j, atm, and

R_1 = gas constant, 1.98717 cal/g-mole °K.

Program Printout

A list of the symbols printed by the computer program and the properties they represent are given in the following table.

Symbol	Property	Units
P	pressure	atm
T	temperature	°R
MW	molecular weight	lb_m/lb-mole
S	entropy	BTU/lbm °R
RHO	density	lb_m/ft^3
MU	viscosity	lb_m/ft sec
CP-EQ	equilibrium heat capacity	BTU/lb_m °R
CP-FR	frozen heat capacity	BTU/lbm °R
K-EQ	equilibrium thermal conductivity	BTU/ft sec °R
K-FR	frozen thermal conductivity	BTU/ft sec °R
PR-EQ	equilibrium Prandtl number	- - -
PR-FR	frozen Prandtl number	- - -
H	enthalpy (referred to elements in their thermodynamic standard state at 298°K)	BTU/lb_m

To convert these properties from the cgs units to the units indicated above, the following conversion factors are used:

1 ca/g °K	=	0.9993312 BTU/lb_m °R
1 ca/g	=	1.798796 BTU/lb_m
1 g/cm sec	=	0.0671969 lb_m/ft sec
1 cal/cm sec °K	=	0.06715196 BTU/ft sec °R

REFERENCES

1. "JANAF Thermochemical Tables, "The Dow Chemical Company, Midland, Michigan.

2. Hirschfelder, Joseph O., Curtiss, Charles F., and Bird, R. Byron, "Molecular Theory of Gases and Liquids", John Wiley and Sons, Inc., 1954.

3. Svehla, R.A., "Estimated Viscosities and Thermal Conductivities of Gases at High Temperatures", NASA TR R-132, 1962.

4. Brokaw, R.S., J. Chem. Phys., 32, 1005 (1960).

APPENDIX B

COMPUTER PROGRAM NO. 5002 FOR DETERMINATION OF HEATING LOADS IN A ROCKET THRUST CHAMBER

DESCRIPTION

This program determines the gas film heating coefficient parametrically as a function of chamber pressure, combustion gas temperature, gas sidewall temperature and area ratio. Output parameters are printed out in non-dimensional form or as a function of inside thrust chamber diameter.

In order to determine the ratio of specific heats in the subsonic and supersonic zones, two approaches were required to determine the Mach number, sonic speed and gas velocities. A constant gamma was used in the subsonic zone and a variable gamma was utilized in the supersonic zone. Subsequent to finding the values of Mach number, sonic speed and gas velocities, the remaining portion of the program will be identical to both zones.

This program may be used over a large range of temperature differentials between combustion gas and gas sidewall as well as a complete range of gas velocities.

METHOD

A. Subsonic Zone

Values of total pressure, combustion temperature, required gas sidewall temperature, and required area ratio are input boundary conditions. The molecular weight at total or stagnation conditions is entered as a table look-up. The density at total and static conditions respectively is:

$$\rho_o = \frac{(MW)_o \, P_o}{RT_o}$$

and

$$\rho_s = \frac{(MW)_s \, P_s}{RT_s}$$

The ratio of specific heat, γ , at constant entropy can now be computed:

$$\gamma = \frac{\text{Log} \quad P_{o/P_s}}{\text{Log} \quad \rho_{o/\rho_s}}$$

The local Mach number may then be found implicitly from the following relationship for a selected area ratio; gamma being constant in all cases.

$$\frac{A}{A+} = \frac{1}{M}\left[\frac{1 + \left(\frac{\gamma - 1}{2}\right) M^2}{\frac{\gamma + 1}{2}}\right]^{\frac{\gamma + 1}{2(\gamma - 1)}}$$

After establishing γ and M, and knowing P_o and T_o, the static pressure and static temperature may be found by:

$$\frac{P_o}{P_s} = \left[1 + \left(\frac{\gamma - 1}{2}\right) M^2\right]^{\frac{\gamma}{\gamma - 1}}$$

and

$$\frac{T_o}{T_s} = 1 + \left(\frac{\gamma - 1}{2}\right) M^2$$

The $(\text{Prandtl Number})_s$ is a table look-up functionally related to T_s. The recovery factor, $(=Pr^{1/3})$, is then computed:

The sonic speed is calculated

$$C_s = \left[\frac{\gamma g RT_s}{(MW)_s}\right]^{1/2}$$

Finally the velocity is calculated by $V=MC_s$

B. Supersonic Zone

The static pressure and temperature are found by a table look-up as a function of area ratio. Total enthalpy and static enthalpy are also found by a table look up as a function of area ratio. Hence, the velocity of the combustion gas can be found by the equation

$$V = \sqrt{2g J (H_o - H_s)}$$

The ratio of specific heat, γ, is then found by the relation $\gamma = \frac{\text{Log } P_o/P_s}{\text{Log } \rho_o/\rho_s}$ as shown in the subsonic zone. The sonic speed now is: $C_s = \sqrt{\frac{\gamma g RT}{(M.W.)_s}}$

and the Mach number $M = V/C_s$

At this point, the method of approach for both zones is identical and follows as such.
T_w, wall temperature, boundary condition Enthalpy of wall, H_w, table look-up
Total enthalpy, H_o, table look-up
Static enthalpy, H_s, table look-up

The recovery enthalpy is described as:

$$H_r = H_s + Pr^{1/3} (H_o - H_s)$$

The recovery temperature T_r is found by a table look-up.

The reference enthalpy H_{ref} is described as:

$$H_{ref} = H_s + 0.5 (H_w - H_s) + 0.22 (H_r - H_s)$$

$$\text{Reynolds Number} = \frac{\rho_{ref} DV}{\mu_{ref}}$$

$(\text{Prandtl})_{ref}$ is obtained from a table look-up.

At H_{ref} the resultant heat flux is defined as:

$$\frac{\dot{q}}{a} = \frac{\bar{K}_G \quad \rho_{ref} \quad V_{ref} \quad (H_r - H_w)}{\left(\frac{\rho VD}{\mu}\right)_{ref}^{0.2} \qquad Pr^{2/3}}$$

hence: $h_g = \frac{\dot{q}/a}{T_r - T_w}$

LIST OF SYMBOLS

A/A*	Area Ratio
C_s	Sonic Speed ft/sec
D	Hydraulic Diameter ft
g	Gravitational Constant 32.2 ft/sec^2
H	Enthalpy BTU/lb
h	Convective Coefficient BTU/hr $ft^2 {}^\circ F$
J	Mechanical Equivalent of Heat 778 $\frac{\text{ft lb}}{\text{BTU}}$
$\bar{K}_G$	Gas Film Coefficient
M	Mach number

MW	Molecular weight	lb/MOL
P	Pressure	lb/ft^2
$\dot{q}/a$	Heat flux BTU/hr	ft^2
R	Universe gas constant	$\frac{ft\ lb}{lb\ ^\circ R}$
T	Temperature	$^\circ R$
V	Velocity	ft/sec

SUBSCRIPTS

g	Combustion Gas
o	Total Conditions
r	Recovery Conditions
s	Static Conditions
w	Wall Conditions
ref	Reference

GREEK

γ	Ratio of Specific Heats	
ρ	Density	lb/ft^3
μ	Viscosity	lb/ft sec

APPENDIX C

COMPUTER PROGRAM USED TO DETERMINE TEMPERATURE AND PRESSURE DISTRIBUTIONS THROUGH THE ENGINE

COMPUTER PROGRAM 3812

THE THICK WALLED MULTI-PASS HEAT EXCHANGER DIGITAL COMPUTER PROGRAM

A sophisicated three-dimensional approach was developed in order to determine the temperature distribution through thick walled passages experiencing thermal radiation interchange. The program accounts for up to six different wall materials, the thermal conductivity of each being a function of temperature. The program is extremely versatile, limited only by the ingenuity of the analyst (within the constraints of computer size) in describing a wide variety of cooling system configurations, i.e., any configuration of multiple flow passages including counter or cross-flow with variable area may be represented mathematically by dividing the system into finite elements and writing the energy balance for each.

From equations of conservation of energy, conservation of momentum, and continuity the temperature and pressure relationships between two arbitrary fluid stations in a flowing system can be obtained. The equations are expressed in the following form:

Conservation of energy:

$$(T_{i+1} - T_i) = \frac{1}{2gJ\bar{C}_p}\left(V_i^2 - V_{i+1}^2\right) + \frac{\dot{Q}}{\dot{W}\bar{C}}$$

Temperature changes of hydrogen between stations — Kinetic energy change stations — Temperature change due to heat to the hydrogen

Conservation of momentum

$$(P_{i+1} - P_i) = \frac{\dot{W}}{g}\left(\frac{V_{i+1} - V_i}{\bar{A}}\right) + \frac{2f\,\rho\,\bar{V}^2\,\Delta X}{144\,g\bar{D}_H}$$

Pressure difference of hydrogen between stations — Pressure change due to change in momentum — Pressure dissipated as friction

Continuity

$$\dot{W} = \rho_i A_i V_i = \rho_{i+1} A_{i+1} V_{i+1}$$

The wall node temperatures are obtained by satisfying the steady-state heat balance equations (written below) for each location in the system.

$$\sum_{j=1}^{j=6} \bar{k}\left(\frac{b_{ij}}{a_{ij}}\left[T_j - T_i\right]\right) + \sum_{j=1}^{2} U_{oi}\,(T_{Lj} - T_i)$$

convection

$$+ \sum \sigma A_i F_{ij}\left[T_j^4 - T_i^4\right] + \Delta S_i \left\{\left(\frac{\dot{q}_{cw}}{T_r}\right)(T_r - T_i)\right.$$

radiation — aerodynamic heating

$$\left. + \left(\frac{\dot{Q}}{A}\right)_i - \sigma \epsilon_{oi} T_i^4 \right\} = 0$$

external heat flux — emitted energy from surface

The friction factor f for smooth tubes is computed from the Karman-Nikuradse expression for Reynolds numbers in excess of 3000 (Reference 1), and for Reynolds numbers less than 2000, the Hagen-Poiseville expression (Reference 1) is employed to compute the friction factor. A linear interpolation between the two is employed in the range of transition.

The overall conductance term U_{oi} for heat transfer from they hydrogen to the wall employs the McCarthy and Wolf expression, (Reference 2), for computing the convective heat transfer coefficient over most of the range of super critical temperatures. However, at near critical temperatures the Hess and Kunz relationship (Reference 3) is employed.

$$U_{oi} = 518{,}400\frac{a_{ij}}{kb_{ij}} + \frac{1}{h_{ij}A_j}$$

where for $60^\circ R \leq T_{L_j} \leq 100^\circ R$

Hess and Kunz:

$$h_{ij} = 0.932\ (10\text{-}4)\ \phi_{ij}\left(\frac{\dot{W}}{A}\right)^{0.8} \frac{1}{\left(\bar{D}_H\right)^{0.2}}\left[\frac{C_p^{0.4}\ K^{0.6}}{\mu^{0.4}}\right]_{\text{Film}} \left[\frac{T_{L_j}}{T_i}\right]^{0.8}\left[1 + 0.0145\ \frac{V_W}{V_L}\right]$$

and for $T_{L_j} > 200^\circ R$

McCarthy and Wolf:

$$h_{ij} = 1.093\ (10^{-4})\ \phi_{ij}\left(\frac{W}{A}\right)^{0.8} \frac{1}{\left(\bar{D}_H\right)^{0.2}}\left[\frac{C_P^{0.4}\ K^{0.6}}{\mu^{0.4}}\right]_{\text{Bulk}}\left[\frac{T_{L_j}}{T_i}\right]^{0.55}$$

McCarthy and Wolf for hydrogen flow in straight heated tubes over a relatively wide range of supercritical temperatures, pressures and wall temperature ratios, however, recent data (Reference 4) indicates that the correlation of Hess and Kunz is more accurate in the near critical range of temperatures.

The governing equations already defined are set up in matrix form in two separate subroutines, i.e., temperature and pressure.

The computer inverts the temperature (fluid and wall nodes) matrix based on the properties of hydrogen at the estimated initial pressure distribution.

Thus, having obtained an initial temperature solution for each node, the pressure matrix is inverted using the initial values of nodal temperatures. The temperatures are iteratively solved until the current solution is within a designated accuracy. Subsequently, a final check of pressures is made. Although the generality of the program requires considerable input ingenuity, the computer running time is reasonable (30 minutes duration for a typical 135 nodes case). The computer time may be minimized by using the results of the thin wall program previously described to obtain initial estimates of fluid temperatures and pressures.

The thick wall program considers the following variable geometries and/or boundary conditions:

(a) fluid node lengths
(b) passage cross-sections
(c) multipass, cross or counter flow
(d) internal convective area
(e) external heated areas
(f) external heat flux
(g) aerodynamic heating
(h) emittance from the external surfaces
(i) radiation interchange
(j) wall material (from 1 to 6)
(k) manifold location
(l) inlet temperatures, inlet pressures and flow rates for a system with multiple inlets.

The hydrogen transport properties used in initial studies were stored in the computer as sets of "look-up tables" obtained from Reference 5, 6, and 7. However, the program was revised to obtain the hydrogen properties directly through the use of a computational technique described in Reference 8. The various thermodynamic, state, and transport properties are computed from approximate analytical expressions and data tabulations to cover the range from melting temperatures to limits imposed by appreciable dissociation for pressures up to 340 atmospheres. It should be noted that the subroutine is very accurate, i.e., characterized by 1 1/2% in state, 1% in enthalpy and 5% in specific heats.

The Hess and Kunz correlation has been used for the calculation of hydrogen convective heat transfer coefficients at hydrogen bulk temperatures of less than 100°R, i.e., near critical. The McCarthy and Wolf correlation has been used for hydrogen bulk temperatures greater than 200°R. Between the two temperature limits an interpolation value for heat transfer coefficient was used.

The Hess and Kunz expression correlates experimental data from 69°R to 85°R and T_W/T_B (hot wall to hydrogen bulk temperature) ratio from 0.33 to 1.76 and pressures from 213 to 315 psia. The McCarthy and Wolf expression correlates experimental data in the ranges from 224 to 773°R, T_W/T_B from 1.50 to 9.25 and pressure 26 to 1354 psia.

Since the present engine will have hydrogen pressures greater than 550 psia, high bulk to wall ratios > 5 and hydrogen temperatures for the most part > 85°R, the McCarthy and Wolf expression appears more applicable.

The two expressions are:

$$h_L = 0.0244 \left(\frac{(W)}{A}\right)^{0.8} \frac{1}{D^{0.2}} \left[\frac{C_p^{0.4} K^{0.6}}{\mu^{0.4}}\right]_B \left[\frac{T_B}{T_W}\right]^{0.55}$$

Hess and Kunz

$$h_L = 0.0208 \left(\frac{(W)}{A}\right)^{0.8} \frac{1}{D^{0.2}} \left[\frac{C_p^{0.4} K^{0.6}}{\mu^{0.4}}\right]_F \left[\frac{T_B}{T_W}\right]^{0.55} \frac{(1+0.0145\ V_W)}{V_B}$$

where

h_L = convective heat transfer coefficient BTU/in.^{2} sec °R

W/A = flow rate of hydrogen lb/in.^{2} sec

D = hydraulic diameter inches

C_p = specific heat of hydrogen BTU/lb °R

K = thermal conductivity BTU-in./in.^{2} - sec - °R

M = viscosity lb/in. sec

T = temperature °R

B = subscript, properties evaluated at hydrogen bulk temperature

F = subscript, properties evaluated at film temperature

W = subscript, properties evaluated at wall temperature

V = kinematic viscosity in.^{2}/sec

In conclusion the utilization of the above correlations over the proposed temperature ranges for each expression is considered to best cover the present design.

Distribution List for Design Report NASA CR-72320
"Investigation of Advanced Regenerative Thrust Chamber Designs"
Contract NAS3-7968
Bell Aerosystems Company
Buffalo, New York

	Copies
National Aeronautics and Space Administration Lewis Research Center 21000 Brookpark Road Cleveland, Ohio 44135	
Attention: Contracting Officer, MS 500-210	1
Liquid Rocket Technology Branch, MS 500-209	12
Technical Report Control Office, MS 5-5	1
Technology Utilization Office, MS 3-16	1
AFSC Liaison Office, MS 4-1	2
Library	2
Office of Reliability and Quality Assurance, MS 500-203	1
E.W. Conrad, MS 100-1	1
E.W. Roberts, MS 3-17	1
D.L. Nored, MS 500-209	1
National Aeronautics and Space Administration Washington, D.C. 20546	
Attention: Code MT	1
RPX	2
RPL	2
SV	1
Scientific and Technical Information Facility P.O. Box 33 College Part, Maryland 20740	
Attention : NASA Representative Code CRT	6
National Aeronautics and Space Administration Ames Research Center Moffett Field, California 94035 Attention: Library	1
National Aeronautics and Space Administration Flight Research Center P. O. Box 273 Edwards, California 93523 Attention: Library	1
National Aeronautics and Space Administration Goddard Space Flight Center Greenbelt, Maryland 20771 Attention: Library	1
National Aeronautics and Space Administration John F. Kennedy Space Center Cocoa Beach, Florida 32931 Attention: Library	1
National Aeronautics and Space Administration Langley Research Center Langley Station Hampton, Virginia 23365 Attention: Library	1
National Aeronautics and Space Administration Manned Spacecraft Center Houston, Texas 77001 Attention: Library	1
J. G. Thibodaux	1
National Aeronautics and Space Administration George C. Marshall Space Flight Center Huntsville, Alabama 35812 Attention: Library	
Keith Chandler, R-P&VE-PA	1
Jet Propulsion Laboratory 4800 Oak Grove Drive Pasadena, California 91103 Attention: Library	1
Dave Evans	1
Office of the Director of Defense Research and Engineering Washington, D C 20301 Attention: Dr. H.W. Schulz, Office of Asst. Dir. (Chem. Technology)	1
RTD(RTNP) Bolling Air Force Base Washington, D.C. 20332	1
Arnold Engineering Development Center Air Force Systems Command Tullahoma, Tennesee 37389 Attention: AEOIM	1
Advanced Research Projects Agency Washington, D.C. 20525 Attention: D.E. Mock	1
Wright-Patterson Air Force Base Dayton, Ohio 45433 Attention: AFML (MAAE)	1
Air Force Systems Command (SCLT/Capt. S.W. Bowen) Andrews Air Force Base Washington, D.C. 20332	1
Air Force Rocket Propulsion Laboratory (RPRRE) Edwards, California 93523 Attention: Roy Silver	

	Copies
Air Force Rocket Propulsion Laboratory (RPM) Edwards, California 93523	1
Air Force FTC (FTAT-2) Edwards Air Vorce Base, California 93523 Attention: Col. J.M. Silk	1
Air Force Office of Scientific Research Washington, D.C. 20333 Attention: SREP, Dr. J.F. Masi	1
U.S. Air Force Washington 25, D.C. Attention: Col. C.K. Stanbaugh, Code AFRST	1
Commanding Officer U. S. Army Research Office (Durham) Box CM, Duke Station Durham, North Carolina 27706	1
U. S. Army Missile Command Redstone Scientific Information Center Redstone Arsenal, Alabama 35808 Attention: Chief, Document Section	1
Bureau of Naval Weapons Department of the Navy Washington, D. C. Attention: J. Kay, Code RTMS-41	1
Commander U. S. Naval Missile Center Point Mugu, California 93041 Attention: Technical Library	1
Commander U. S. Naval Ordnance Test Station China Lake, California 93557 Attention: Technical Library	1
Commanding Officer Office of Naval Research 1030 E. Green Street Pasadena, California 91101	1
Director (Code 6180) U. S. Naval Research Laboratory Washington, D. C. 20390 Attention: H. W. Carhart	1
Picatinny Arsenal Dover, New Jersey Attention: I. Forsten, Chief Liquid Propulsion Laboratory	1
U. S. Atomic Energy Commission Technical Information Services P. O. Box 62 Oak Ridge, Tennessee Attention: A. P. Huber, Code ORGDP Box P	1
Air Force Aero Propulsion Laboratory Research and Technology Division Air Force Systems Command United States Air Force Wright-Patterson AFB, Ohio 45433 Attention: APRP (C. M. Donaldson)	1
Aerojet-General Corporation P. O. Box 296 Azusa, California 91703 Attention: Librarian	1
Aerojet-General Corporation 11711 South Woodruff Avenue Downey, California 90241 Attention: F. M. West, Chief Librarian	1
Aerojet-General Corporation P. O. Box 1947 Sacramento, California 95809 Attention: Technical Library 2484-2015A	1
Aeronutronic Division of Philco Corporation Ford Road Newport Beach, California 92600 Attention: Technical Information Department	1
Aeroprojects, Incorporated 310 East Rosedale Avenue West Chester, Pennsylvania 19380 Attention: C. D. McKinney	1
Aerospace Corporation P. O. Box 95085 Los Angeles, California 90045 Attention: Library-Documents	1
ARO, Incorporated Arnold Engineering Development Center Arnold AF Station, Tennessee 37389 Attention: Dr. B. H. Goethert Chief Scientist	1
Battelle Memorial Institute 505 King Avenue Columbus, Ohio 43201 Attention: Report Library, Room 6A	1
Beech Aircraft Corporation Boulder Facility P. O. Box 631 Boulder, Colorado Attention: J. H. Rodgers	1
Bell Aerosystems Company P. O. Box 1 Buffalo, New York 14240 Attention: Librarian	1
The Boeing Company Aero Space Division P. O. Box 3707 Seattle, Washington 98124 Attention: Ruth E. Peerenboom (1190)	1
Chemical Propulsion Information Agency Applied Physics Laboratory 8621 Georgia Avenue Silver Spring, Maryland 20910	1
Chrysler Corporation Space Division New Orleans, Louisiana Attention: Librarian	1

	Copies
Curtiss-Wright Corporation Wright Aeronautical Division Woodridge, New Jersey Attention: G. Kelley	1
Douglas Aircraft Company, Inc. Santa Monica Division 3000 Ocean Park Blvd. Santa Monica, California 90405 Attention: J. L. Waisman	1
General Dynamics/Astronautics P. O. Box 1128 San Diego, California 92112 Attention: Library and Information Services (128-00)	1
Convair Division General Dynamics Corporation P. O. Box 1128 San Diego, California 92112 Attention: Mr. W. Fenning Centaur Resident Project Office	1
General Electric Company Re-Entry Systems Department P. O. Box 8555 Philadelphia, Pennsylvania 19101 Attention: F. E. Schultz	1
General Electric Company Flight Propulsion Lab. Department Cincinnati 15, Ohio Attention: D. Suichu	1
Grumman Aircraft Engineering Corporation Bethpage, Long Island, New York Attention: Joseph Gavin	1
Hercules Powder Company Allegheny Ballistics Laboratory P. O. Box 210 Cumberland, Maryland 21501 Attention: Library	1
IIT Research Institute Technology Center Chicago, Illinois 60616 Attention: C. K. Hersh, Chemistry Division	1
Kidde Aero-Space Division Walter Kidde & Company, Inc. 675 Main Street Belleville 9, New Jersey Attention: R. J. Hanville, Director of Research Engineering	1
Lockheed Missiles and Space Company P. O. Box 504 Sunnyvale, California Attention: Technical Information Center	1
Lockheed-California Company 10445 Glen Oaks Blvd., Pacoima, California Attention: G. D. Brewer	1
Lockheed Propulsion Company P. O. Box 111 Redlands, California 92374 Attention: Miss Belle Berlad, Librarian	1
Lockheed Missiles and Space Company Propulsion Engineering Division (D.55-11) 1111 Lockheed Way Sunnyvale, California 94087	1
Marquardt Corporation 16555 Saticoy Street Box 2013 - South Annex Van Nuys, California 91404 Attention: Librarian	1
Martin-Marietta Corporation Martin Division Baltimore 3, Maryland Attention: John Calathes (3214)	1
McDonnell Aircraft Corporation P. O. Box 6101 Lambert Field, Missouri Attention: R. A. Herzmark	1
North American Rockwell Corp. Space and Information Systems Division 12214 Lakewood Boulevard Downey, California 90242 Attention: Technical Information Center, D/096-722 (AJ01)	1
Northrop Space Laboratories 1001 East Broadway Hawthorne, California Attention: Dr. William Howard	1
Republic Aviation Corporation Farmingdale, Long Island New York Attention: Dr. William O'Donnell	1
Rocket Research Corporation 520 South Portland Street Seattle, Washington 98108	1
North American Rockwell Corp. Rocketdyne Division 6633 Canoga Avenue Canoga Park, California 91304 Attention: Library, Department 596-306	1
Rohm and Haas Company Redstone Arsenal Research Division Huntsville, Alabama 35808 Attention: Librarian	1
Space-General Corporation 777 Flower Street Glendale, California Attention: C. E. Roth	1
Texaco Experiment, Incorporated P. O. Box 1-T Richmond, Virginia 23202 Attention: Librarian	1

Copies

Thiokol Chemical Corporation
Alpha Division, Huntsville Plant
Huntsville, Alabama 35800
Attention: Technical Director 1

Thiokol Chemical Corporation
Reaction Motors Division
Denville, New Jersey 07834
Attention: Librarian 1

Thiokol Chemical Corporation
Redstone Division
Huntsville, Alabama
Attention: John Goodloe 1

TRW Systems, Incorporated
1 Space Park
Redondo Beach, California 90200
Attention: STL Tech Lib Doc Acquisitions 1

TRW, Incorporated
TAPCO Division
23555 Euclid Avenue
Cleveland, Ohio 44117
Attention: P. T. Angell 1

United Aircraft Corporation
Corporation Library
400 Main Street
East Hartford, Connecticut 06118
Attention: Dr. David Rix 1

United Aircraft Corporation
Pratt & Whitney Division
Florida Research and Development Center
P. O. Box 2691
West Palm Beach, Florida 33402
Attention: Library 1

United Aircraft Corporation
United Technology Center
P. O. Box 358
Sunnyvale, California 94088
Attention: Librarian 1

Vought Astronautics
Box 5907
Dallas 22, Texas
Attention: Warren C. Trent 1

Camin Laboratories, Inc.
104-14 South Fourth Street
Brooklyn, New York 11211
Attention: S. Fialkoff 1